Targeting Non-Genetic Kinase-Dependent Signaling Pathways to Prevent Group 3 Medulloblastoma Tumor Relapse

by

Ujala Chawla

A thesis submitted to the Faculty of Graduate and Postdoctoral Studies of
The University of Manitoba
In partial fulfillment of the requirements of the degree of

MASTER OF SCIENCE

Department of Pathology
Rady Faculty of Health Sciences
University of Manitoba
Winnipeg, MB

Abstract

Medulloblastoma (MB) is the most common pediatric brain tumor, accounting for about 25% of childhood brain tumor cases. Among its molecular subgroups, Group 3 (G3) is particularly aggressive, marked by high rates of metastasis at diagnosis and a devastating 30% recurrence rate that is nearly fatal because of its therapy-resistant nature. Although the transcriptional programs driving primary tumors are well characterized, the molecular mechanisms underlying the transition to therapy resistance remain poorly understood. This challenge is further complicated by the extreme scarcity of matched primary and recurrent patient specimens.

To overcome this challenge, we established a clinically relevant experimental model in which G3 MB cells were treated with standard-of-care chemoradiotherapy (CRT), and living cells were isolated. We then mapped signaling adaptations in these CRT-surviving cell populations, discovering that the non-receptor tyrosine kinase SRC and its downstream effectors were significantly upregulated following CRT. Interestingly, this adaptive increase was exclusive to the G3 MB and was not observed in the SHH subgroup, Group 4 MB, normal human astrocytes, or neural stem cells.

Functional validation through genetic ablation or pharmacological inhibition showed that SRC acts as a central survival anchor for these cells. Disrupting SRC affected the stemness circuitry, involving key factors such as SOX2, NOTCH1, OCT4, and NANOG, and further hindered both migratory and proliferative capabilities. The loss of progenitor identity was accompanied by increased expression of the neuronal marker TUBB3, indicating a forced shift toward terminal lineage differentiation. This fundamental change effectively stripped the cells of their plasticity, initiating dual-mode programmed cell death through both apoptotic and necroptotic pathways.

Finally, repurposing the blood-brain-barrier-permeable SRC inhibitor, Saracatinib, in combination with standard CRT in patient-derived orthotopic xenograft models led to a significant reduction in tumor burden and an extension of overall survival, all without causing neurotoxicity. By uncovering a previously hidden mechanism of recurrence in G3 MB, our research provides a rationale for the clinical application of SRC inhibitors. This approach offers a transformative, neuro-sparing opportunity in pediatric oncology by specifically targeting the signaling pathways that enable the most aggressive tumors to survive, adapt, and recur.

Acknowledgements

First and foremost, I would like to express my deepest gratitude to my supervisor, Dr. Tanveer Sharif, for being a constant source of support, encouragement, and belief in me throughout this journey. His dedication to both science and his students' growth makes him a truly inspiring mentor.

I would also like to extend my heartfelt thanks to Dr. Emma Martell, whose mentorship has exceeded all expectations. Providing guidance with care and wisdom, patiently walking through experiments to help us understand complex technical and theoretical concepts, you have been an incredible source of knowledge and encouragement.

To my amazing lab members, both past and present, Helgi Kuzmychova, Harshal Senthil, Esha Kaul, Akaljot Grewal, Charul Jain, and Kayshana Ramnauth, it has been a privilege to work alongside you. Thank you for creating a collaborative and supportive environment where learning and teaching went hand in hand. None of this work would have been possible without the spirit of teamwork and friendship we built together.

I am also thankful to the Central Animal Care staff, especially Agnes Fresnoza, for her technical expertise and dedication in performing the brain tumor xenograft surgeries that were vital to my research. I would also like to thank Rhonda Kelley, Shawn Blum, Barry (Dean) Jeske, Denise Borowski, and Mike Jackson. Their expertise and training support were essential to my mastery of the critical steps in the animal experiments.

I also want to express my sincere thanks to our collaborators at McMaster University, Dr. Sheila Singh and Dr. Chitra Venugopal, for generously providing samples essential to this study. Additionally, I am deeply grateful to my committee members, Dr. Jody Haigh and Dr. Brad Doble.

Their constructive feedback and steady encouragement throughout this journey were instrumental in shaping this work.

Special thanks to the Department of Pathology at the University of Manitoba and the Faculty of Graduate Studies, particularly Dr. Gabor Fisher, Department Head, and Dr. Yvonne Myal, former Graduate Chair, for creating a supportive academic environment that allowed me to thrive.

Finally, I would like to express my deepest love and gratitude to my family - my parents, my brothers, Kanwal, Sunny, and Nikesh, and my fiancé, Rohan - for being my most incredible supporters. Your endless prayers, sacrifices, love, and encouragement have given me the strength to rise after every setback and keep moving forward. This thesis is not only the result of my efforts but also a reflection of your unwavering support and belief in me. For that, I am forever grateful.

Dedication

This thesis is dedicated to my loving family, my parents, and my brothers, but above all, to my eldest brother, Kanwal. His sacrifices have laid the foundation for everything I have achieved. A decade ago, he left the comfort of home and crossed oceans, carrying the weight of responsibility on his shoulders, to give his siblings a life of dignity, opportunity, and hope. He's the one who first sparked my curiosity for research and guided me along this path, even though his own journey was far from the field of science. He taught me never to give up, listened to my fears, and reminded me that every ending carries the promise of something better. Without him, none of this would have been possible.

I also dedicate this work to all minorities in Pakistan who continue their tireless struggle for equality and justice. They often fight unseen battles, yet they carry immeasurable strength in their hearts. I owe my respect and solidarity; their courage reminds the world that actual progress is born from perseverance and hope.

Finally, I dedicate this thesis to the brave patients battling Medulloblastoma, one of the most devastating diseases. Your unwavering courage, resilience, and stories inspire me deeply. I hope that my research contributes to easing your burden, lighting your path, and strengthening your hope for brighter tomorrows.

TABLE OF CONTENTS

List of Tables

List of Figures

Abbreviation

AML	Acute Myeloid Leukemia
AR	Androgen Receptor
BBB	Blood-Brain Barrier
Ca^{2+}	Ionic calcium
cAMP	Cyclic Adenosine Monophosphate
CBFA	Core Binding Factor Alpha
CML	Chronic Myeloid Leukemia
CNS	Central Nervous System
CRPC	Castration-Resistant Prostate Cancer
CRT	Chemoradiotherapy
CRT-Res	CRT-Resistant
CSCs	Cancer Stem Cells
CSK	C-Terminal Src Kinase
DOX	Doxycycline
DSPs	Dual-Specificity Kinases
EGF	Epidermal Growth Factor
EGL	External Germinal Layer
EMT	Epithelial-To-Mesenchymal Transition
ERK	Extracellular signal-regulated kinases
FAK	Focal Adhesion Kinase
G3	Group 3
G4	Group 4
GBM	Glioblastoma
GCPs	Granule Cell Precursors
GPCRs	G Protein-Coupled Receptors
IVC	Individually vented cage
KO	Knock-Out
LRL	Lower Rhombic Lip
MB	Medulloblastoma
Nec-1	Necrostatin-1
NICG	NOTCH1 Intracellular Domain
NOTCH1	Neurogenic Locus Notch Homolog Protein 1
nRTKs	Non-Receptor Tyrosine Kinases
NSCs	Neural Stem Cells
NTM	NOTCH1 Transmembrane/Cytoplasmic
OCT3/4	Octamer-Binding Transcription Factor 3/4
PARP1	Poly (ADP-Ribose) Polymerase-1
PC	Prostate Cancer
PCW	Post-Conception Weeks
PDOX	Patient-Derived Orthotopic Xenograft
p-SRC	Phosphorylated-SRC

RIP3K	Receptor-Interacting Protein Kinase 3
RL	Rhombic Lip
RL^{SVZ}	Subventricular Zone Rhombic Lip
RL^{VZ}	Ventricular Zone Rhombic Lip
ROS	Reactive Oxygen Species
RTKs	Receptor Tyrosine Kinases
SFKs	SRC Family Kinases
SHH	Sonic Hedgehog
SOX2	SRY-Box Transcription Factor 2
STAT3	Signal Transducer and Activator of Transcription 3
STKs	Serine/Threonine Kinases
TKs	Tyrosine Kinases
TNBC	Triple-Negative Breast Cancer
TUBB3	βIII-tubulin
UBCs	Unipolar Brush Cells
URL	Upper Rhombic Lip
VEGF	Vascular Endothelial Growth Factor
VZ	Ventrical Zone
WHO	World Health Organization
WNT	Wingless-related integration site
Z-VAD-FMK	N-Carbobenzoxy-Valyl-Alanyl-Aspartyl-Fluoromethyl Ketone

CHAPTER 1. INTRODUCTION

1.1. Medulloblastoma

1.1.1. Overview and Epidemiology of Pediatric Brain Tumors

Cancer has a significant impact on the Canadian population, with current estimates showing that nearly 2 in 5 Canadians will be diagnosed with some form of cancer in their lifetime, and approximately 1 in 4 are expected to succumb to some sort of cancer[1]. Within this wider perspective, pediatric oncology stands out as particularly distressing. On average, 1000 children under the age of 15 are diagnosed with cancer in Canada each year[2]. While significant advancements in treatment have been made, approximately 150 of these children die annually from it[2, 3]. Among Canadian children, leukemia is the most common form of cancer, accounting for 33% of all cancer cases[2, 4]. However, tumors of the brain and central nervous system (CNS) are the second most prevalent, representing 20% of the total cancer burden[2, 3, 5].

Although CNS tumors are the second most common type of cancer in terms of incidence, there has been a significant shift in mortality rates. Since 2016, brain tumors have become the leading cause of cancer-related deaths in children and adolescents aged 0 to 19, surpassing leukemia[6, 7]. This trend is especially evident in the United States and Canada, where advancements in leukemia treatment have greatly improved survival rates[8]. In contrast, high-grade CNS malignancies have not seen similar progress[4]. Brain tumors are now recognized as the leading cause of solid cancer deaths in individuals under the age of 20 worldwide[9], highlighting an urgent need for more effective treatment options.

1.1.2. Classification of Pediatric Brain Tumors

The biological framework of pediatric brain tumors is fundamentally distinct from that of adult tumors, requiring a specialized research focus. Adult neuro-oncology is often defined by

tumors that develop as a result of the genetic alterations and environmental exposures accumulated over decades[10, 11]. By contrast, pediatric brain tumors are primarily seen as developmental disorders[12, 13]. These tumors often originate from undifferentiated neural progenitor cells that remain trapped in a primitive state of continuous self-renewal[14]. Their molecular characteristics are often distinguished by a low mutational burden but are heavily influenced by unique epigenetic landscapes and specific developmental driver mutations[15]. These factors retain the cells in an embryonic state of proliferation, preventing the maturation and differentiation required for normal CNS development[16].

According to the current World Health Organization (WHO) classification of CNS tumors, these pediatric malignancies are grouped into several broad categories, including gliomas, ependymomas, and embryonal tumors[17-19]. Among these categories, embryonal tumors are particularly recognized for their aggressive nature and high-grade[18, 20]. Medulloblastoma (MB) is the most common embryonal tumor, arising in the cerebellum and accounting for nearly 20-25% of all pediatric brain tumors[21]. Its tendency to spread through the cerebrospinal fluid, a process known as leptomeningeal dissemination, presents a considerable challenge even for the most intensive multimodal therapies[22].

1.1.3. *Origin of Medulloblastoma*

The cerebellum, essential for motor coordination and higher-order cognitive processing, has an exceptionally protracted developmental timeline compared to other cortical structures[23]. The majority of cerebellar neurons originate from two distinct, spatially segregated germinal zones: the ventricular zone (VZ), which produces GABAergic lineages, and the rhombic lip (RL), which serves as the primary source for all glutamatergic populations[24-26].

In humans, the development of the cerebellum shows a level of structural complexity that is significantly different from that seen in mouse models and even in non-human primates[25]. A key characteristic of this species-specific development is the compartmentalization of the upper RL (URL) around 11 post-conception weeks (PCW)[26, 27]. During this critical period, the URL is divided by a specialized vascular plexus into two distinct germinal environments: ventricular zone RL (RL^{VZ}) and the subventricular zone RL (RL^{SVZ})[26, 27].

The RL^{VZ} serves as a protected reservoir for multipotent stem cell populations, preserving the long-term regenerative potential of the hindbrain[24]. By contrast, the RL^{SVZ} acts as a specialized factory for transit-amplifying progenitor cells[24]. These progenitors migrate rostrally to form the external germinal layer (EGL), where they give rise to granule cell precursors (GCPs) and unipolar brush cells (UBCs)[24, 27]. MB is essentially a developmental glitch that occurs within these specific lineages. It arises when these cells fail to exit the cell cycle and become trapped in a state of continuous embryonic proliferation[28].

1.1.4. *Molecular Classification: Subgroups of Medulloblastoma*

Recent advancements in single-cell transcriptomics and epigenomic mapping have enabled researchers to classify MB into four molecular subgroups **(Table 1)**. Each subgroup is explicitly defined by its specific progenitor cells of origin and distinct anatomical locations within the developing hindbrain, such as the RL and external VZ has unique clinical, biological, and prognostic features[29, 30].

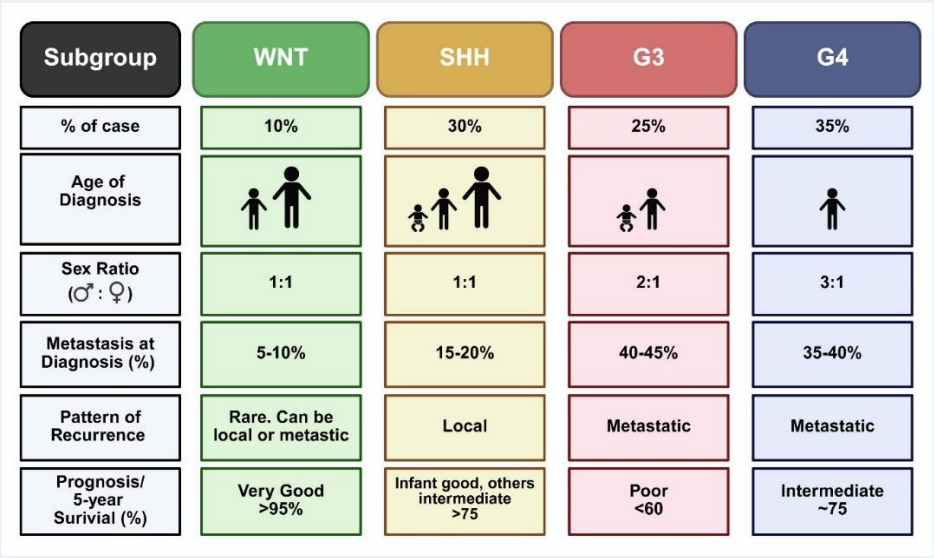

Subgroup	WNT	SHH	G3	G4
% of case	10%	30%	25%	35%
Age of Diagnosis				
Sex Ratio (♂:♀)	1:1	1:1	2:1	3:1
Metastasis at Diagnosis (%)	5-10%	15-20%	40-45%	35-40%
Pattern of Recurrence	Rare. Can be local or metastic	Local	Metastatic	Metastatic
Prognosis/ 5-year Surivial (%)	Very Good >95%	Infant good, others intermediate >75	Poor <60	Intermediate ~75

Table 1. Clinical and Molecular Features of Medulloblastoma (MB) Subgroups.

The Wingless (WNT) subgroup, which accounts for approximately 10% of all MB cases, is remarkably distinct, originating not from the cerebellum itself but from the lower RL (LRL) of the dorsal hindbrain and the adjacent embryonic dorsal brainstem[27, 31, 32]. The primary driver of these tumors is the constitutive activation of the WNT signaling pathway, which typically occurs due to missense mutations in the *CTNNB1* gene, which encodes *β*-catenin[33]. These mutations prevent the degradation of *β*-catenin, allowing it to accumulate in the nucleus, where it functions as a transcription factor to drive the aberrant expression of target genes[33]. As a result of their origin in this specific LRL niche, WNT tumors are anatomically localized to the fourth ventricle and the brainstem[33, 34]. This localization contributes to their distinct clinical presentation and the most favorable outcomes among all MB subgroups, with 5-year overall survival rates exceeding 90%[34].

The Sonic Hedgehog (SHH) subgroup accounts for 30% of MB cases and is directly linked to the URL-EGL axis[35, 36]. These tumors originate from the GCP lineage. During normal development, GCPs undergo a significant expansion phase in the EGL, which is stimulated by SHH ligands. However, genetic alteration in *PTCH1*, *SMO, SUFU*, or downstream effectors causes

cells to disregard the regulatory stop signals that typically control development[31, 37, 38]. As a result, the GCPs enter a persistent state of proliferation, failing to migrate to the external granule layer and instead forming a malignant mass on the surface of the cerebellum.

SHH MB is a clinically diverse subgroup of tumors, where patient outcomes are significantly influenced by factors such as age, histopathology, and specific genetic drivers, particularly the *TP*53 tumor suppressor gene[39, 40]. While infants and a large portion of the adult population often have more favorable outcomes, the prognosis changes dramatically for children aged 5 to 16[40]. Simultaneous activation of the SHH pathway and *TP*53 somatic mutations leads to significant genomic instability and strong resistance to conventional treatments[39]. This molecular distinction is so fundamental to the disease's behavior that the WHO has classified SHH tumors based on their *p*53 status. Consequently, the subset of tumors with *p*53 mutations presents a significant therapeutic challenge, as these tumors have an advanced ability to evade apoptotic checkpoints and continue to grow malignantly, even in the face of aggressive treatments[39, 41].

While WNT and SHH MBs originate from clearly separated niches, Group 3 (G3) and Group 4 (G4) are considered as part of a developmental continuum arising from the glutamatergic lineages of the URL[42, 43]. High-resolution cellular mapping has demonstrated that these two subgroups are not entirely distinct; instead, they represent different stages along a single maturation pathway[43]. G3 MB represents the most primitive and lethal end of the disease spectrum, accounting for approximately 25% of all cases[30]. These tumors are believed to arise from early progenitor cells within the RL^{VZ} and are characterized by significant *MYC* amplification or overexpression[30, 37, 44, 45]. This molecular driver functions as a developmental handbrake, keeping cells in an undifferentiated, stem-like state while promoting uncontrolled proliferation and self-renewal. Due to its embryonic characteristics, G3 MB is exceptionally versatile and aggressive,

often leading to metastasis in about 40% of patients at the time of diagnosis[30, 44, 45]. In contrast to the WNT or SHH subgroups, G3 MB cells lack clinically actionable molecular vulnerabilities, making them notoriously difficult to treat[46, 47]. Furthermore, G3 MB exhibits tumor relapses, affecting approximately 30% of G3 MB patients. These relapses are uniformly fatal, as the tumor evolves to resist standard radiation and chemotherapy treatments. As a result, patients face poor outcomes, with 5-year survival rates often falling below 60%[48].

G4 MB is the most common yet complex subtype, accounting for approximately 35% of all cases[37, 48]. These tumors are believed to originate from progenitor cells that have migrated into the RL^{SVZ} and have aligned with the UBC lineage[24, 49]. Although these cells have advanced beyond the primitive state observed in G3, their maturation is hindered by genetic disruptions, particularly through enhancer hijacking and the abnormal activation of the *PRDM6* oncogene[50]. This disruption affects the activity of the Core Binding Factor Alpha (*CBFA*) complex (*CBFA2T2 and CBFA2T3*), which impairs the cell's ability to remodel chromatin and activate the gene programs required for terminal differentiation[37, 48]. Clinically, G4 presents a unique paradox: although it has a high metastasis rate at diagnosis, patients generally have an intermediate-to-favorable prognosis compared to G3, with 5-year survival rates typically exceeding 75%[48].

The identification of four distinct molecular subgroups **(Table 1)** has fundamentally redefined MB, transforming it from a single clinical diagnosis into a collection of biologically distinct diseases[48]. This shift has propelled the field toward a precision medicine approach, where the unique molecular characteristics of each tumor guide its clinical management. In practice, this means we can now consider therapy de-escalation for WNT MB patients, aiming to reduce long-term treatment toxicity while maintaining high survival rates. By contrast, for the SHH subgroup,

research focuses on the development and clinical testing of targeted inhibitors to specifically block the oncogenic signaling driving those tumors[51].

The clinical reality for G3 MB patients highlights a significant and urgent gap in our current treatment options. G3 represents the most challenging therapeutic issue in pediatric neuro-oncology due to its primitive, stem cell-like biology, which confers inherent resistance to standard treatments[30, 45, 48]. Lacking viable molecular targets, these patients often face limited options beyond aggressive, high-toxicity regimens that frequently fail to prevent relapse[47]. Addressing the unique resilience of G3 tumors is a critical priority for the next generation of MB research.

1.1.5. *Tumor Recurrence in G3 MB*

The current clinical standard-of-care for G3 MB involves a combination of surgical resection, craniospinal irradiation, and cytotoxic chemotherapy[52-54]. This approach aims to dismantle the tumor and its ability to proliferate. However, even with these aggressive interventions, G3 MB tumors have a high rate of recurrence[54]. This recurrence is increasingly linked to a specialized group of cancer stem cells (CSCs) **(Figure 1),** which act as a reservoir for relapses[55, 56]. CSCs do not just survive treatment; they actually thrive afterward by actively remodeling their tumor microenvironment. As therapy eliminates the majority of sensitive cells, the resulting empty niche becomes a fertile ground for the surviving CSCs, which secrete growth factors and modify the extracellular matrix. This effectively protects them from further therapeutic attacks and prepares the area for regrowth[55-57].

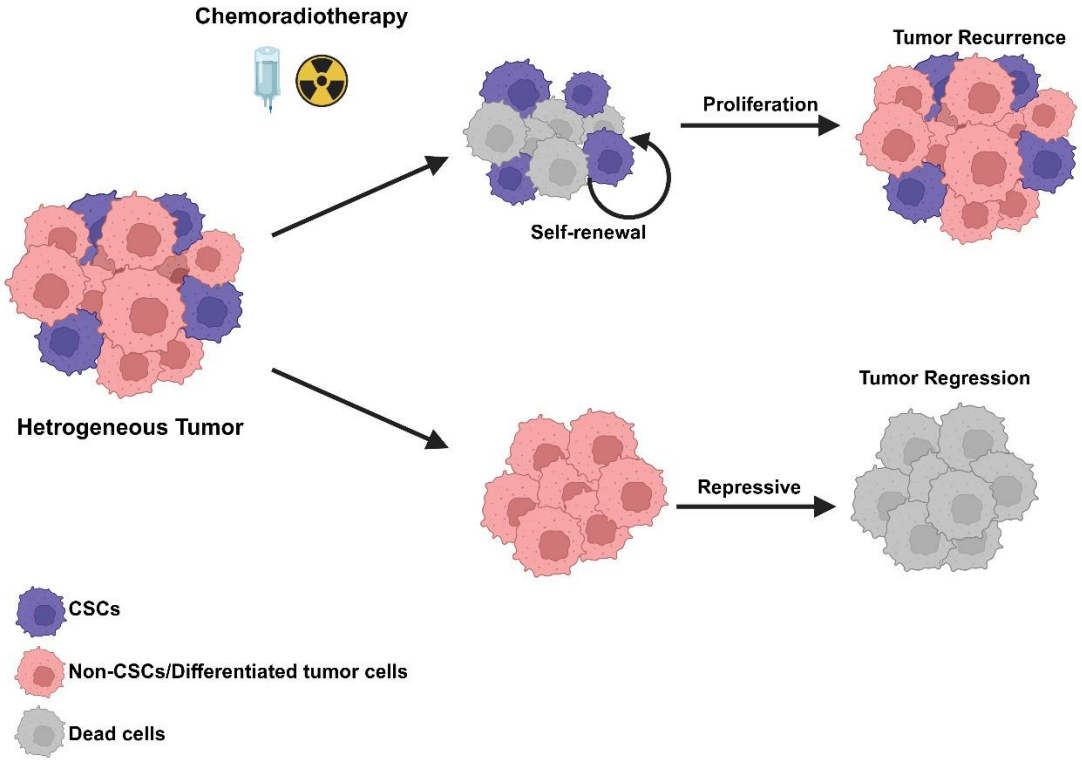

Figure 1. Cancer Stem Cell Survival and Post-Therapy Tumor Proliferation.
Treatment-resistant Cancer Stem Cells (CSCs) survive therapy to drive tumor recurrence through self-renewal and proliferation, whereas sensitive non-CSCs result in tumor regression.

What makes G3 MB relapse particularly dangerous is its remarkable genetic stability. Longitudinal studies comparing patient-matched primary tumors and their relapsed counterparts show that these cancers rarely acquire new driver mutations[51, 58]. Instead, the tumor's memory for survival and regrowth is influenced by non-genetic adaptations. This indicates that the transition from a primary treatable tumor to a fatal relapse is not due to changes in the DNA, but rather a significant shift in the cellular signaling networks that execute the genetically encoded plans.

1.2. Cell Signaling

1.2.1. Overview of Cell Signaling

Cell signaling is the essential biochemical language that allows a cell to sense its environment and respond with precise physiological changes[59, 60]. In multicellular organisms, cells do not exist in isolation; instead, they are part of a vast, interconnected network that requires constant communication to maintain homeostasis[61]. This signaling network acts like a biological operating system, governing crucial decisions that a cell makes, such as whether to grow, divide, move, or undergo cell death[61, 62]. At its core, cell signaling involves converting an extracellular stimulus into a specific intracellular response. Without this process of interpreting extracellular signals, tissues would lose their structural integrity, and the coordinated development of complex organs would be impossible. In a healthy state, these signaling pathways operate within a strict system of checks and balances, ensuring that a cell initiates growth or movement only when it receives a clear, verified signal from its surroundings[59, 61, 62].

1.2.2. Signal Processing: Membrane to Nucleus

The journey of a message from the cell surface to the nucleus is a remarkable example of biological engineering known as signal transduction[63]. This process begins when a ligand, such as a hormone, growth factor, or neurotransmitter, binds to a specific transmembrane receptor. Some of these ligands cannot cross the lipid bilayer of the cell membrane; therefore, they depend on receptors to transmit their signals. Two major classes of receptors are G Protein-Coupled Receptors (GPCRs), which activate intracellular secondary messengers, and Receptor Tyrosine Kinases (RTKs), which possess intrinsic enzymatic activity[64, 65]. When a ligand binds to its receptor, the receptor undergoes a conformational change, effectively signaling that an external event has taken place and allowing communication with the cell's interior[65].

Once the signal crosses the cell membrane, it enters a phase of rapid amplification. This process primarily involves a phosphorylation cascade, a high-speed relay race in which enzymes called kinases add phosphate groups (PO_4^{3-}) to downstream proteins[66]. This step is crucial because a single ligand can activate thousands of effector molecules, creating a biological waterfall effect. To facilitate this flow, cells use second messengers such as cyclic adenosine monophosphate (cAMP) and calcium ions (Ca^{2+}), which diffuse rapidly to reach various organelles[66]. This internal communication is rarely linear; rather, it resembles a complex network where multiple pathways engage in crosstalk, allowing the cell to integrate conflicting signals before committing to a specific course of action.

The final destination for this relay is the nucleus. When a signal aims to change a cell's long-term identity, the pathway culminates in the activation of specific transcription factors. These proteins translocate to the nucleus and bind to cis-regulatory elements, such as enhancers and promoters, to initiate targeted gene transcription[67]. This coordinated shift in the transcriptional program enables the cell to produce the specific proteins required for its next functional phase, whether that involves DNA replication for mitosis or the synthesis of metabolic enzymes. Beyond the nucleus, signaling also drives immediate structural changes, such as cytoskeletal remodeling, where actin polymerization generates the mechanical force necessary for chemotaxis toward a wound or pathogen[64, 68].

To maintain homeostasis and prevent diseases such as cancer, cells must eventually silence certain signals. This termination can occur through several mechanisms, such as ligand degradation, receptor internalization via endocytosis, or the action of phosphatases, which act as an off switch by removing the phosphate groups that kinases add[68]. A key concept in this process is the kinome, the complete collection of kinases that serve as the cell's primary signaling hub. As

the decision-makers of the phosphorylation cascade, kinases play a critical role as gatekeepers of cellular behavior.

1.2.3. *Classification of Kinases*

The human kinome represents one of the most refined regulatory systems in biology, functioning like a sophisticated circuit board that translates signals from outside the cell into precise genomic and proteomic responses. The human genome encodes around 518 protein kinases, but their diversity is governed by a structural and evolutionary hierarchy[69].

At a fundamental level, these enzymes are classified into three types based on their substrate specificity, which refers to the specific chemical binding sites they select for attaching a phosphate group. The majority of protein kinases are Serine/Threonine kinases (STKs), which modify the hydroxyl groups on these specific amino acids to alter protein function. These kinases often function as the essential components of intracellular signaling pathways[70]. Notable examples include AKT, which plays a central role in regulating metabolism and cell survival, and mTOR, responsible for integrating nutrient sensing with cell growth. Another important group within this class is the ERK/MAPK family, which acts as a main channel for transmitting growth signals from the cell membrane to the nucleus to initiate transcription[70, 71].

By contrast, the second type, Tyrosine kinases (TKs), evolved later and serve as specialized communicators in multicellular organisms, often acting as high-fidelity receptors for growth factors. Lastly, a smaller group, known as dual-specificity kinases (DSPs), has the unique ability to act on all three types of residues (serine, threonine, and tyrosine), enabling them to connect different signaling pathways and serve as critical integration points for cellular logic[70].

In the hierarchy of TKs, it is important to differentiate between RTKs and non-Receptor TKs (nRTKs). RTKs are transmembrane proteins that serve as the cell's main antennas, featuring

an extracellular ligand-binding domain, a single transmembrane helix, and an intracellular catalytic domain. When external growth factors, such as EGF (epidermal growth factor) or VEGF (vascular endothelial growth factor), bind to these receptors, the RTKs dimerize and recruit lipid kinases like PI3K[70, 72]. Although PI3K primarily phosphorylates lipids rather than proteins, it plays a crucial role as a partner of TKs by generating the chemical signals necessary to recruit and activate downstream STKs, such as AKT. This coordination is essential for translating external environmental signals into cellular decisions related to growth and differentiation[70].

nRTKs play a crucial role in cellular signaling. Unlike RTKs, which have ligand-binding domains on the outer surface of the cell membrane, nRTKs are either found in the cytoplasm or anchored to the inner side of the cell membrane[72, 73]. They are activated by intracellular signals, including those from GPCRs and interactions with the cell matrix. Examples of nRTKs include the SRC and ABL families. These kinases act as flexible hubs within the cell, integrating signals from various cell-surface receptors and directing them to specific internal targets. For instance, they can transmit signals to the cytoskeleton to facilitate movement or to the cell's survival mechanisms. By serving as a link between the cell's outer environment and its internal processes, nRTKs ensure that the cellular response to external stimuli is amplified and accurately targeted[72-74].

Altogether, the coordination among these kinases creates a layered regulatory control system. RTKs and associated lipid kinases, such as PI3K, often serve as primary sensors of extracellular signals. nRTKs and STKs, including the ERK and mTOR pathways, function within an integrated signaling cascade to mediate downstream biological effects. This delicate balance of phosphorylation is maintained by the counteracting actions of phosphatases, ensuring that the off

switches are strictly regulated to prevent uncontrolled signaling, often seen in pathological conditions[75, 76].

1.2.4. *The SRC Family of Non-Receptor Tyrosine Kinases*

The SRC Family Kinases (SFKs) consist of nine nRTK members that are highly conserved and serve as central hubs for integrating intracellular signaling. SFKs include SRC, FYN, YES, BLK, FGR, HCK, LCK, LYN, and YRK. These kinases play a vital role in translating extracellular signals into organized biochemical pathways that influence cell fate. Although they share a structural similarity, the kinases have evolved to have distinct functional specializations, resulting in unique expression profiles and regulatory functions across various human tissues[77, 78].

SFKs are divided into three main groups based on their spatial expression patterns. The first group, known as the ubiquitous group, includes SRC, FYN, and YES; these members are expressed across a wide range of cell types and maintain essential homeostatic processes, including mitogenesis, cytoskeletal reorganization, and survival signaling. By contrast, the second group, the hematopoietic-restricted group, consists of BLK, FGR, HCK, LCK, and LYN. These kinases are primarily found in immune cell lineages, where they coordinate the complex signaling required for leukocyte activation and inflammatory responses. Finally, a distinct member of this family is YRK. Unlike its siblings, YRK is not found in the human genome; it is an avian-specific ortholog originally characterized in chicken cells[79, 80].

Despite their differing biological roles, members of the SFK family share a common mechanical framework. Each member of this family employs a conserved allosteric snap-lock mechanism that allows them to switch between an inactive dormant state and an active catalytic conformation. The uniqueness of each kinase does not arise from the catalytic domain, but rather from a region known as the Unique region **(Figure 2A-B)**. The structural plasticity of the unique

region serves as a selective interface, allowing each kinase to identify and engage a specific subset of molecular partners. This structural characteristic ensures that even when multiple kinases are present in the same cytoplasm, a particular kinase, such as SRC, can perform its unique signaling functions with high precision and minimal interference from others[81].

1.2.5. *Conformational Dynamics of SRC*

SRC is a prototypical member of the nRTK family. Its discovery as the first cellular proto-oncogene transformed our understanding of how intracellular signaling regulates life and death at the molecular level[82]. Unlike receptor kinases, which require an external ligand to activate them, SRC functions as an internal processor. It integrates upstream signals to control the cell's mechanical, chemical, and structural responses[81].

In the domain of nRTKs, SRC serves as a key model for understanding how proteins connect complex intracellular signals. The human SRC protein consists of 536 amino acids and showcases a modular structure that allows it to shift between a dormant state and an active signaling site[83]. The N-terminus begins with the SH4 domain **(Figure 2A)**, which undergoes a covalent lipid modification known as myristoylation at Glycine 2. This modification anchors the protein to the inner layer of the plasma membrane, positioning it near its upstream activators. Next to this anchor is the unique region **(Figure 2A)**, an intrinsically disordered region (IDR) that facilitates specific protein-protein interactions and allosteric regulation. This IDR is essential for SRC's functional specificity, enabling it to interact with unique cellular partners that other SRC family members cannot recognize[84].

The regulatory core of the protein comprises the SH3 and SH2 domains **(Figure 2A)**, which facilitate protein-protein interactions by binding to proline-rich sequences and phosphorylated tyrosine residues, respectively. These domains are located before the SH1 catalytic domain, which

contains the ATP-binding pocket and the activation loop, serving as the protein's enzymatic engine. **(Figure 2A)** For the enzyme to achieve its full catalytic potential, it must undergo autophosphorylation at Tyrosine 419 (Y419), a residue located within the activation loop that stabilizes the catalytic site in a conformation that is favorable for substrate binding. Regulation of this enzymatic activity is accomplished through an internal snap-lock mechanism[81, 82, 84].

In healthy, resting cells, SRC is maintained in a closed, inactive conformation by the C-terminal Src Kinase (CSK) **(Figure 2B)**. CSK phosphorylates a regulatory tyrosine at the C-terminal tail (Y530), which acts as an internal ligand that bends backward to bind to SRC's own SH2 domain. At the same time, the SH3 domain clamps onto a linker region between the SH2 and SH1 domains, physically shielding the catalytic site and preventing unwanted signaling. Activation, or the opening of the molecule, is a dynamic process that begins when specific phosphatases remove the inhibitory phosphate at Y530 **(Figure 2B)**. Higher-affinity external partners, such as activated growth factor receptors or integrin-associated proteins, can recruit the SH2/SH3 domains. This release enables the protein to transition to an extended open state, facilitating the autophosphorylation of Y419 and the recruitment of downstream substrates[81, 82, 84].

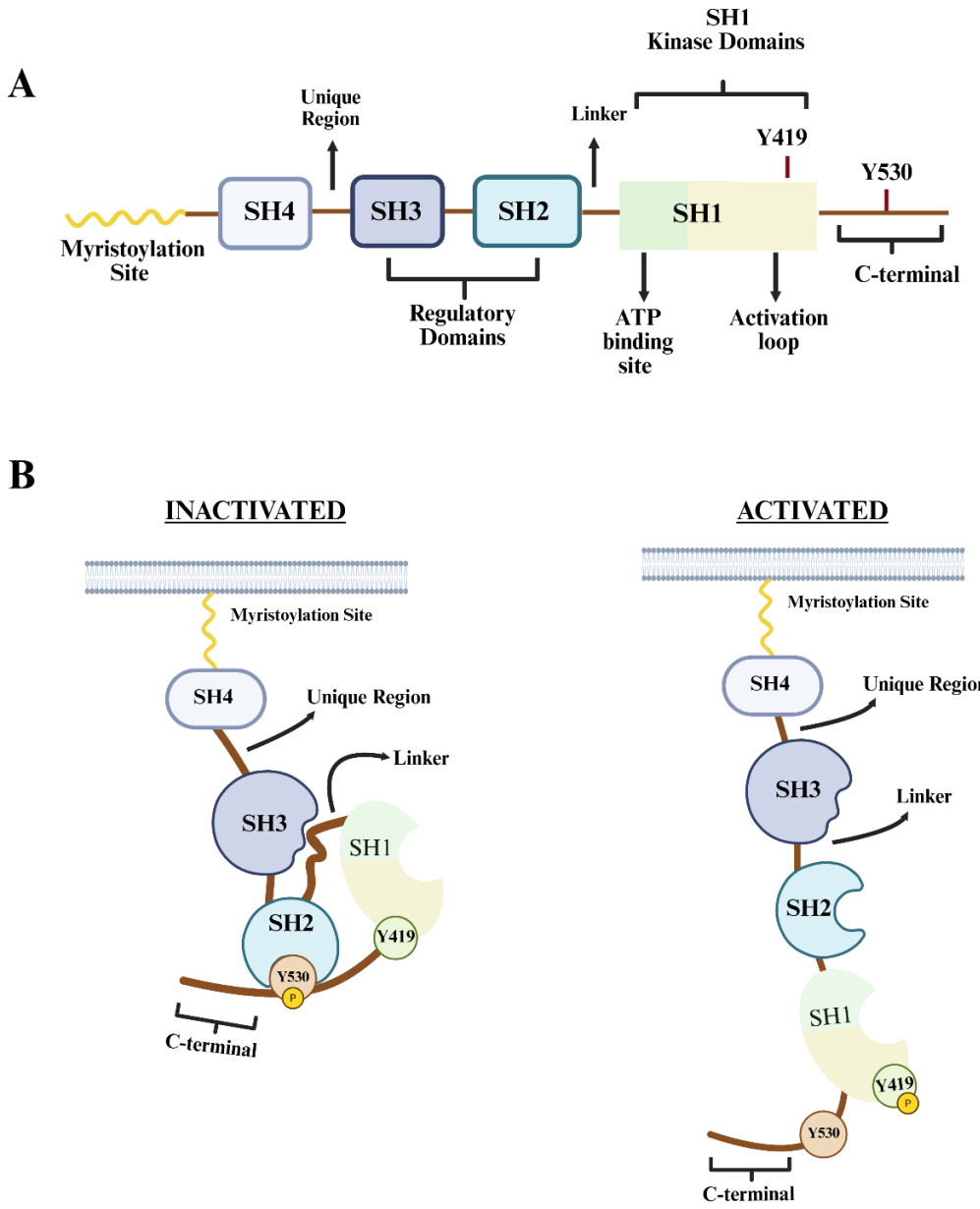

Figure 2. Structure and activation of SRC (A) Schematic representation of the SRC kinase domain. **(B)** SRC kinase configuration with Y530 phosphorylation in inactivated or Y419 phosphorylation in activated, respectively.

1.2.6. Role of SRC in Cellular Homeostasis and Fate

Under physiological conditions, SRC serves as an essential regulator for interactions between cells and their environment. It does this through the Integrin Focal Adhesion Kinase (FAK) axis, which allows SRC to detect mechanical signals from the extracellular matrix. This detection helps to regulate the actin cytoskeleton and promotes cell migration. The process

involves the phosphorylation of proteins like p130Cas and paxillin, which are essential for the turnover of focal adhesions, enabling the cell to move through its surroundings[85, 86]**(Figure 3)**. Furthermore, SRC plays a vital role in amplifying signals from RTKs, such as EGF and VEGF receptors. This amplification triggers important survival and growth pathways, including the Ras-ERK and PI3K-AKT cascades **(Figure 3)**. These pathways ensure that cell growth and movement occur only in response to appropriate environmental signals, thereby maintaining strict cellular homeostasis[87].

The influence of SRC extends deeply into the regulation of cell survival, actively suppressing mechanisms that lead to apoptosis, or programmed cell death. SRC sends a strong inhibitory signal against the activation of Caspase-3, the main protease responsible for the systemic breakdown of cells **(Figure 3)**. It achieves this inhibition through the PI3K-AKT survival pathway, which phosphorylates and inactivates pro-apoptotic proteins. Additionally, SRC regulates the BCL-2 family of proteins, known as the mitochondrial apoptosis regulators, both directly and indirectly[87-89].

Moreover, SRC signaling is closely associated with PARP1 (Poly (ADP-ribose) polymerase 1). PARP1 is crucial for detecting single-strand DNA breaks and initiating repair processes. However, when PARP1 is hyperactivated, it can lead to cellular energy depletion and a form of programmed cell death **(Figure 3)**. SRC's signaling cascades often modulate PARP1 recruitment and activity at sites of damage, ensuring that the cell focuses on repairing DNA and maintaining genomic integrity rather than initiating apoptosis[90]. In situations where the apoptotic pathway is bypassed, SRC can also affect necrotic-like death pathways. This occurs through its interactions with the RIP3K (Receptor-Interacting Protein Kinase 3) complex **(Figure 3)**, which

determines the switch between cell survival and necroptosis, particularly under conditions of inflammation or genotoxic stress[91, 92].

Beyond survival and death, SRC plays a critical role in regulating cellular identity by preserving stemness and preventing premature differentiation. It serves as a central hub for the Signal Transducer and Activator of Transcription 3 (STAT3) pathway **(Figure 3)**. When phosphorylated by SRC, STAT3 forms homodimers and translocates to the nucleus. Within neural stem and progenitor cells (NPCs), nuclear STAT3 collaborates with the Notch Receptor 1 (NOTCH1) intracellular domain (NICD) to transactivate a core self-renewal program. This network directly supports SRY-box Transcription Factor 2 (SOX2) expression, a master transcription factor that maintains the undifferentiated, multipotent state[93, 94]. This stem-like signature is vital during neural development, as it helps prevent the exhaustion of the progenitor pool.

As the cell commits to a specific lineage, regulation of the stemness axis is reduced, allowing the expression of mature structural proteins. This change marks the final transition into a differentiated neuronal state[95]. By carefully balancing these signals, SRC ensures that the transition from a progenitor state to a specialized cell occurs in synchrony with developmental requirements.

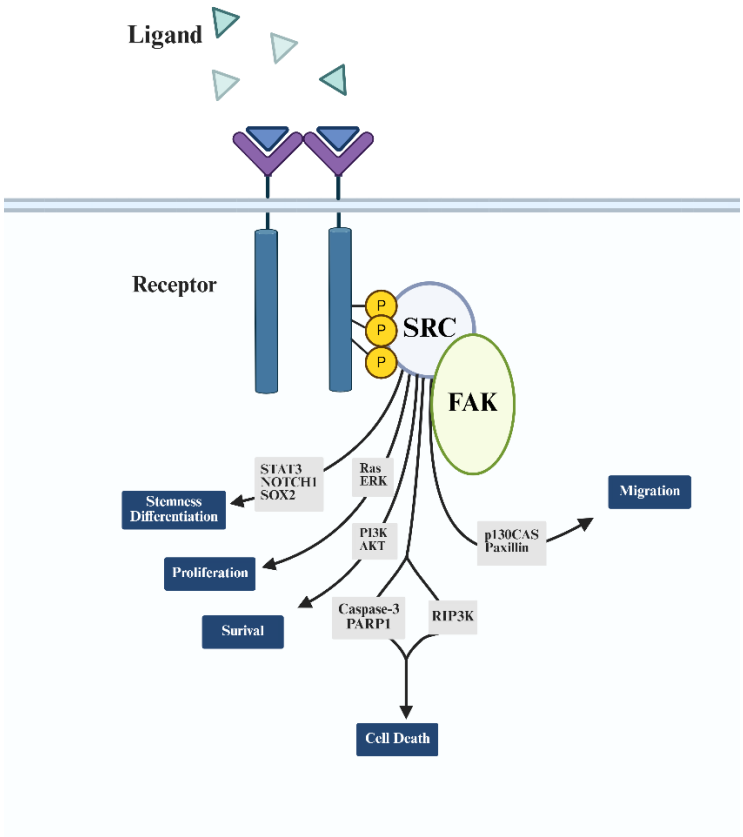

Figure 3. SRC Kinase as a Central Regulatory Hub for Downstream Signaling Pathways and Cellular Homeostasis. SRC kinase acts as a central signaling hub that integrates extracellular signals to regulate migration via the FAK axis, proliferation and survival through Ras-ERK and PI3K-AKT, and stemness and differentiation via the STAT3-NOTCH1-SOX2 pathway. It further maintains cellular homeostasis by balancing survival signals against cell death pathways involving Caspase-3, PARP1, and RIP3K.

1.2.7. Kinase Dysregulation: Hallmarks of Cancer

The transformation of a normal cell into a malignant one is primarily due to rewiring in intracellular communication, a concept introduced by Hanahan and Weinberg in their influential work on the hallmarks of cancer[96]. Their first paper identified essential biological capabilities that tumors acquire, and nearly all of them, especially self-sufficiency in growth signals and evasion of programmed cell death, revolve around the alteration of protein kinase signaling.

In a healthy state, kinases operate as part of a tightly regulated system. However, during oncogenesis, they can become continuously active[97]. This deregulation functions like a short circuit in a cellular network, allowing kinases to bypass the need for external signals and provide

an ongoing, autonomous stimulus for cell survival[98]. As a result, kinases play a crucial role in acquiring and maintaining the hallmarks of cancer by promoting stemness, driving unchecked cell proliferation, and enforcing a blockade against differentiation, keeping cells in a primitive and aggressive state.

1.2.8. *Kinases as Therapeutic Targets for Cancer*

Understanding that kinases are primary drivers of oncogenic signaling has revolutionized clinical oncology, shifting the focus away from broad-spectrum cytotoxic treatments to precision molecular medicine. This change is highlighted by the development of small-molecule inhibitors and monoclonal antibodies that target specific ATP-binding sites or extracellular domains of abnormal kinases. Since the landmark FDA approval of Imatinib (Gleevec) in 2001, a BCR-ABL1 inhibitor that changed Chronic Myeloid Leukemia from a terminal diagnosis to a manageable chronic condition, the field has experienced a surge in drug development[99].

Currently, over 80 kinase inhibitors have been approved by the FDA, targeting various proteins such as EGFR for non-small cell lung cancer, HER2 for breast cancer, and BRAF for melanoma. These therapies have provided many patients with rapid tumor regression and a significant extension of progression-free survival by precisely dismantling the signaling networks that sustain the hallmarks of cancer[99]. However, while these advancements in kinase-targeted therapies have shown remarkable effectiveness in primary tumor settings, their role in managing recurrent and therapy-resistant tumors, especially the childhood brain cancer MB, remains poorly understood.

1.3. Study Rationale, Hypothesis, and Objectives

1.3.1. Rationale

Historically, most research on MB has focused on primary tumors. While these studies are crucial for understanding how tumors form, they do not address the most pressing clinical issue: recurrent disease. In patients with G3 MB, relapses are the leading cause of mortality, yet the biology of these recurrent tumors remains largely unknown. This lack of understanding creates a barrier to developing effective treatments for the most lethal stage of the disease.

One major reason for this knowledge gap is the scarcity of patient-derived recurrent tumor samples. Unlike primary tumors, where surgical resection is the first line of therapy due to their localized clinical representation, recurring tumors often display as diffuse and metastatic diseases. This makes surgical removal both technically challenging and medically risky. Furthermore, families of pediatric patients are understandably reluctant to subject their children to invasive procedures. As a result, the lack of recurrent tumor samples directly hinders our understanding of the largely unknown mechanisms underlying relapses, such as how cancer cells adapt to survive the initial intensive therapy, leaving doctors with no effective options for their most vulnerable patients.

To address this knowledge gap, we have developed specialized *in vitro* and *in vivo* models that recapitulate the environment of therapy-resistant and recurrent G3 MB. These models provide a high-fidelity platform for investigating molecular changes following chemoradiotherapy (CRT). Unlike studies that focus solely on primary cells, our models capture the clinical context of relapses, offering a much more accurate depiction of the disease's evolution. By using these models, we are prioritizing a drug repurposing strategy that identifies new uses for existing FDA-approved medications. Because existing drugs have previously cleared safety requirements, we may skip the lengthy development timeline for a novel chemical and proceed directly to clinical

trials. Our goal is to transform these research results into rapid, life-saving measures for children who currently lack effective treatment options.

1.3.2 Hypothesis

Given that recurrent G3 MB often lacks significant new genomic alterations, this suggests that the observed phenotypic changes are likely due to a shift in cellular signaling. We hypothesize that these non-genomic changes in cell signaling are a crucial factor in therapy resistance and tumor recurrence of G3 MB. Specifically, reorganization of signaling pathways following CRT may act as a master regulator, maintaining a reservoir of cells in a stem-like state. This preservation inhibits differentiation and promotes cell survival under therapeutic stress. Given the availability of FDA-approved inhibitors, these kinase-driven pathways present an attractive target for reducing G3 MB recurrence. Targeting these critical signaling nodes may disrupt the survival of the stem-like progenitor cell pool and ultimately improve patient outcomes.

1.3.3. Objectives

Aim 1: **Mapping the Adaptive Kinome**: profile the phospho-kinase proteome to identify the signaling signatures that emerge post-treatment. By comparing primary and CRT-resistant MB models, we will pinpoint the specific molecular switches that allow G3 MB to survive CRT.

Aim 2: Deciphering the Mechanism of Resistance: dissect the kinase-mediated circuits that drive cellular stemness, migration, and survival. This aim focuses on how these activated pathways allow CRT-resistant MB models to bypass cell death signals and maintain their regenerative potential, ultimately leading to relapse.

Aim 3: Therapeutic Evaluation of SRC Inhibitors: evaluate combinatorial strategies by pairing FDA-approved kinase inhibitors with standard treatment. Through *in vitro* and *in vivo* testing, we

will determine if these targeted combinations can effectively suppress tumor growth and prevent recurrence.

CHAPTER 2: METHODS & MATERIALS

2.1. Cell Model

2.1.1. Cell Culture

Primary human pediatric MYC-amplified MB cell cultures were obtained from collaborators as kind gifts; Dr. Till Milden (German Cancer Research Center) provided HD-MB03, a treatment-naïve large cell/anaplastic G3 MB cell model isolated from a male patient ≤ 3 years old at the time of surgical intervention[100]. SU_MB002 cells were generously provided by Dr. Yoon-Jae Cho (OHSU Doernbecher Children's Hospital). Cells were derived from an autopsy specimen of the leptomeningeal compartment from a pediatric patient with treatment-refractory, metastatic G3 MB after receiving cyclophosphamide treatment[101]. MB3W1, anaplastic G3 MB cells, were derived from the malignant cells found in the pleural effusions of a male patient ≤ 3 years old and kindly provided by Dr. Matthias Wölfl (Universitätsklinikum Würzburg)[102]. Dr. Sheila Singh (McMaster University) kindly provided us with matched human pediatric primary D425 and recurrent D458 G3 MB cells[103]. The D283 G3/G4 MB cell line was established from malignant ascites cells and a peritoneal metastasis from a male patient, G3/4 MB, between 6 and 10 years old, and was purchased from the American Type Culture Collection (ATCC, Rockville, MD, USA)[103, 104].

Dr. Sheila Singh generously provided primary human pediatric BT992 SHH MB cells. These cells were originally isolated from a pediatric patient who later relapsed with the disease. The collection and use of these samples were conducted with fully informed consent obtained from the patient and their family, in accordance with ethical guidelines and under the approval of the Hamilton Health Sciences/McMaster Health Sciences Research Ethics Board[105]. DAOY cells, derived from a 4-year-old patient with desmoplastic SHH MB, were purchased from the ATCC[106].

HD-MB03, SU_MB002, and MB3W1 G3 MB cells were cultured as tumourspheres in serum-free Knockout DMEM/F12 media (Life Technologies) with 1X GlutaMAX (Life Technologies), 20 ng/mL of EGF (STEMCELL Technologies), 10 ng/mL of bFGF (STEMCELL Technologies), 1X NeuroCult SM1 Supplement (STEMCELL Technologies), 1X N2 Supplement (STEMCELL Technologies), 2 µg/mL Heparin (STEMCELL Technologies), and 1X antibiotic-antimycotic (Life Technologies).

Human pediatric primary D425 G3 MB cells were grown in MEM media (Life Technologies) with 0.5X D-glucose (Life Technologies), 1X antibiotic-antimycotic, 20% fetal bovine serum (FBS; Life Technologies), and 1X Sodium pyruvate (Life Technologies). In contrast, human pediatric matched D458 G3 MB were grown in DMEM media (Life Technologies) with 1X GlutaMax, 1X antibiotic-antimycotic, 10% FBS, and 1X Sodium pyruvate (Life Technologies). Three days prior to performing any functional assays, cells were transferred to serum-free medium.

D283 G3/G4 MB cells were cultured in MEM media (Life Technologies) with 1X antibiotic-antimycotic,10% FBS, and 1X Sodium pyruvate.

BT992 cells were expanded with the BTIC enrichment medium (Life Technologies) supplemented with 10% FBS. DAOY cells were expanded in DMEM high-glucose media (Life Technologies), supplemented with 1X GlutaMAX, 1 mM sodium pyruvate, 1X non-essential amino acids (NEAA; Life Technologies), and 1X antibiotic-antimycotic. BT992 and DAOY cells were cultured in serum-free BTIC enrichment medium for at least 48h prior to experiments.

Human astrocytes were purchased from ScienCell Research Laboratories (Carlsbad, CA, USA) and maintained in complete Astrocyte Medium (ScienCell Research Laboratories). Human neural stem cells (NSCs) are isolated from embryonic brain tissue at 8–11 weeks of age. Samples were collected with informed written consent from patients in strict accordance with institutional

and legal ethical guidelines. These cells were provided by Dr. Sheila Singh. Samples were dissociated in artificial cerebrospinal fluid containing 0.2 Wunisch U/mL Liberase (Roche) and incubated at 37 °C in a shaker for 15 min. The dissociated tissue was then filtered through a 70 µm cell strainer and collected by centrifugation at 300 *g* for 3 min. Human HSCs were cultured in serum-free DMEM/F12 media (Life Technologies) with 20ng/mL of EGF (STEMCELL Technologies), 10ng/mL of bFGF, 1× NeuroCult SM1 Supplement, 1× N2 Supplement, 2µg/mL Heparin, and 1× antibiotic antimycotic.

All cells were grown in 10 cm tissue culture plates in a humidified incubator at 37 °C with 5% CO_2 and 95% air. Once the plates reached 80% confluency, tumorspheres were centrifuged at 500 *g* for 5 minutes. The spheres were dissociated by gentle pipetting and replated at 20% of the resuspended volume. To maintain a healthy population, cells were typically passaged 2-3 times per week.

2.1.2. In vitro *Chemoradiotherapy Treatment*

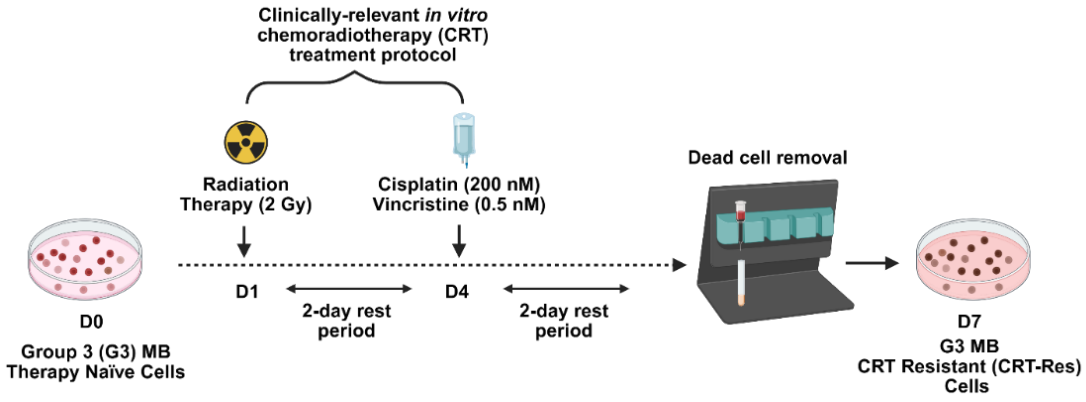

Figure 4: Clinically-relevant in vitro chemoradiotherapy treatment protocol.

To model the standard-of-care treatment received by MB patients, we employed a clinically-relevant *in vitro* CRT protocol. This regimen spans 7 days and consists of an initial dose of radiation followed by chemotherapy. When the cells reached about 80% confluency, they were

exposed to 2 Gray units (Gy) of X-ray radiation using the Rad Source 2000, designated as Day 1 of treatment. On Day 2, both treated and control cells were harvested, tumorspheres were dissociated, and cells were replated at a density of 2 million cells per 10 cm tissue culture plate to ensure consistent growth conditions. Day 3 served as a recovery day, allowing cells to rest before subsequent treatments.

On Day 4, treatment plates were exposed to the chemotherapeutic agents cisplatin (MedChemExpress, Cat. # HY-17394) and vincristine (MedChemExpress, Cat. #HY-N0488). Cisplatin was prepared as a 5 mM stock solution and stored at −80 °C until use. At the time of treatment, the stock was diluted in 1X PBS to generate a 200 µM working solution. Similarly, vincristine was stored as a 1 mM stock at −80 °C and diluted in 1X PBS to obtain a 500 nM working solution. For treatment, half of the media from each plate was collected into sterile tubes, and the working solutions of cisplatin and vincristine were added at a volume of 1 µL per mL of total media, resulting in final concentrations of 200 nM cisplatin and 0.5 nM vincristine. The media was gently mixed by flipping the tubes 10–15 times and then returned to the plates to restore the original volume.

Cells were carefully observed on a daily basis from Day 5 through Day 7 in order to monitor their growth and overall health. During this period, cultures were split when necessary to avoid over-confluency and to maintain cells in optimal growth conditions. On Day 8, the live cell population was separated from dead cells using appropriate techniques.

2.1.3. *Live Cell Separation*

Due to changes in cell populations following CRT treatment, we started with approximately 3 times as many plates for treated cells as for therapy-naïve cells. Living cells were isolated using the Dead Cell Removal Kit (Miltenyi Biotec, Cat. #130-090-101) according to the manufacturer's

instructions. This kit contains magnetic MicroBeads that specifically bind to designated cell-surface markers. Cells were first pelleted by centrifugation at 500 × g for 5 minutes, then washed with 1X Binding Buffer (provided in the kit) to remove residual media and centrifuged again at 500 × g for 5 minutes. Cells were then counted using trypan blue and resuspended in 100 µL of Dead Cell Removal MicroBeads per 10^7 living cells, followed by a 15-minute incubation at room temperature. The cell-bead mixture was diluted with 1X Binding Buffer to a final volume of 3 mL per tube, then loaded onto an LS MACS® Column in a MACS magnetic separator (Miltenyi Biotec, Cat. #130-042-401) in 1 mL increments to separate dead cells from live cells. Flow-through containing the enriched live cell population was collected into a tube, centrifuged at 500 × g for 5 minutes, and resuspended in 1 mL of medium. Cell viability was confirmed by trypan blue exclusion, demonstrating an increased proportion of live cells following separation. Lastly, the surviving cells were replaced under control conditions and subsequently treated for downstream experimental analyses.

2.1.4. *CRISPR-Cas9 Gene Editing*

Tetracycline-inducible (Tet-ON) Cas9 lentivirus particles were purchased from Dharmacon (Horizon Discovery, Cat. No. VCAS11227) and used to establish a stable Cas9-inducible cell line. G3 MB cells were seeded at a density of $5x10^4$ cells in a 24-well plate. Immediately, after seeding, cells were transduced with Tet-ON Cas9 lentiviral particles at a multiplicity of infection (MOI) of 0.3 in the presence of 5 µg/mL of sequabrene (Millipore Sigma, Burlington, MA, USA) to enhance viral uptake. To further increase transduction efficiency, the plate was centrifuged at 800 × g for 1 hour at 32 °C. Following centrifugation, the plate was transferred to a 37 °C incubator with a humidified atmosphere containing 5% CO_2 and maintained under standard culture conditions.

24-hours post-transduction, the virus-containing medium was carefully aspirated and replaced with fresh growth medium supplemented with 5 µg/mL blasticidin (Invitrogen, Cat. # A1113903) to select for stably transduced cells. Blasticidin selection was continued for two weeks, during which the media was refreshed every 2–3 days until a resistant population was established. Two weeks after selection, cells were transduced with two different lentivirus clones containing pre-designed guide RNA (gRNA) targeting SRC, purchased from Dharmacon (clone #1: Cat. No VSGHSM_38240064, and clone #2: Cat. No VSGHSM_38240069). Transduction was performed using the same protocol described above. Following viral exposure, cells were selected in culture medium containing 2 µg/mL puromycin (Millipore Sigma, Cat. # P9620) to ensure expression of the integrated gRNAs. Cells were continuously maintained in media containing the selection markers blasticidin and puromycin throughout all experiments to prevent loss of the lentiviral constructs.

For induction of Cas9 expression and activation of CRISPR-mediated genome editing, cells were treated with 0.5 µM doxycycline hyclate (DOX; Millipore Sigma, Cat. #D5207). DOX was freshly prepared and added to the culture medium daily for three consecutive days to achieve robust induction of Cas9 protein expression. Treated cells were subsequently expanded and used for downstream experimental validation.

2.1.5. In vitro *Treatment*

To validate the successful acquisition of a treatment-resistant cell population following live cell separation, the cells were challenged with either re-irradiation at 2 Gy, high-dose cisplatin (500 mM), or vincristine (1 nM).

To achieve pharmacological inhibition of SRC, MB cells were treated with one of the following small-molecule inhibitors: 10 µM Saracatinib (MedChemExpress, Cat. # HY-10234), 5

μM Bosutinib (MedChemExpress, Cat. # S1014), or 5 μM SU6656 (TOCRIS, Cat. # 6475). Cells were exposed to these inhibitors 24 hours prior to harvest for downstream analyses.

To investigate the contribution of cell death pathways, *SRC* knockout (KO) cells were subjected to a sequential DOX-induced KO protocol, combined with inhibition of apoptosis or necroptosis. On Day 1, cells were treated with DOX to induce *SRC* KO. On Day 2, cells received DOX in combination with 10 μM of pan-caspase apoptosis inhibitor N-benzyloxycarbonyl-Val-Ala-Asp (OMe)-fluoromethylketone (Z-VAD-FMK: Selleckchem, Cat. # S7023) or 10 μM of necroptosis inhibitor Necrostatin-1 (Nec-1; Selleckchem, Cat. #S8037). On Day 3, cells received DOX alone. In each case, cells were incubated for 24 hours prior to sample collection.

Z-VAD-FMK and Nec-1 were prepared in dimethyl sulfoxide (DMSO; Invitrogen, Cat. # D12345). To account for solvent-related effects, control cells received an equivalent concentration of DMSO as a vehicle control. All chemical reagents were freshly prepared in appropriate solvents immediately prior to use, according to the manufacturer's recommendations.

2.2. *In Vitro* Model

2.2.1. *Human Proteome Profiler Phospho-kinases Array*

Phospho-kinase array profiling was performed using the Proteome Profiler Human Phospho-Kinase Array Kit (R&D Systems, Cat. # ARY003C) according to the manufacturer's specifications and guidelines. Briefly, cells were lysed using the lysis buffer provided in the kit, supplemented with protease and phosphatase inhibitors. Protein concentration was quantified using the colorimetric Micro BCA assay kit (Life Technologies, Cat. # 23235), and 300 μg of total protein was incubated with the pre-blocked array membranes overnight at 4°C on a rocking platform. The following day, membranes were washed 3 times for 10 minutes each, then incubated with an antibody detection cocktail (provided in the kit) for 1 hour at room temperature. Membranes were then washed 3 times for 10 minutes each, followed by incubation with

streptavidin-HRP reagent (provided in the kit) for 30 minutes at room temperature. Membranes were again washed three times, 10 minutes each, before being covered with the chemiluminescent detection reagents (provided in the kit). Membranes were imaged using the iBright FL1500 Imaging System under chemiluminescent settings, with multiple exposure times applied to capture the optimal signal. The intensity of kinase spots was quantified using ImageJ software (National Institutes of Health), and relative phosphorylation levels were determined by normalizing internal reference spots on the membrane.

2.2.2. *Protein Extraction*

Suspension cells were transferred into 15 mL tubes and washed with cold 1X PBS; adherent cells were harvested by scraping, transferred into 15 mL tubes, and similarly washed with cold 1X PBS. The tubes were centrifuged at 500 x *g* for 5 minutes, after which the supernatant was decanted. The cells were then washed with 200 µL of cold 1X PBS, transferred to 1.5 mL Eppendorf tubes, and pelleted at 700 x *g* for 5 minutes at 4°C. Following aspiration of the supernatant, pellets were resuspended in RIPA lysis buffer (25 mM Tris-HCl, pH 7.6, 150 mM NaCl, 1% NP-40, 1% sodium deoxycholate, 0.1% SDS) supplemented with 1% protease and phosphatase inhibitor cocktail (PIC; Life Technologies, Cat. # 78425). Lysates were incubated on ice for 45 minutes, then sonicated for 1 minute. Finally, the samples were centrifuged at 20,000 *g* for 15 minutes at 4°C, and the protein-containing supernatants were collected.

2.2.3. *Protein Quantification*

Protein concentration within the lysates was quantified using the Micro BCA Protein Assay Kit in a 96-well flat-bottom plate. The working reagent was prepared by mixing three components in the ratio 25:24:1, 25 parts of reagent A, 24 parts of reagent B, and 1 part of reagent C. This colorimetric assay relies on the reduction of Cu^{+2} to Cu^{+1} by specific amino acids (cysteine,

cystine, tryptophan, and tyrosine) followed by the chelation of Cu^{+1} with bicinchoninic acid (BCA).

To ensure absorbance values remained within the spectrophotometer's linear range, protein lysates were diluted 1:2 in ddH_2O. To each well containing 150 µL of the prepared working reagents, 5 µL of either the diluted sample or a BSA standard (ranging from 0.2 to 2.0 mg/mL) was added in duplicate. The plate was covered and incubated at room temperature on a microplate shaker for 45 minutes. Following incubation, absorbance was measured at 570 nm using a SpectraMax Microplate Reader. Final protein concentrations were extrapolated by comparing the optical densities of the unknown samples to the generated BSA standard curve

2.2.4. *SDS-PAGE and Western Immunoblotting*

Polyacrylamide gels were prepared and resolved by standard SDS–PAGE procedures. Resolving gels (6–15%) were prepared fresh using distilled water, 30% acrylamide/bis-acrylamide solution (Bio-Rad, Cat. # 1610156), Tris-HCl buffer (pH 8.8), 10% sodium dodecyl sulfate (SDS; Millipore Sigma, Cat. # 289957), 10% ammonium persulfate (APS; Invitrogen, Cat. # 401161000), and tetramethylethylenediamine (TEMED; Millipore Sigma, Cat. # 411019). Once the resolving layer polymerized, a 6% stacking gel was prepared using the same reagents (distilled water, 30% acrylamide/bis-acrylamide solution, 10% SDS, 10% APS, and Tris-HCl buffer (pH 6.8)).

Cell lysates were quantified as described above, and equal amounts of protein (5–50 µg) were prepared for electrophoresis. Samples were mixed with loading buffer (95% 2× Laemmli sample buffer (Bio-Rad, Cat. # 1610737) and 5% β-mercaptoethanol (Millipore Sigma, Cat. # M6250) and denatured at 95 °C for 5 minutes.

Proteins were separated on gels using the Mini Trans-Blot® Cell and Criterion™ Blotter system (Bio-Rad). Electrophoresis was performed in 1× SDS running buffer (25 mM Tris, 200

mM glycine, 0.1% SDS) freshly prepared from a 10× stock using 64.8% Tris-base (ThermoScientific; Cat # BP152-1), 32.4% UltraPure™ Glycine (Invitrogen, Cat. # 15527013), 2.8% SDS. A two-step voltage program was used: 80 V for 15 minutes to concentrate proteins into the resolving gel, followed by 110 V for approximately 1.5 hours until optimal separation was achieved. Following electrophoresis, proteins were transferred onto Immobilon-P PVDF membranes (Millipore Sigma, Cat. # IPVH00010) using the wet-transfer method in transfer buffer (25 mM Tris, 192 mM glycine, 20% methanol, pH 8.3) at 110V for 1.5 hours.

To normalize protein loading, membranes were stained with No-Stain™ Protein Labeling Reagent (Invitrogen, Cat. # A44717) according to the manufacturer's protocol. Briefly, membranes were rinsed twice with ddH_2O for two minutes each, then incubated for 10 minutes at room temperature in a freshly prepared No-Stain™ Protein labeling solution (20 µL No-Stain Activator, 20 µL No-Stain Derivatizer, 0.5 mL 10X No-Stain Labeling buffer, and 9.5 mL ddH_2O) under gentle rocking. After incubation, membranes were washed three times for two minutes in ddH_2O to remove unbound reagent. Labeled proteins were visualized using the iBright FL1500 Imaging System under universal acquisition settings.

Membranes were then blocked with 5% non-fat dry milk prepared in PBST for 45 minutes at room temperature on a rocker. Following blocking, membranes were then incubated overnight at 4 °C with the indicated primary antibodies (diluted 1:1000 in PBST containing 1% BSA). The next day, membranes were washed three times in PBS (5 minutes each) and incubated with horseradish peroxidase (HRP)-conjugated secondary antibodies (1:10,000 dilution in 5% milk/PBST) for 1.5 hours at room temperature.

After secondary antibody incubation, membranes were washed three times in PBS (5 minutes each). Protein signals were detected using the Clarity Western ECL Substrate (Bio-Rad,

Cat. # 1705061) prepared at a 1:1 ratio and imaged using the iBright FL1500 Imaging System under chemiluminescence acquisition settings.

Protein band intensities were quantified using ImageJ software (National Institutes of Health). The total protein signal obtained from No-Stain™ labeling was used as a loading control for normalization of target proteins, providing a robust, reproducible method that avoids the variability associated with traditional housekeeping protein detection.

ANTIGEN	HOST	DILUTION	SOURCE	Cat. No.
p-SRC	Rabbit	1:1000	R&D systems	AF2685
Total SRC	Rabbit	1:1000	Cell Signaling	2109S
Cas9	Mouse	1:1000	Cell Signaling	14697S
SOX2	Rabbit	1:1000	Cell Signaling	3579S
TUBB3	Mouse	1:1000	R&D systems	MAB1195
Cleaved Caspase-3	Rabbit	1:1000	Cell Signaling	9661S
Caspase-3	Rabbit	1:1000	Cell Signaling	9662S
RIP3K	Rabbit	1:1000	Cell Signaling	95702S
PARP1	Mouse	1:667	Santa Cruz	SC-8007
Nanog	Rabbit	1:1000	Cell Signaling	3580S
OCT3/4	Mouse	1:667	Santa Cruz	SC-5279
p-Stat3	Rabbit	1:1000	Cell Signaling	9145T
Total Stat3	Mouse	1:1000	Cell Signaling	9139T

Table 2. List of primary antibodies used for western blotting used in this study.

ANTIGEN	HOST	DILUTION	SOURCE	Cat. No.
HRP CONJUGATED SECONDARY ANTI-RABBIT	Goat	1:10 000	Jackson Immunoresearch	111-035-114
HRP CONJUGATED SECONDARY ANTI-MOUSE	Goat	1:10 000	Jackson Immunoresearch	115-035-003

Table 3. List of secondary antibodies used for western blotting used in this study.

2.2.5. *Trypan Blue Cell Counting*

Cell proliferation was evaluated using the Trypan blue exclusion assay, a standard technique that identifies live cells based on membrane integrity. This method uses trypan blue dye, which is selectively excluded by the intact membranes of living cells. Conversely, cells with compromised membranes, indicative of cell death, internalize the dye and appear blue under light microscopy, allowing for a clear distinction between living and non-living cell populations.

The experimental workflow began by seeding cells at a density of 5×10^4 cells/mL into 12-well tissue culture plates. To allow initial stabilization, the plates were incubated for 2 hours under standard culture conditions (37 °C, 5% CO_2, humidified atmosphere) before treatment with either the designated drug or an equivalent volume of vehicle control. At predetermined time points following treatment, the cells were harvested, centrifuged at 300 *g* for 5 minutes, washed with PBS, and then resuspended in an appropriate volume of PBS for counting.

An aliquot of the cell suspension was mixed with 0.4% trypan blue solution (Millipore Sigma, Cat. # 93595) at a 1:1 ratio. Finally, 10 µL volume of this mixture was loaded onto a hemocytometer and examined under a light microscope. Living, unstained cells were manually counted across the hemocytometer quadrants. The final concentration of living cells was calculated using the following formula: Average cell counts per quadrant $\times 10^4 \times$ Dilution factors.

2.2.6. *Prestoblue Cell Viability*

Cell viability was quantitatively assessed using the PrestoBlue™ HS Cell Viability Reagent (Invitrogen, Cat. # P50201), a resazurin-based assay that serves as a sensitive indicator of metabolic health by measuring the reducing potential of living cells. In metabolically active cells,

the non-fluorescent resazurin-based compound is reduced to highly fluorescent resorufin; the resulting fluorescence intensity is directly proportional to the number of viable cells in the population

For the experimental procedure, cells were seeded at a density of 1×10^3 cells per well in sterile, flat-bottom 96-well plates in 100 µL of media. The plates were incubated overnight at 37 °C in a humidified atmosphere (5% CO_2) to allow for cell attachment and recovery. Following this stabilization period, cells were treated with the designated drug or a vehicle control. All experimental conditions were performed in triplicate to ensure statistical plate consistency, and additional wells containing only culture media were maintained as background controls to account for non-specific signals.

At specified time points post-treatment, 10 µL of PrestoBlue™ HS reagent (final concentration of 1×) was added to each well and mixed gently. The plates were then incubated at 37°C for 15 minutes, protected from light, to facilitate the metabolic reduction of the reagent. Fluorescence intensity was subsequently measured using a microplate reader with excitation at 560 nm and emission at 590 nm.

To determine relative viability, the average background fluorescence from the media-only wells was subtracted from all experimental readings. Data were then normalized to the untreated control group, which was set to 100% viability, allowing determination of the relative impact of the treatment on cell health.

2.2.7. *Tumorsphere Formation Assay*

Tumorsphere formation assays were performed to assess the self-renewal capacity of cells under serum-free, non-adherent conditions. Cells were first dissociated into single-cell suspensions by gentle trituration through repeated pipetting to minimize cellular clumping while maintaining

viability. Single cells were counted as described above to ensure accurate seeding density. Cells were plated at a low density of 2.5×10^3 cells per well in 1mL of serum-free growth media into ultra-low attachment 24-well plates to prevent adherence and promote sphere formation.

Plates were incubated at 37 °C in a humidified incubator with 5% CO_2, and cultures were maintained for 5 days to allow tumorsphere development. During this period, cells were treated with either the designated drug or the vehicle control. Treatments were added gently along the sides of the well to avoid disturbing the non-adherent cultures and to ensure minimal disruption to the forming spheres. At the end of the 5-day incubation, brightfield images of tumorspheres were captured from multiple random fields of view per well using a light microscope equipped with a digital camera.

For secondary sphere formation assays, primary tumorspheres were collected, gently dissociated into single-cell suspensions by trituration, and live cells were counted. Cells were then re-seeded at the same density of 2.5×10^3 cells per well into fresh ultra-low attachment 24-well plates under identical culture conditions. Secondary tumorspheres were imaged after 5 days of culture.

Quantification of tumorsphere formation was performed using ImageJ software (National Institutes of Health). Images were analyzed to measure the diameter of cell aggregates, and only spherical colonies with a minimum diameter of ≥50 μm were scored as tumorspheres. This cutoff was selected to exclude non-proliferative cell clusters and to ensure that only spheres resulting from clonal expansion were included in the analysis.

2.2.8. *Migration Assays*

To evaluate the migratory potential of MB cells, eGFP-expressing G3 MB cells were harvested and resuspended in serum-free MB medium to establish a baseline for chemotactic

induction. The cells were seeded at a density of 2×10^4 cells per well into the upper chamber of Corning® Transwell® 12-well polycarbonate membrane inserts (8.0 μm pore size, 6.5 mm diameter; Cat. #3422). To facilitate directional migration, the lower chamber was filled with 600 μL of MB medium supplemented with 10% FBS as a chemoattractant. Transwell plates were incubated at 37°C in a 5% CO_2 atmosphere for 72 hours, during which cells were treated with designated drugs or a vehicle control.

Following incubation, migration was assessed via direct fluorescence visualization to preserve cell integrity and eGFP signal intensity without the use of chemical fixatives. The upper chamber inserts were briefly removed, and migrated eGFP-positive cells situated on the basal surface of the membrane were imaged using an EVOS® FL Cell Imaging System. To ensure statistical robustness and an unbiased representation of migratory patterns, fluorescence micrographs were captured across multiple randomly selected fields of view for each experimental condition. The number of migrated cells was quantified using ImageJ software (National Institutes of Health).

2.3. Patient Data Analysis

To evaluate gene expression differences between primary and recurrent MB, a publicly available dataset of paired tumor samples from Okonechnikov et al[107]. was used. This data was accessed via the R2: Genomics Analysis and Visualization Platform (http://r2.amc.nl) under the name “Tumor Medulloblastoma-Korshunov-86-rpkm-mbffpe.” Normalized gene expression data were downloaded and processed within the R statistical environment using the markeR, ggplot2, and ggpubr packages for data orchestration and visualization. GAUTSCHI_SRC_SIGNALING GSEA molecular signature was employed to assess SRC activity.

The magnitude of change in this SRC activity signature between paired primary and recurrent states was quantified using Cohen's *d,* a standardized measure of effect size. This metric measured the distance between group means in standard deviation units, with values of approximately 0.2, 0.5, and 0.8 categorized as small, medium, and large effects, respectively. Within this analytical framework, a positive Cohen's *d* reflects a higher mean signature expression in the primary tumors, while a negative value indicates an enrichment of the SRC signaling signature in the recurrent tumors.

2.4. *In Vivo* Model

2.4.1. *Ethics Statement*

All experiments involving animals were approved by the University of Manitoba's Animal Care Committee (Protocol #24-059). Non-obese diabetic (NOD) severe combined immunodeficient (SCID) IL2R gamma null (NSG) mice (NOD.Cg-*Prkdc*^{scid} *Il2rg*^{tm1Wjl}/SzJ) were obtained from the CancerCare Manitoba Research Institute and used for all procedures. Animals were housed in individually vented cage (IVC) and maintained in accordance with the Guidelines of the Canadian Council on Animal Care and the Animal Care and Use Policy of the University of Manitoba.

Irradiated feed was used, and caging and bedding were sterilized by steam autoclave. Animals had continuous access to food and water. The room ambient temperature was 21–23°C, with a relative humidity target of 50% but within a range of 30–60%. Light cycle was 12 h on/12 h off, beginning with lights on at 6:00 a.m.

2.4.2. G3 MB Recurrent Model

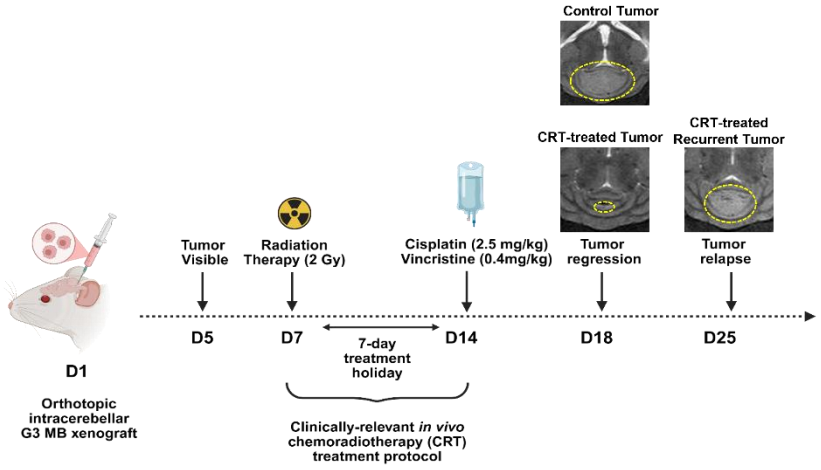

Figure 5: Clinically-relevant *in vivo* chemoradiotherapy treatment protocol.

To establish the model for progression of recurrent G3 MB tumors, 7–9-week-old NSG mice were anesthetized with isoflurane (5% induction, 2.5% maintenance) and positioned in a stereotactic frame. A suspension of 1×10^5 HD-MB03 or SU_MB002 cells in 5 µL of sterile PBS was injected into the cerebellum. Injections were performed in a non-randomized and non-blinded manner. Based on prior experience with this model, tumors typically become detectable and clinically significant by day 5 post-engraftment, reflecting the highly aggressive nature of these cells[108].

On day 7 post-engraftment, mice were randomized into treatment cohorts. The first group served as placebo-treated therapy-naïve controls and received no active drug intervention. The second group received standard CRT. Animals in the CRT group were subjected to craniospinal irradiation (2 Gy) on day 7 using the Rad Source 2000 irradiator. To limit irradiation exposure, a custom-fitted cerrobend shield was used to protect the thoracic and abdominal regions while ensuring uniform exposure of the cranium and upper spine. One week following irradiation (day 14 post-engraftment), chemotherapy was initiated with intraperitoneal (I.P.) administration of cisplatin (2.5 mg/kg) and vincristine (0.4 mg/kg). Control animals received volume-matched saline injections via the IP route.

Mice were closely monitored following treatments. Humane endpoints were defined by the University of Manitoba's Animal Care Committee as a ≥20% reduction in peak body weight or the onset of significant clinical deterioration, including neurological symptoms (e.g., paralysis, head tilt, seizures) or signs of pain and distress. Once humane endpoints were reached, animals were anesthetized, perfused with formalin, and their brains were harvested. Tissues were post-fixed in 10% neutral-buffered formalin for 5–7 days prior to paraffin embedding, sectioning, and slide preparation for histopathological and immunohistochemical analyses.

2.4.3. *G3 MB Survival Studies*

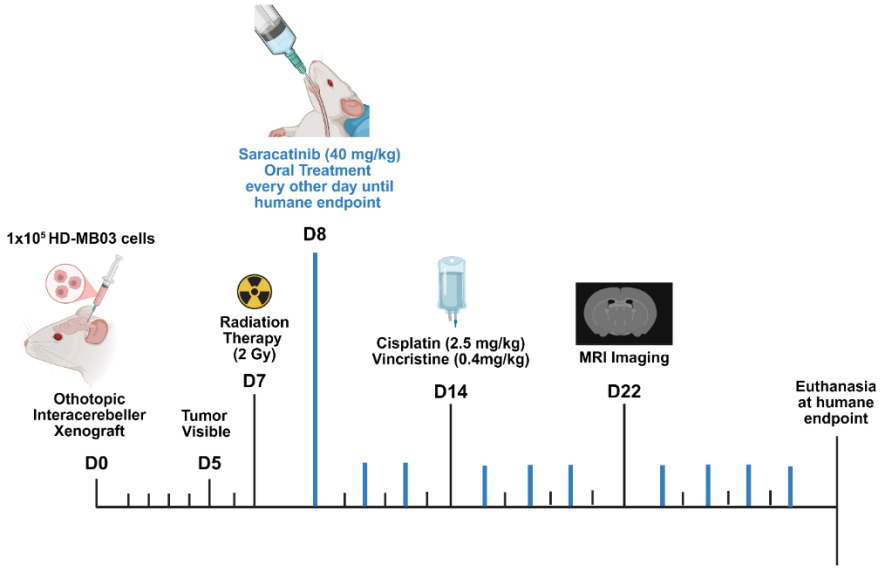

Figure 6: In vivo experimental design used for survival studies.

For survival studies, a similar protocol was followed. NSG mice (7–9 weeks old) were engrafted orthotopically with 1 × 10^5 HD-MB03 cells suspended in 5 µL PBS under stereotactic guidance. On day 7 post-engraftment, animals were randomized into three treatment groups: 1. placebo controls, 2. CRT, and 3. CRT + Saracatinib combination therapy. CRT-treated animals received craniospinal irradiation and chemotherapy as described above. Mice in the combination

therapy group also received Saracatinib (40 mg/kg) by oral gavage every other day (QOD) starting on day 8 (1 day after irradiation) and continuing until endpoint. Saracatinib was prepared in a 0.5% methylcellulose (Millipore Sigma, Cat. # H7509-25G) suspension. Control animals received volume-matched vehicle treatments, consisting of saline I.P. injections and oral gavage with 0.5% methylcellulose containing no active drug.

Animals in all groups were weighed and monitored daily for signs of morbidity and neurological deficits. Humane endpoint criteria were applied as described above. One mouse in the CRT group died from complications unrelated to experimental treatments and was excluded from survival analysis. At the time of sacrifice, mice were perfused with formalin, and brains were collected, fixed, embedded, and sectioned for subsequent histopathological evaluation.

2.4.4. *T2 MRI Imaging*

T2-weighted MRI was performed using a cryogen-free 7T FlexiScan system (MR Solutions, Guildford, Surrey, UK) to monitor tumor growth non-invasively. Tumor volumes were calculated from the acquired MRI images using ImageJ software. For each sample, 18 consecutive coronal sections (300 μm thickness) were analyzed, and the tumor area in each slice was delineated using the freehand selection tool. The volume of each section was calculated, and the total tumor volume was determined by summing the volumes of all individual slices, providing an accurate estimate of overall tumor burden.

2.4.5. *Tissue Processing and Immunofluorescence*

Paraffin-embedded tissue sections were first dewaxed to remove the embedding medium. Slides were incubated in an oven at 60 °C for 30 minutes or until the paraffin layer was visibly melted. Dewaxing was further achieved by immersing the slides in four consecutive xylene washes, each for 5 minutes, to ensure complete removal of paraffin. Following dewaxing, the tissue

sections were rehydrated through a graded ethanol series. Slides were first immersed in two successive washes of 100% ethanol for 1 minute each, followed by 95% ethanol for 1 minute, 70% ethanol for 1 minute, and finally rinsed under running tap water for 1 minute at room temperature.

Antigen retrieval was performed using citrate buffer (diluted 1× from a 10× stock; Sigma-Aldrich, Cat. # C9999). Slides were submerged in preheated citrate buffer (95–100 °C) and heated in a microwave for 20 minutes. Slides were then allowed to cool gradually in the citrate buffer to room temperature. Following antigen retrieval, slides were washed twice in 1× PBS for 2 minutes each to remove residual buffer.

To block non-specific binding, slides were incubated with 10% sheep serum in a humidity chamber at room temperature for 45 minutes. After blocking, excess solution was gently removed, and primary antibodies diluted in 1% sheep serum were applied to the tissue sections. Slides were incubated in a covered hydration chamber at 4 °C overnight to allow specific binding of primary antibodies.

The following day, slides underwent three washes in 1X PBST for 5 minutes each to remove unbound primary antibodies. Secondary antibodies, diluted 1:200 in PBST, were then applied and incubated in a covered hydration chamber for 1 hour and 30 minutes at room temperature. Three additional 5-minute washes in 1X PBST removed excess secondary antibody. Slides were immediately mounted using ProLong™ Diamond Antifade Mountant with DAPI (Invitrogen, Cat. # P36971) and covered with glass coverslips (Sigma Aldrich, Cat. # CLS29752230) to preserve fluorescence and counterstain nuclei.

Fluorescent images were captured using a Zeiss AxioImager Z2 microscope within the Quantitative Imaging, Phenotyping and Sorting (QuIPS) Platform at the Paul Albrechtsen Research Institute, CancerCare Manitoba. Quantification of fluorescence intensity was performed

using ImageJ software (National Institutes of Health). For single-cell correlation analyses, tissue sections were segmented under DAPI guidance, and the mean gray value per cell was measured. For overall fluorescence assessment, full-tissue scans were analyzed to quantify total fluorescent signal intensity across the tumor section.

ANTIGEN	HOST	DILUTION	SOURCE	Cat. No.
p-SRC	Rabbit	1:50	R&D systems	AF2685
Total SRC	Rabbit	1:400	Cell Signaling	2109S
SOX2	Mouse	1:400	Novus Biologicals	NBP2-29623
TUBB3	Mouse	1:21	R&D systems	MAB1195
Cleaved Caspase-3	Mouse	1:50	R&D systems	MAB835
RIP3K	Rabbit	1:400	Cell Signaling	95702S
IBA1/AIF-1	Rabbit	1:800	Cell Signaling	20825S

Table 4. List of primary antibodies used for Immunofluorescence used in this study.

ANTIGEN	HOST	DILUTION	SOURCE	Cat. No.
ALEXA FLUOR 647-CONJUGATED ANTI-MOUSE	Goat	1:100	Jackson Immunoresearch	115-605-003
ALEXA FLUOR 594-CONJUGATED ANTI-RABBIT	Goat	1:100	Jackson Immunoresearch	111-585-144

Table 5. List of secondary antibodies used for immunofluorescence in this study.

2.4.6. *Bielschowsky Silver Staining*

Neuronal fibers were visualized using the Bielschowsky Silver Stain Kit (Abcam, Cambridge, UK, Cat. No. ab245880) according to the manufacturer's protocol. After deparaffinization in an oven at 60 °C for 30 minutes or until the paraffin layer was visibly melted, slides were hydrated by washing 3 times in distilled water for 3 minutes each. A staining jar containing 25 mL of 20% Silver Nitrate Solution (provided with the kit) was pre-warmed in a

water bath for 10 minutes, and slides were incubated for 15 minutes at 40 °C. Tissue slides were rinsed in 4 changes of distilled water for 5 minutes each, then incubated in Ammoniacal Silver Solution (provided with the kit) for 10 minutes at 40 °C. Afterward, slides were placed in the Developer Solution with gentle agitation until a yellow-brown coloration appeared (5-20 s), then transferred to Ammonia Water for 30 seconds. Slides were fixed in 5% Sodium Thiosulfate Solution (provided with the kit) for 2 minutes, rinsed, dehydrated in ethanol, and mounted with Parmount (Fisher Scientific) using glass coverslips (Sigma Aldrich, Cat. # CLS29752230). Images were captured using a Zeiss Axio Imager.

2.5. Declaration of Generative AI and AI-Assisted Technologies

No generative AI tools were utilized in the conceptualization, data analysis, or drafting of this thesis. The use of AI-assisted technologies was strictly limited to refining grammar, syntax, and linguistic clarity to improve the overall readability of the text. The thesis was thoroughly reviewed and remains the sole responsibility of the author.

2.6. Statistical Analysis

All data analyses were performed using Microsoft Excel and GraphPad Prism software. Unless otherwise indicated, error bars represent the mean ± standard error of the mean (SEM). Statistical comparisons were conducted using either an unpaired two-tailed Student’s t-test or one-way or two-way analysis of variance (ANOVA), followed by either a Fisher's Least Significant Difference (LSD) test or, when all pairs of datasets were compared, Tukey’s multiple comparisons test was performed. When every mean was only compared to the control mean, Dunnett’s multiple comparisons test was performed, as specified in the corresponding figure legends. For all tests, a p-value of <0.05 was considered statistically significant.

CHAPTER 3. RESULTS

3.1. Therapy-resistant G3 MB cells exhibit elevated SRC phosphorylation

To evaluate the cellular signaling adaptations driving recurrence and therapy resistance in G3 MB, we used a clinically relevant CRT regimen that mimics the patient's standard-of-care treatment. Three patient-derived G3 MB cell lines (HD-MB03, SU_MB002, and MB3W1) were treated with 2 Gy radiation followed by cisplatin (200 nM) and vincristine (0.5 nM) treatment. Following treatment, dead cells were removed via magnetic bead sorting, yielding a cell population that survived CRT treatment **(Figure 4).**

These persistent cell populations were re-challenged with either 2 Gy RT or higher doses of chemotherapeutic agents (500 nM cisplatin or 1 nM vincristine). Quantification of cell viability via the PrestoBlue metabolic assay revealed that the persistent cells exhibited a significant reduction in sensitivity compared with therapy-naïve cells **(Figure 7)**. This divergence confirms the establishment of a CRT-resistant (CRT-Res) phenotype, providing a robust *in vitro* experimental model for exploring the signaling architectures specifically associated with acquired therapy resistance.

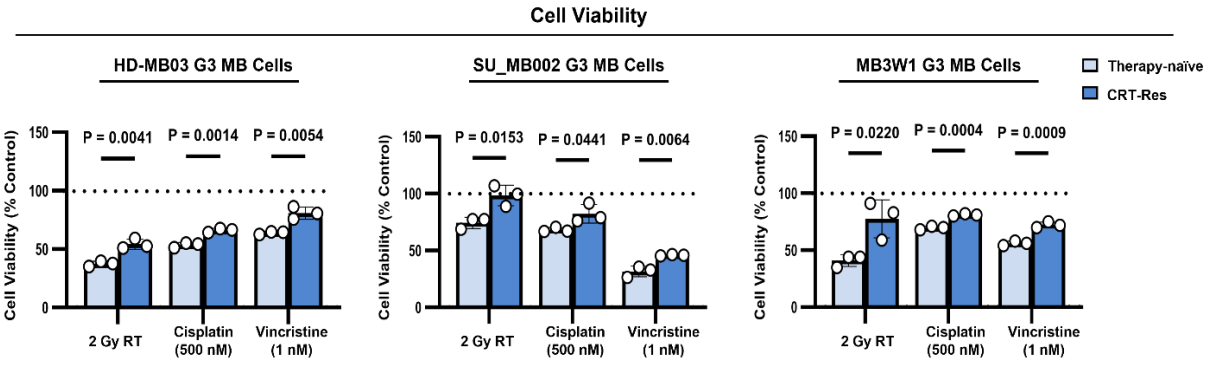

Figure 7: Validation of CRT-Resistance phenotype in G3 MB cells.
Cell viability of therapy-naïve and CRT-ResHD-MB03, SU_MB002, and MB3W1 G3 MB cells following treatment with 2 Gy RT, Cisplatin (500 nM), or Vincristine (1 nM) measured using PrestoBlue. Data represent mean ± s.e.m; from $n = 3$ experimental replicates. Unpaired two-tailed t-tests.

Following validation of the CRT-Res phenotype, we sought to map the specific kinase signaling adaptations in these cells. We employed a proteome profiler phospho-kinase array to simultaneously screen the phosphorylation status of 37 distinct kinases **(Appendix Figure 1)**.

Densitometric analysis of the array dot blots revealed a significant and consistent upregulation of SRC phosphorylation at its activating residue, tyrosine 419 (p-SRC Y419), in CRT-Res SU_MB002 cells **(Figure 8 A-B, Appendix Figure 2A)**. This robust activation identified SRC as a primary signaling junction altered during therapy resistance. Beyond SRC itself, we observed increased phosphorylation in several key downstream effectors of the SRC pathway, p-Lyn, p-PYK2, and p-PLC-γ1 **(Figure 8 A-B, Appendix Figure 2A)**.

Interestingly, while SRC signaling was significantly enriched, canonical oncogenic pathways frequently implicated tumor progression, including p-AKT, p-ERK1/2, and p-JNK, and total p-tyrosine levels remained unaffected by the CRT regimen[109] **(Figure 8 A-B and Appendix Figure 2B)**. This divergence suggests that the transition to a resistant state in G3 MB is not driven by a generalized stress response, but rather by a specific, central adaptation of the SRC signaling architecture.

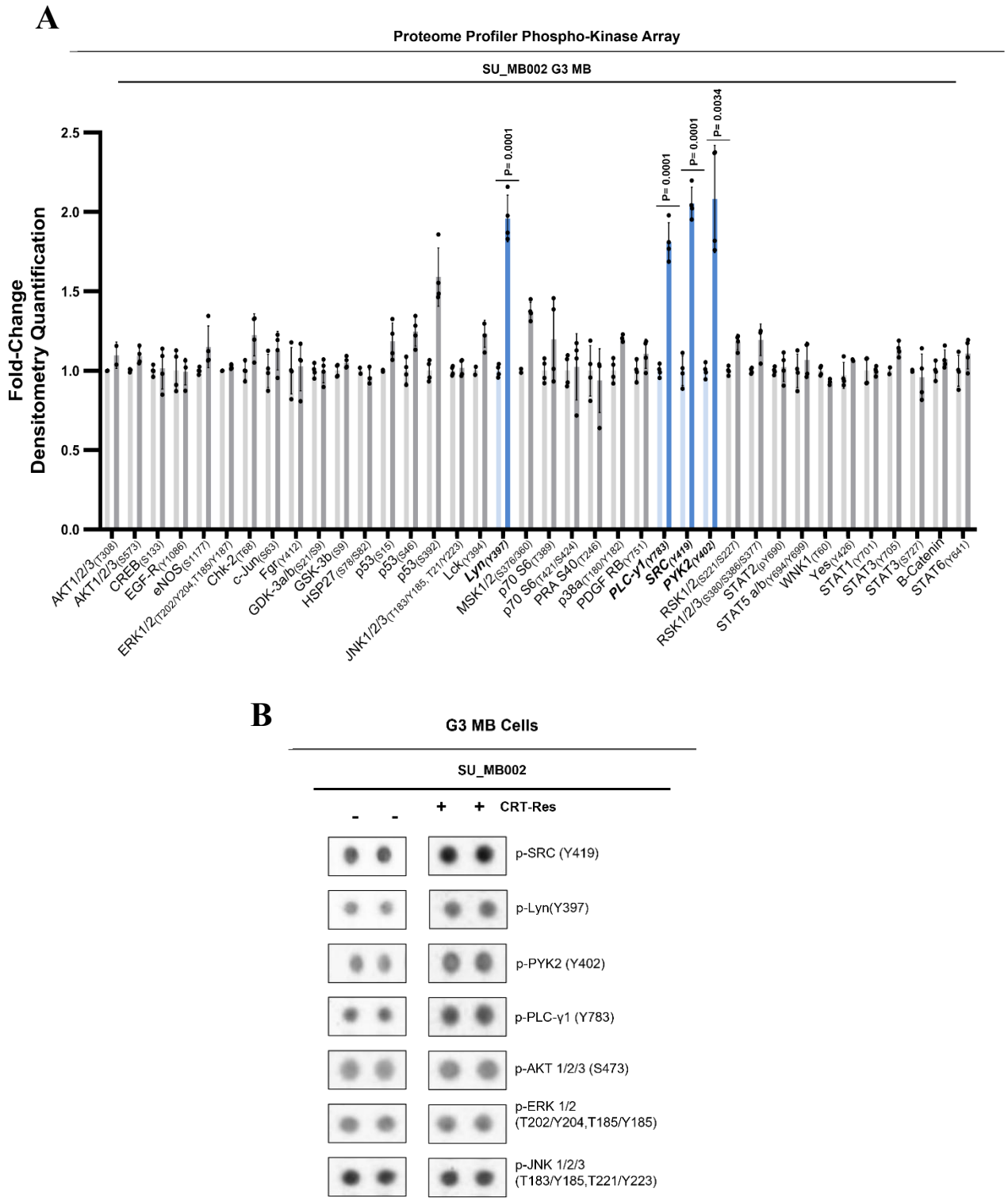

Figure 8: Therapy-resistant G3 MB cells exhibit elevated SRC phosphorylation.
(A) Quantification of Proteome Profiler Phospho-Kinase array results from n = 4 experimental replicates, densitometry quantification measurement normalized to the internal membrane reference spots, presented as mean ± s.e.m; unpaired two-tailed t-tests. **(B)** Representative dot blots of p-SRC (Y419), p-Lyn (Y397), p-PYK2 (Y402), p-PLC-γ1(Y783), p-AKT1/2/3 (S473), p-ERK1/2 (T202/Y204, T185/Y185), and p-JNK1/2/3 (T183/Y185, T221/Y223) spots from the phospho-kinase array membranes comparing therapy-naïve and CRT-Res SU_MB002 G3 MB cells.

These elevated levels of phosphorylated-SRC (p-SRC) were not limited to just one model; they were consistently observed across all three independent G3 MB cell lines **(Figure 9).** Our initial findings collectively suggest that enhanced SRC signaling is a conserved adaptive mechanism that enables G3 MB cells to survive CRT treatment. Consequently, SRC activation may play a crucial role in driving therapy resistance and could be a key factor contributing to recurrence in this aggressive G3 MB.

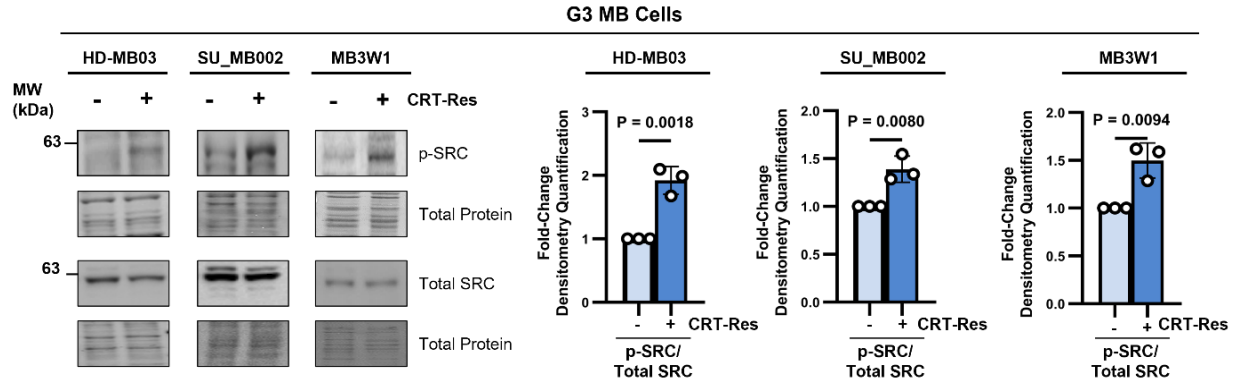

Figure 9: p-SRC Upregulation Across Three CRT-Resistant G3 MB Cell Lines.
Immunoblot of p-SRC (Y419) and total SRC in therapy-naïve and CRT-Res HD-MB03, SU_MB002, and MB3W1 G3 MB. Graphs represent densitometry quantification measurement normalized to the total protein stain of p-SRC/total SRC from *n* = 3 experimental replicates presented as mean ± s.e.m; unpaired two-tailed t-tests.

3.2. Recurrent G3 MB tumors exhibit increased SRC phosphorylation *in vivo*

To determine whether the signaling changes observed *in vitro* are merely temporary responses to acute therapeutic stress or represent long-lasting adaptations that persist in recurrent tumors *in vivo*, we used two PDOX models. In these models, HD-MB03 and SU_MB002 cells were xenografted into the cerebellum of NSG mice. Once the tumors were established, the animals underwent an *in vivo* adapted CRT regimen designed to mimic the treatment received by the MB patient. This treatment included craniospinal radiation (2 Gy), followed by intraperitoneal cisplatin (2.5 mg/kg) and vincristine (0.4 mg/kg) **(Figure 5)**.

Initially, CRT treatment produced a robust therapeutic response, with significant tumor regression compared with untreated, therapy-naïve control groups. However, despite this early response, CRT-treated mice eventually developed large, progressive tumors, effectively recapitulating the clinical phenomenon of disease relapse *in vivo* **(Figure 10)**. IF analysis of paraffin-embedded tumor tissues revealed marked upregulation of p-SRC levels in recurrent tumors from the CRT-treated cohort compared with naïve controls **(Figure 11A-B)**.

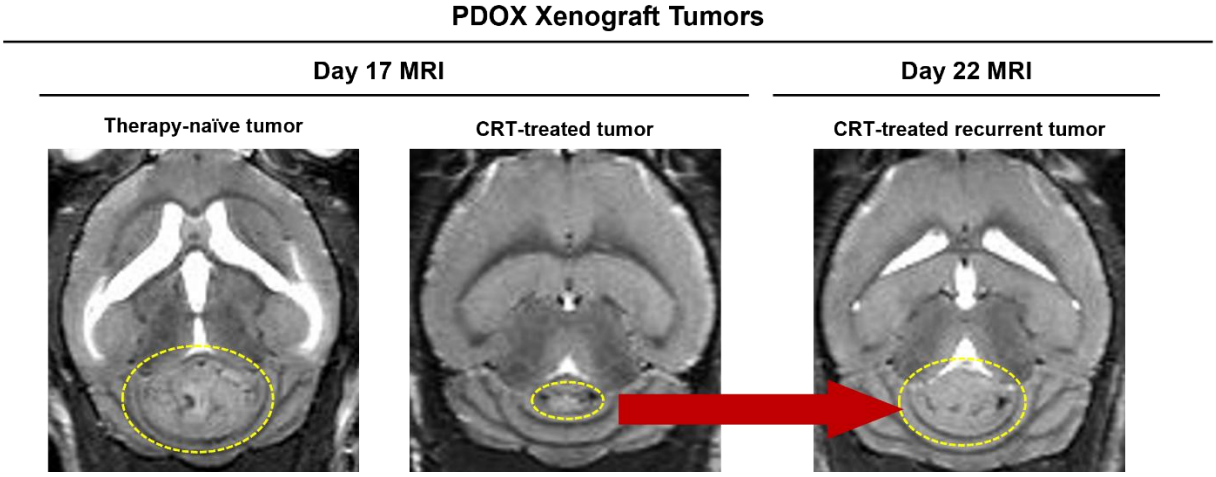

Figure 10: T2-weighted MRI showing therapy-naïve, CRT-treated, and recurrent tumors.

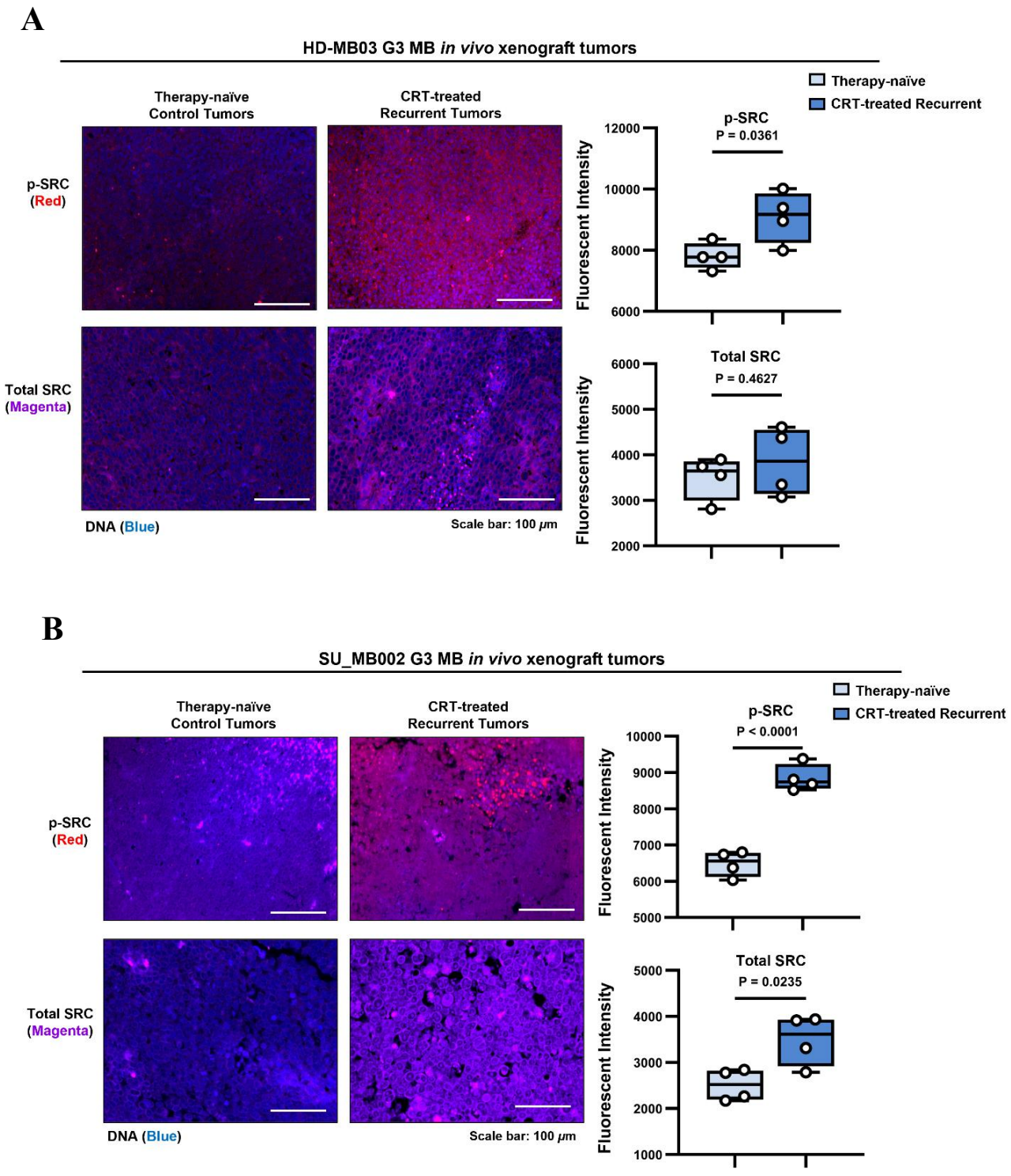

Figure 11 : Recurrent G3 MB tumors exhibit increased SRC phosphorylation *in vivo*
A-B Representative IF images of p-SRC (Y419) (red), total SRC (magenta), and DAPI-stained DNA (blue) in **(A)** HD-MB03 and **(B)** SU_MB002 therapy-naïve control tumors and CRT-treated recurrent tumors. Box-and-whisker plots show quantification of fluorescent intensity from $n = 4$ tumor samples per group, with a solid line at the mean; unpaired two-tailed t-test.

To further strengthen the clinical relevance of our findings, we examined SRC activation in patient-derived primary (D425) and relapsed (D458) G3 MB samples from the same individual. Our Western blot analysis revealed a dramatic increase in both total and p-SRC protein levels in the recurrent D458 sample **(Figure 12A)**. To determine whether this trend extended to a broader patient population, we interrogated a publicly available gene expression dataset of paired primary and recurrent G3 MB patient samples. Although total SRC mRNA expression did not show significant elevation, the overall SRC activity signature, a more robust measure of kinase signaling output, was noticeably upregulated in the recurrent patient samples **(Figure 12B)**.

Taken together, our *in vivo* results closely align with our *in vitro* observations, providing strong evidence that p-SRC upregulation following CRT treatment is not just a transient stress response; rather, it appears to be a long-lasting signaling adaptation maintained *in vivo*. These findings underscore the potential role of sustained p-SRC upregulation as a key factor driving recurrence in G3 MB.

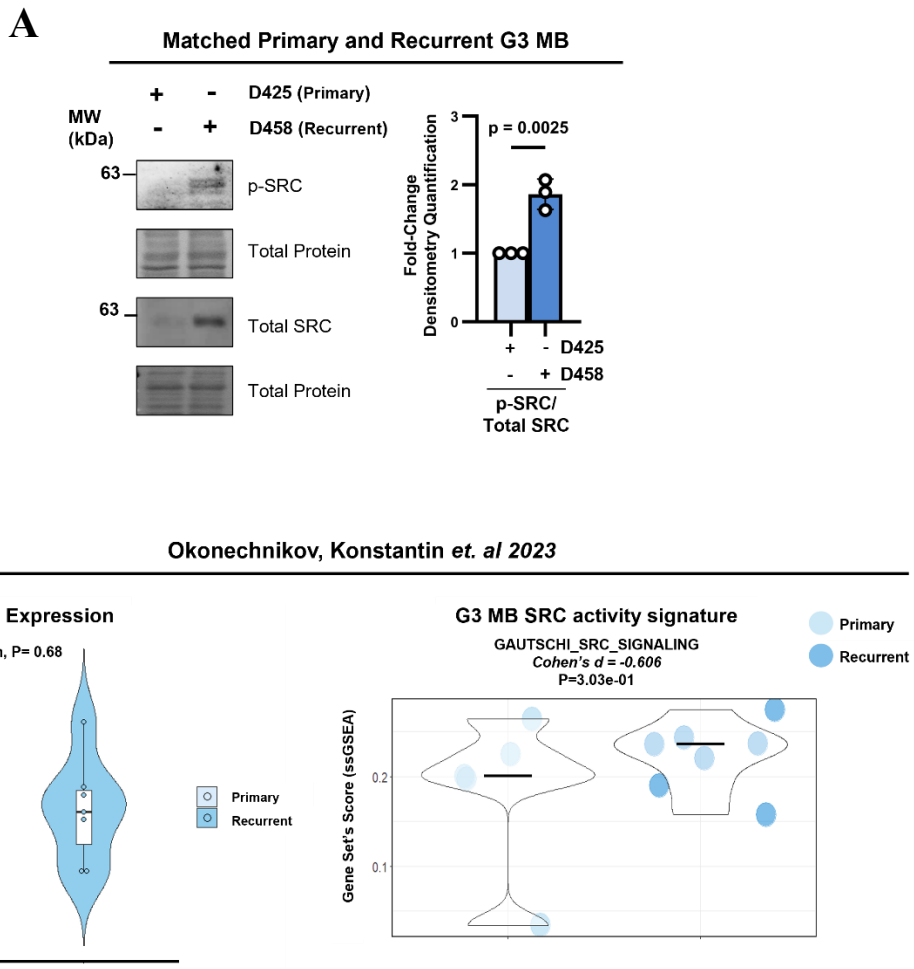

Figure 12: Elevation of SRC signaling in a recurrent G3 MB patient sample.
(A) p-SRC (Y419) and total SRC immunoblots in CRT-treated matched primary (D425) and recurrent (458) G3 MB cells. Graph represents densitometry quantification measurement normalized to the total protein stain of p-SRC/total SRC from n = 3 experimental replicates, presented as mean ± s.e.m; unpaired two-tailed t-tests. **(B)** Violin plot representing SRC expression and SRC activity signature abundance based on the GAUTSCHI_SRC_SIGNALING gene set in the data set from Okonechnikov K. et al. 2023. The Wilcoxon test was used for statistical analysis, and Cohen's d was used to measure effect size.

3.3. CRT-induced SRC activation is a G3 MB tumor- and subgroup-specific response

To determine whether SRC activation is a generalized response to CRT across all MB subgroups, we evaluated its occurrence in the SHH subgroup, which typically has a more favorable clinical prognosis[51, 58]. Using both the well-established DAOY cell line and the patient-derived SHH MB cell line BT99, we applied the same *in vitro* CRT protocol previously utilized for our G3

MB experiments **(Figure 4)**. Western blot analysis of the surviving cell fraction revealed that, in contrast to G3 MB, viable SHH MB cells did not exhibit any upregulation of p-SRC **(Figure 13A)**.

Given that elevated SRC expression is a recognized hallmark of G4 MB[110], we investigated how CRT affects SRC activity in the D283 MB cell line, which has been previously classified as G4 MB. Interestingly, following CRT treatment, both total and p-SRC levels decreased significantly in G4 cells **(Fig. 13B)**. This suggests that G4 tumors employ an adaptive strategy distinct from that of G3 MB. These results imply that SRC activation could be a G3 MB subgroup-specific mechanism of resistance, which may explain why these patients often face a more challenging prognosis.

It is critical to determine whether healthy cell populations use similar survival mechanisms following CRT, as damage to the normal brain, particularly to astrocytes and NSCs, is a primary driver of the long-term neurocognitive deficits seen in MB survivors[53, 54, 111]. To investigate this, we examined p-SRC levels in normal human astrocytes and in NSCs, which were subjected to the same CRT protocol used for our G3 MB models **(Figure 4)**. Notably, these non-malignant cells showed no increase in p-SRC levels post-treatment **(Figure 13C)**, indicating that this signaling shift is a tumor-specific adaptation rather than a general physiological response to the treatment. These findings suggest that targeting CRT-mediated SRC could be a promising therapeutic strategy to selectively eliminate recurrent G3 MB while preserving the integrity of the developing brain.

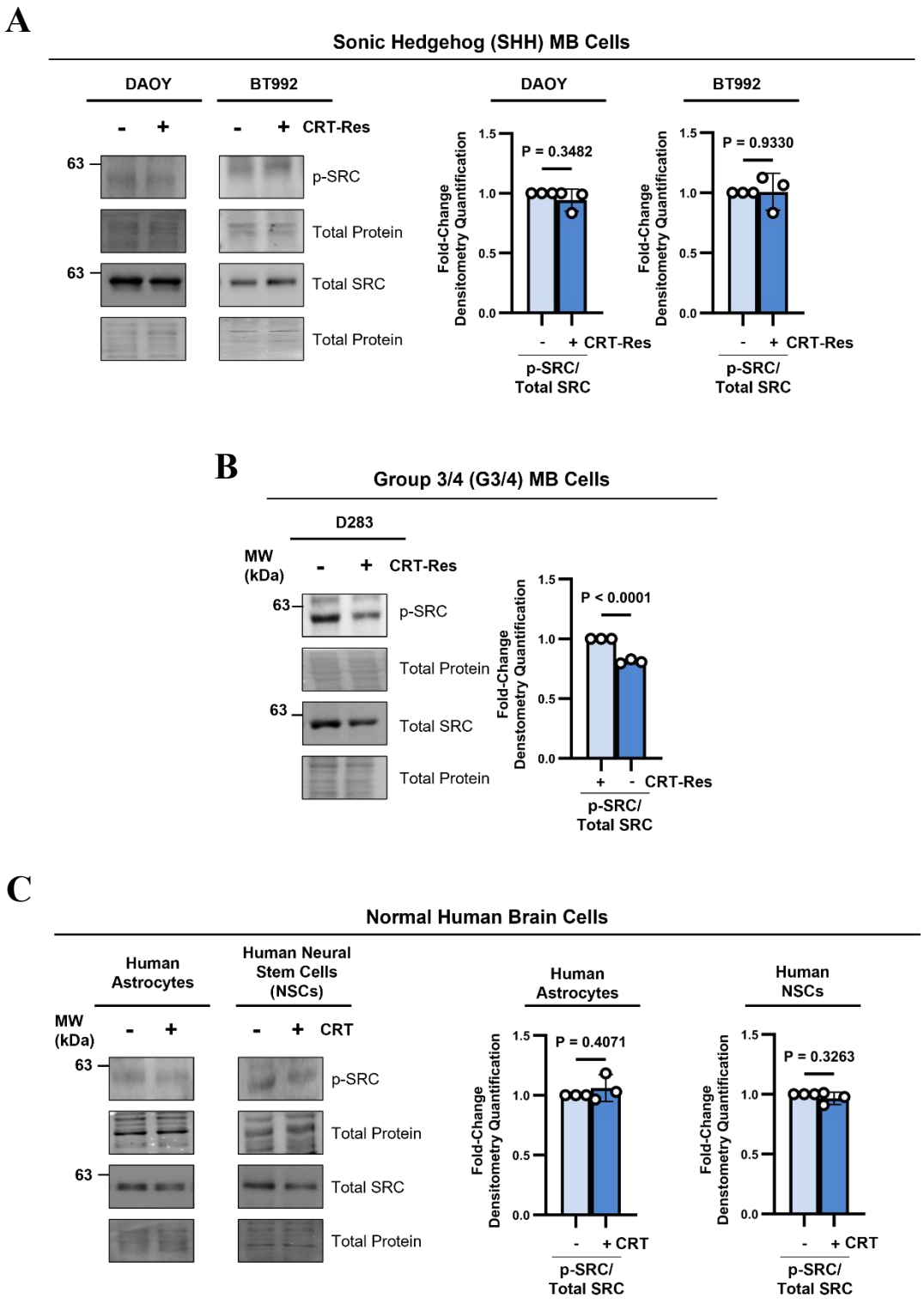

Figure 13: CRT-induced SRC activation is a G3 MB tumor- and subgroup-specific response.
A-C. p-SRC (Y419) and total SRC immunoblots in CRT-treated **(A)** SHH MB cells (DAOY and BT992), **(B)** G3/G4 MB cells (D283), and **(C)** normal human brain cells (human astrocytes and human NSCs). Graphs represent densitometry quantification measurement normalized to the total protein stain of p-SRC/total SRC from $n = 3$ experimental replicates presented as mean ± s.e.m; unpaired two-tailed t-tests.

3.4. SRC activation supports stem-like properties in therapy-resistant G3 MB cells

Our findings establish that SRC activation is a specific, conserved adaptation in G3 MB cells following CRT that persists throughout tumor recurrence *in vivo* as well. To build on this, we investigated the molecular and phenotypic consequences of this activation in CRT-Res G3 MB models. SRC is a versatile kinase known to orchestrate diverse cellular processes, including the maintenance of stemness[93-95]; however, its specific contribution to G3 MB relapse remains poorly understood. In many malignancies, the presence of undifferentiated, stem-like cell populations is a primary driver of aggressive behavior, metastatic potential, and therapeutic failure. Given these associations, we sought to determine whether SRC signaling is a key mediator in the acquisition of these stem-like properties following CRT.

Comparative Western blot profiling of therapy-naïve and CRT-Res HD-MB03 and SU_MB002 G3 MB models revealed a marked enrichment of a core stemness signature following CRT. We observed a significant upregulation of several essential pluripotency transcription factors, including SOX2, octamer-binding transcription factor 3/4 (OCT3/4), and the homeobox protein NANOG **(Figure 14, Appendix Figure 3).** Furthermore, this stem-like shift was accompanied by the robust activation of the Signal Transducer and Activator of Transcription 3 via phosphorylation at its critical tyrosine residue 705 (p-STATE3 Tyro 705) **(Appendix Figure 3)**. In parallel with these transcription factors, we detected the stemness-associated activation of the Notch signaling axis. This was evidenced by the increased proteolytic processing of NOTCH1 into its constituent ligand-binding extracellular (NEC) and transmembrane/cytoplasmic (NTM) domains **(Figure 14).** The concurrent elevation of the SOX2-OCT4-NANOG triad, alongside activated STAT3 and NOTCH1, suggests that G3 MB cells undergo a comprehensive molecular reprogramming toward a highly undifferentiated and resilient state in response to therapeutic pressure.

Conversely, the neuronal differentiation marker TUBB3, a definitive indicator of terminal lineage commitment, was significantly downregulated in CRT-Res G3 MB cell population **(Figure 14)**. The loss of TUBB3 expression, paired with the robust induction of the SOX2-NOTCH1 axis, indicates a profound shift away from neuronal maturation toward a primitive, less differentiated state. This molecular transition highlights a gain in cellular plasticity in response to therapeutic pressure. By reverting to a stem-like phenotype, these cells acquire enhanced survival and self-renewal capacities, enabling clinical recurrence and resistance to multimodal treatment.

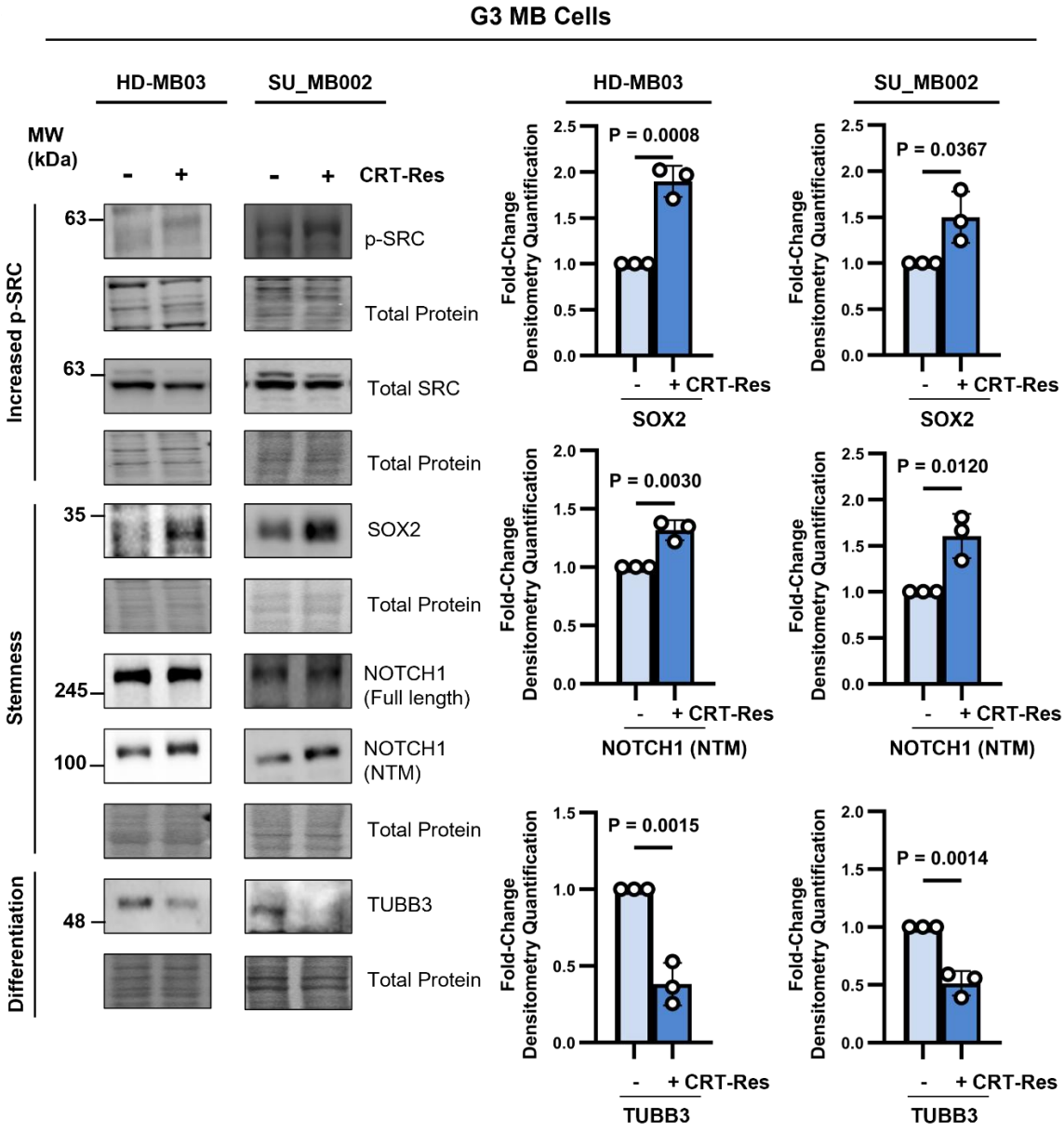

Figure 14: CRT-Resistant cells exhibit stem-like features and reduced differentiation.
Immunoblots of p-SRC (Y419), total SRC, SOX2, NOTCH1 (full length and NTM), and TUBB3 expression in CRT-Res HD-MB03 and SU_MB002 cells. Graphs represent densitometry quantification measurement of SOX2, NOTCH1 (NTM), and TUBB3, normalized to the total protein stain in therapy-naïve and CRT-Res HD-MB03 and SU_MB002 cells from $n = 3$ experimental replicates, presented as mean ± s.e.m; unpaired two-tailed t-test

Similar results were observed in the HD-MB03 and SU_MB002 PDOX models when comparing IF images from therapy-naïve and recurrent tumors, where recurrent tumors showed an upregulation of SOX2, along with a notable downregulation of TUBB3 **(Figure 15 A-B)**. This

molecular pattern further confirms that CRT treatment promotes a shift away from neuronal differentiation toward a more stem-like and plastic state, ultimately enhancing tumor cell survival, resistance, and recurrence.

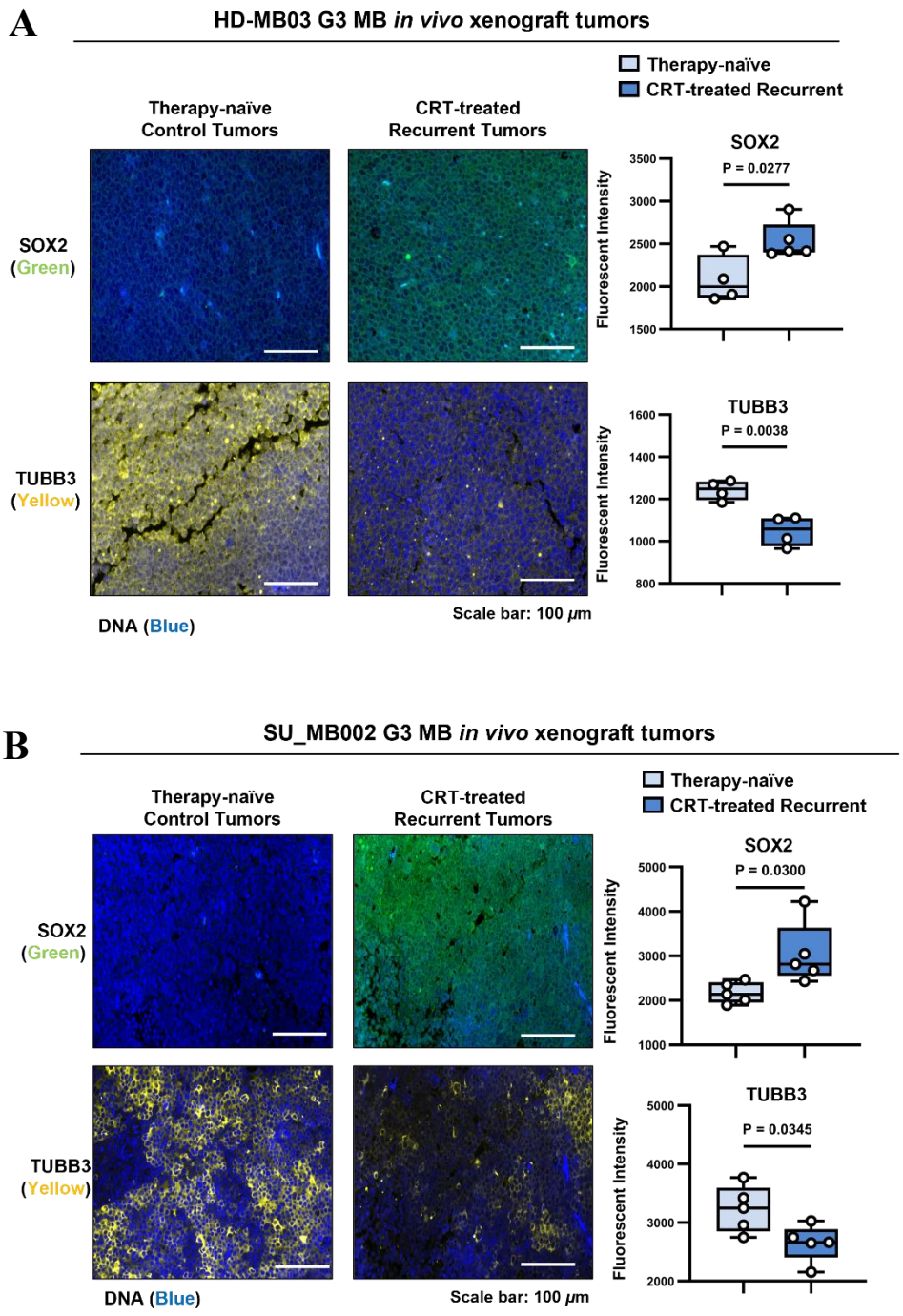

Figure 15: Recurrent tumors exhibit stem-like features and reduced differentiation.
A-B IF images of **(A)** HD-MB03 and **(B)** SU_MB002 tumors from therapy-naïve and CRT-treated recurrent tumors stained with SOX2 (green) and TUBB3 (yellow) with DAPI (blue). Box-and-whisker plots of fluorescent intensity from $n = 4$ tumor samples per group, with a solid line at the mean, unpaired two-tailed t-test.

To investigate whether SRC is required for the maintenance of enhanced stemness in CRT-Res G3 MB cells, we established a DOX-inducible, Tet-ON Cas9-mediated *SRC* knockout (KO) system in HD-MB03 and SU_MB002 lines. Utilizing two independent *SRC*-targeting gRNAs (sg*SRC*) clones. Following CRT administration, we isolated viable CRT-Res populations that harbored the inducible constructs. These cells were then treated with DOX, which successfully depleted both total SRC and p-SRC, correlating with a global reduction in phosphotyrosine levels (**Figure 16-17, Appendix Figure 4).**

Critically, *SRC* depletion led to downregulation of key stemness markers, including SOX2, OCT4, NANOG, and NOTCH1-NTM, and reduced p-STAT3 (**Figure 16-17, Appendix Figure 4)**. This loss of progenitor identity was accompanied by the restoration of the neuronal differentiation marker TUBB3 **(Figure 16-17)**, suggesting that SRC activity is essential for preserving the undifferentiated state of CRT-Res G3 MB cells.

Furthermore, the effects of *SRC* depletion on stemness were also assessed using tumorsphere formation assays, a well-established method for evaluating the self-renewal capacity of cancer stem-like cells. The *SRC* KO resulted in a significant reduction in the number of primary tumorspheres and a diminished ability of the cells to generate secondary tumorspheres upon passaging **(Figure 18-19).**

Importantly, the observed phenotype was reversible; re-expressing active *SRC* via gain-of-function OE in the *SRC* KO CRT-Res G3 MB cells restored both stemness marker expression and the capacity for tumorsphere formation **(Figure 20A-B)**. Conversely, the neuronal differentiation marker TUBB3 was downregulated upon SRC restoration **(Figure 20A)**. These results highlight a critical and direct role for SRC in maintaining the stem-like state of G3 MB cells following CRT treatment.

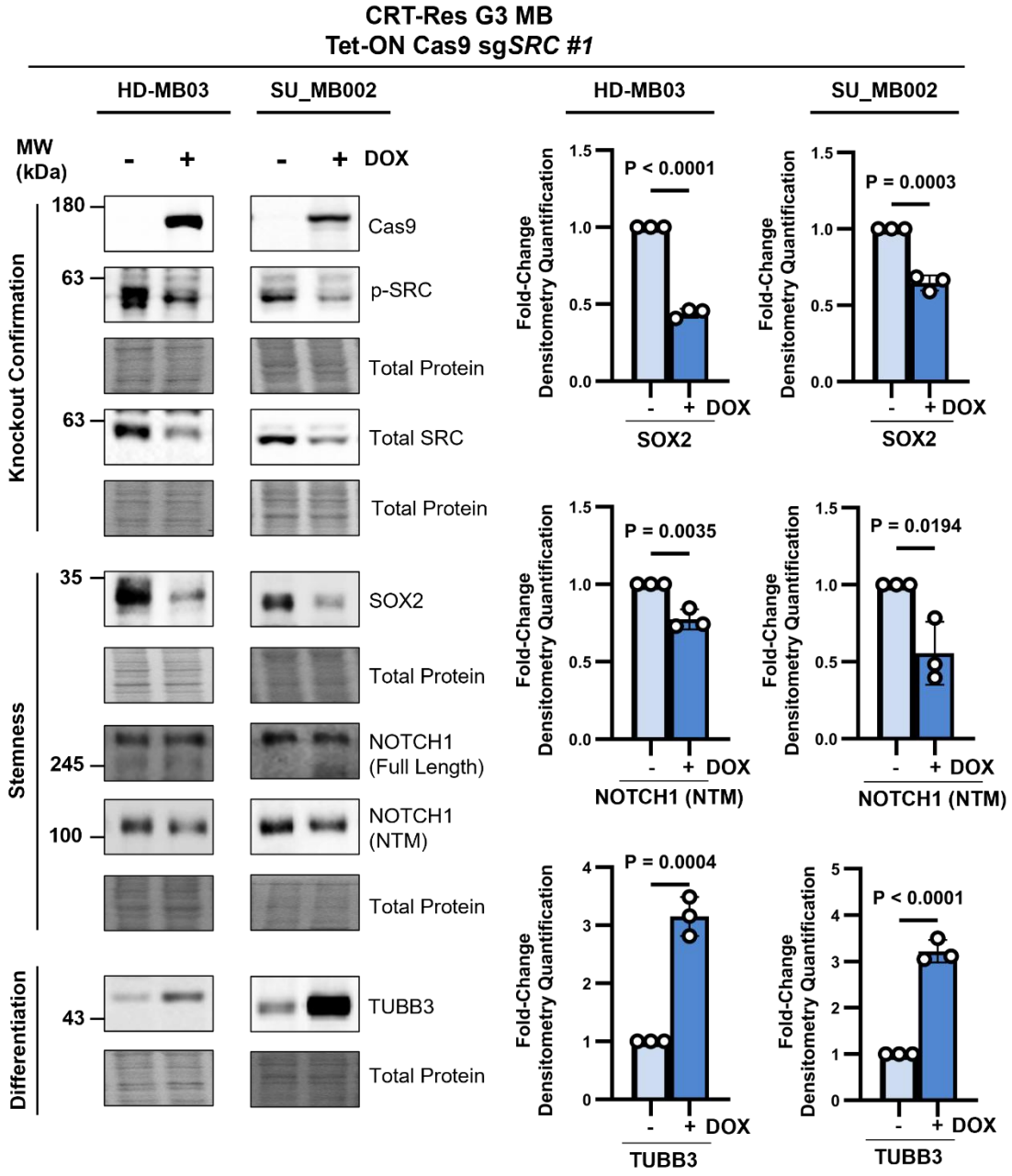

Figure 16: SRC depletion suppresses stem-like features and promotes neuronal differentiation.
Immunoblots of Cas9, p-SRC (Y419), total SRC, SOX2, NOTCH1 (full length and NTM), and TUBB3 in CRT-Res HD-MB03 and SU_MB002 cells expressing Tet-ON Cas9 sg*SRC #1* treated with DOX to induce *SRC* KO. Graphs represent densitometry quantification measurement of SOX2, NOTCH1 (NTM), and TUBB3, normalized to the total protein stain levels from $n = 3$ experimental replicates, presented as mean ± s.e.m; unpaired two-tailed t-test

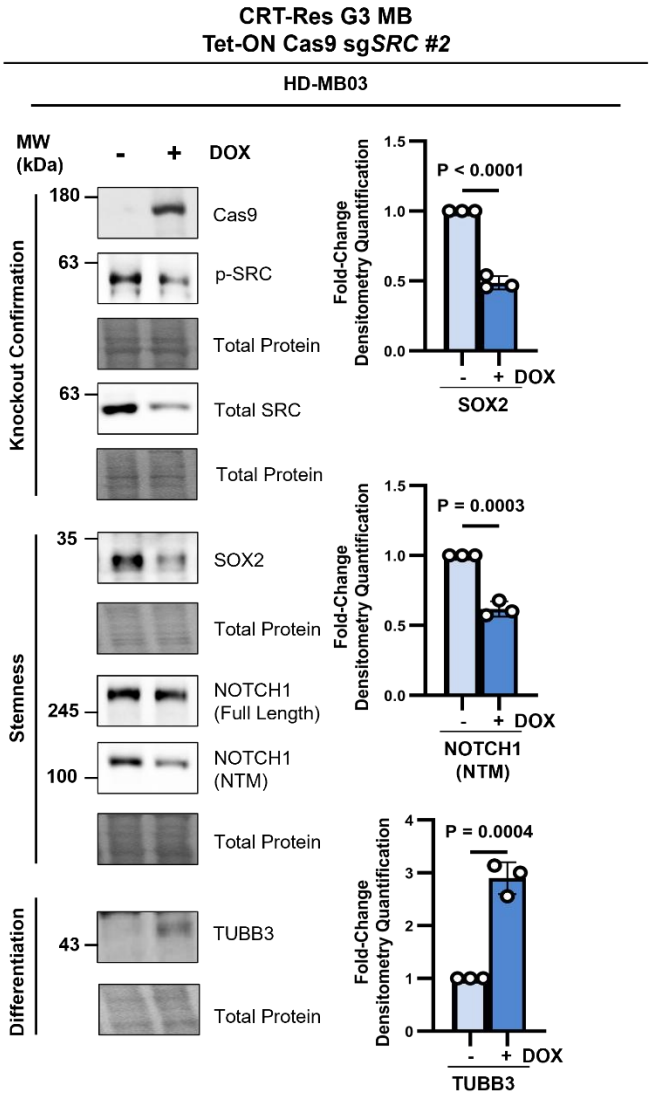

Figure 17: SRC depletion suppresses stem-like features and promotes neuronal differentiation.
Immunoblots of Cas9, p-SRC (Y419), total SRC, SOX2, NOTCH1 (full length and NTM), and TUBB3 in CRT-Res HD-MB03 cells expressing Tet-ON Cas9 sg*SRC* #2 treated with DOX to induce *SRC* KO. Graphs represent densitometry quantification measurement of p-SRC/Total SRC, SOX2, NOTCH1 (NTM), and TUBB3 normalized to the total protein stain levels from $n = 3$ experimental replicates, presented as mean ± s.e.m; unpaired two-tailed t-test.

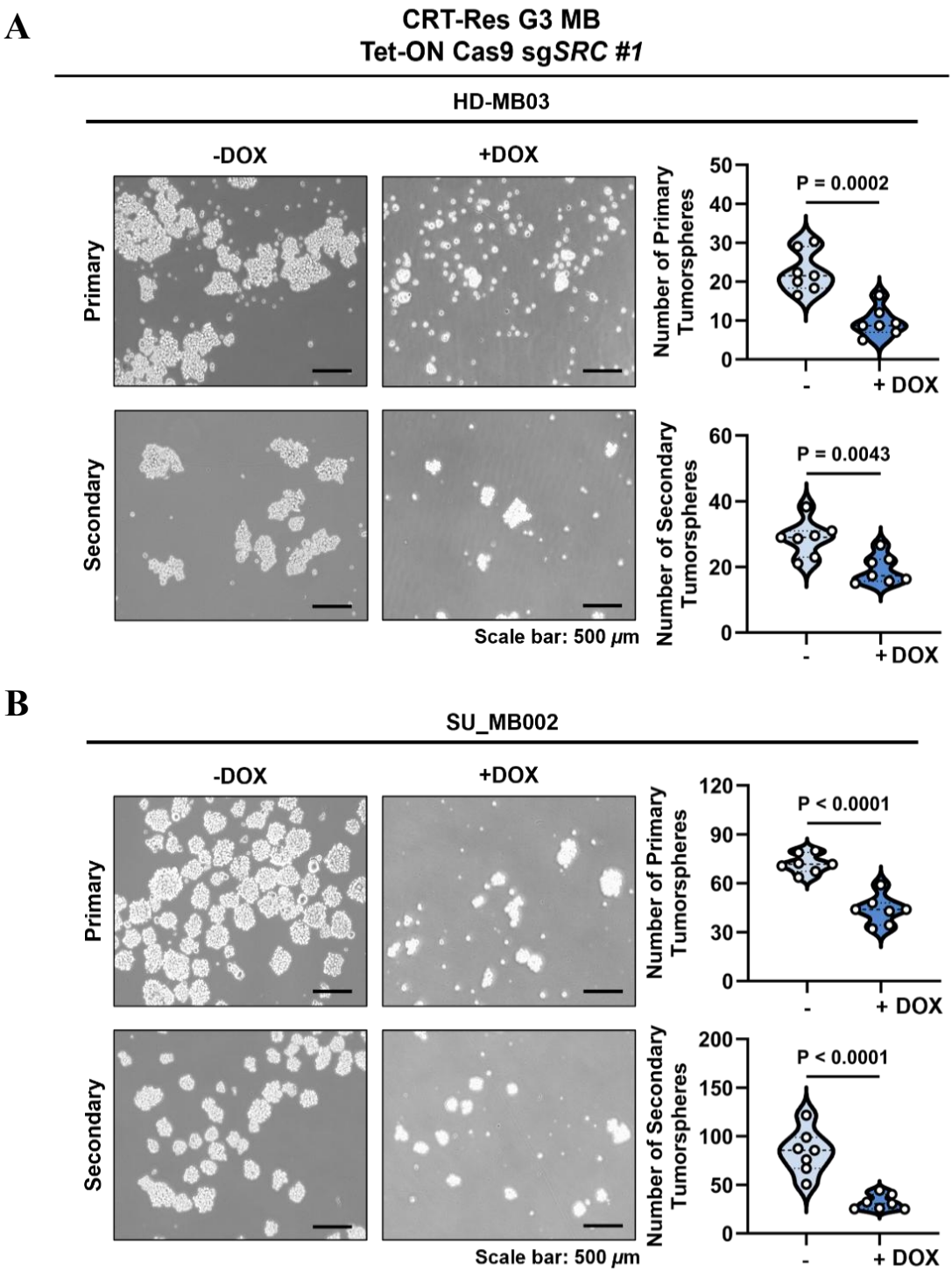

Figure 18: SRC KO impairs self-renewal capacity in CRT-Resistant G3 MB cells.
A-B Primary and secondary tumorsphere formation assay from CRT-Res **(A)** HD-MB03 and **(B)** SU_MB002 cells expressing Tet-ON Cas9 sg*SRC #1* treated with DOX to induce *SRC* KO. A violin plot represents the quantification of the total sphere number from n =7 replicates, with dashed lines at the mean and quartiles; an unpaired two-tailed t-test.

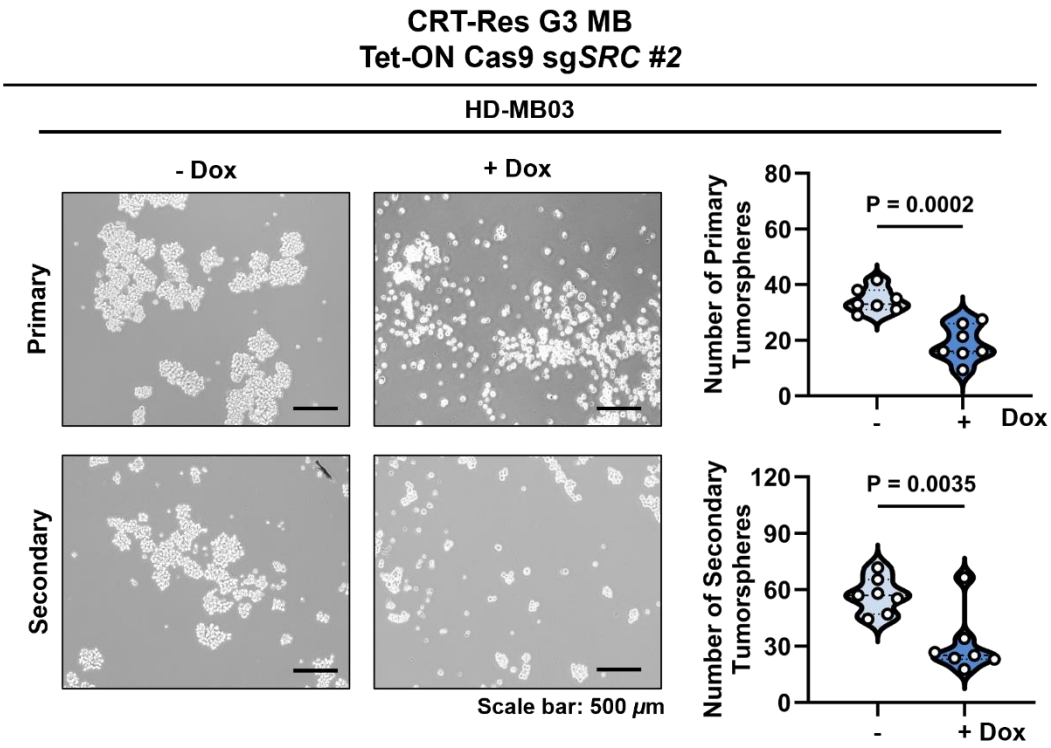

Figure 19: SRC KO impairs self-renewal capacity in CRT-Resistant G3 MB cells.
Primary and secondary tumorsphere formation assay from CRT-ResHD-MB03 cells expressing Tet-ON Cas9 sg*SRC #2* treated with DOX to induce *SRC* KO. A violin plot represents the quantification of the total sphere number from *n* =7 replicates, with dashed lines at the mean and quartiles; an unpaired two-tailed t-test.

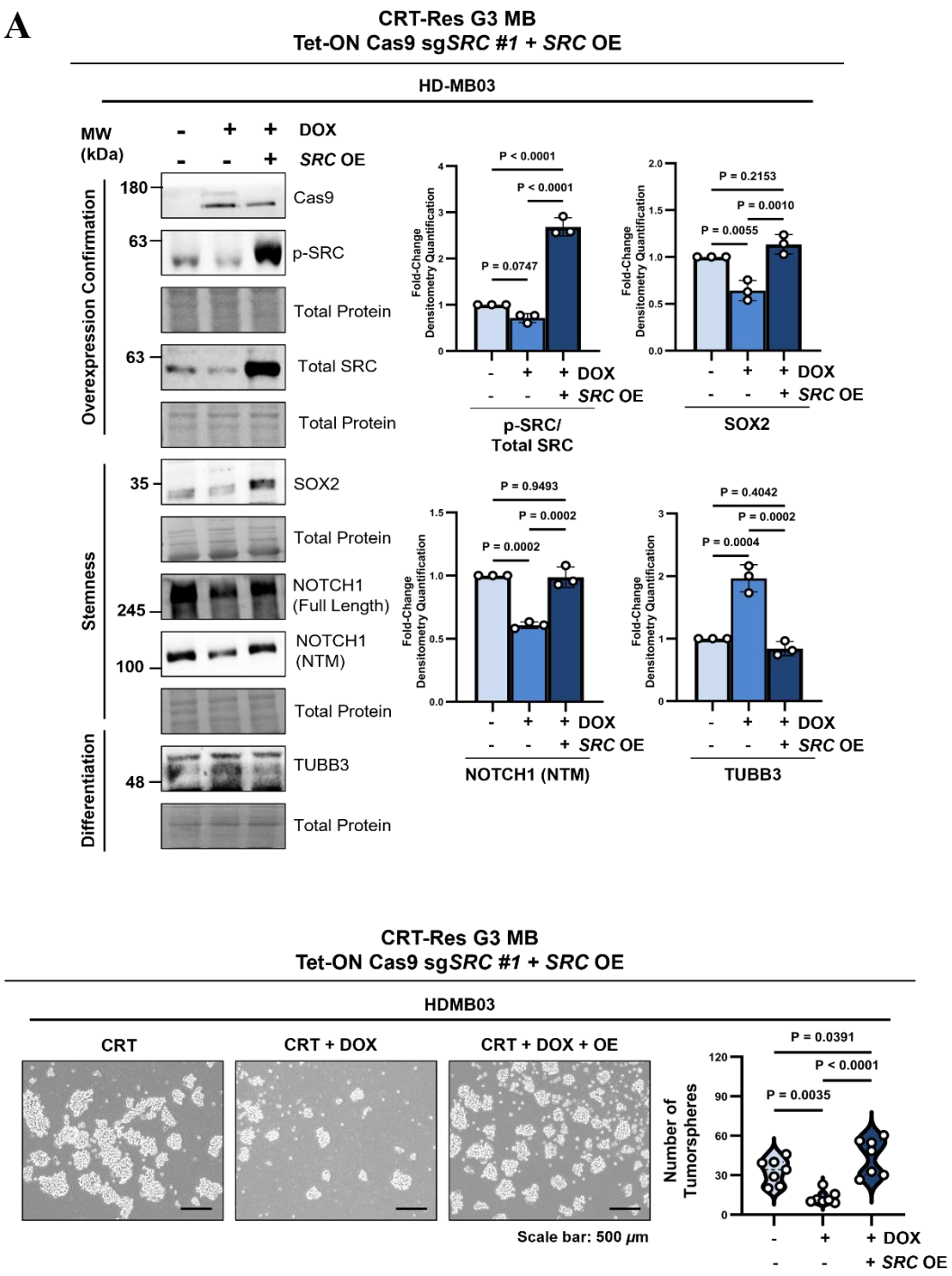

Figure 20: SRC restoration rescues stemness and suppresses neuronal differentiation in SRC-KO CRT-Resistant G3 MB cells.

(A) Immunoblots of Cas9, p-SRC (Y419), total SRC, SOX2, NOTCH1 (full length and NTM), and TUBB3 in CRT-Res HD-MB03 cells expressing Tet-ON Cas9 sg*SRC* #1 treated with DOX and transfected with *SRC* OE. Graphs represent densitometry quantifications of p-SRC/total SRC, SOX2, NOTCH1 (NTM), and TUB33 levels from $n = 3$ experiments; mean ± s.e.m. two-way ANOVA with Tukey's test. **(B)** Tumorsphere formation assay from CRT-Res HD-MB03 expressing Tet-ON Cas9 sg*SRC* #1 treated with DOX and transfected with *SRC* OE, Violin plot represents quantification of total sphere number from $n = 7$ replicates, with dashed lines at the mean and quartiles; two-way ANOVA with Tukey's test

Given the established link between stemness and invasive tumor characteristics, along with high metastatic rates in recurrent G3 MB[32, 51, 58], we assessed the role of SRC in promoting migratory capacity. We conducted transwell migration assays on CRT-Res *SRC* KO HD-MB03 and SU_MB002 cells that expressed GFP for lineage tracking, to determine their ability to migrate across a permeable membrane barrier. Consistent with the observed loss of stemness markers, *SRC* KO also inhibited the migratory ability of CRT-Res G3 MB cells **(Figure 21)**.

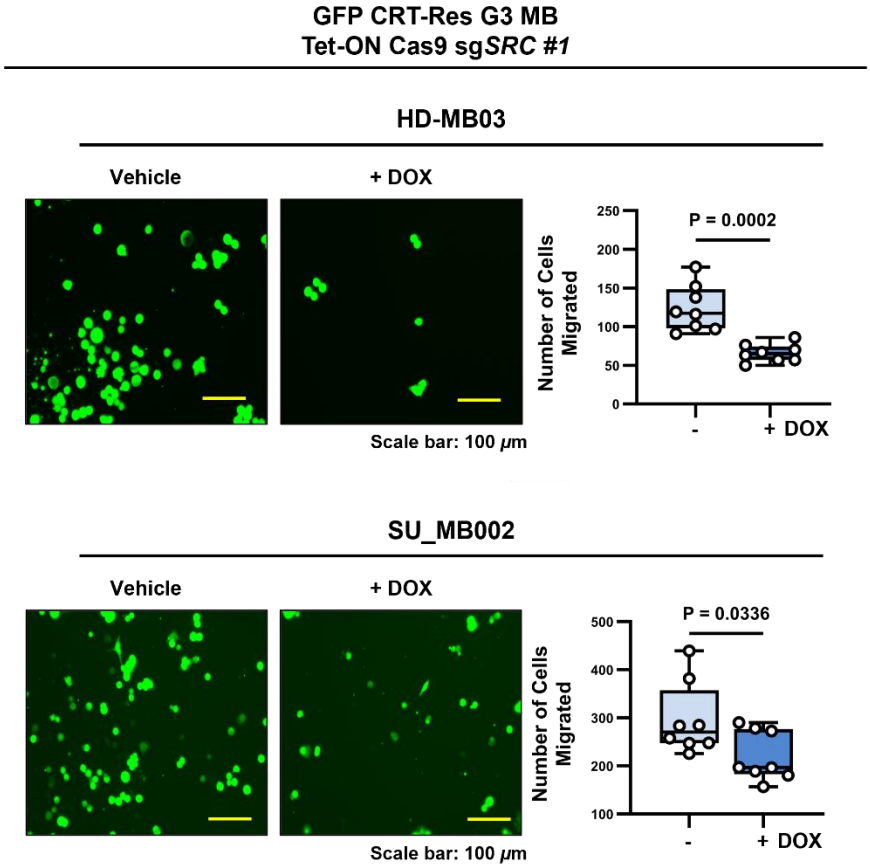

Figure 21: SRC depletion suppresses cell migration in CRT-Resistant G3 MB cells.
Representative images and quantification of migration assays in HD-MB03 and SU_MB002 cells expressing Tet-ON Cas9, sg*SRC #1,* and GFP, treated with DOX to induce *SRC* KO. Box-and-whisker plots represent quantification of migrated cells from $n = 8$ replicates, with a solid line at the mean, unpaired two-tailed t-test.

Collectively, these results indicate that SRC plays a crucial role in maintaining the undifferentiated, stem-like characteristics and aggressive migration of therapy-resistant G3 MB

cells. By sustaining stemness and inhibiting differentiation, SRC enables tumor cells to retain their plasticity and invasive behavior following CRT.

3.5. Loss of *SRC* promotes cell death via apoptotic and necroptotic pathways in therapy-resistant G3 MB

So far, our findings indicate that SRC plays a pro-tumorigenic role in maintaining the aggressive stemness and migratory characteristics of CRT-Res G3 MB cells. While many studies have linked SRC to cell proliferation, survival, and stemness, it is clear that SRC's effects are highly context-dependent. Research suggests that SRC signaling can either promote tumor cell growth or induce cell death[112-114], depending on specific cellular and environmental conditions.

To explore the role of SRC on the viability of CRT-Res G3 MB cells, we conducted viability assays following *SRC* KO in CRT-Res HD-MB03 and SU_MB002 cells. Both Trypan blue exclusion assays and PrestoBlue metabolic viability assays consistently showed that the loss of *SRC* significantly reduced cell number and overall viability **(Figure 22A-C)**.

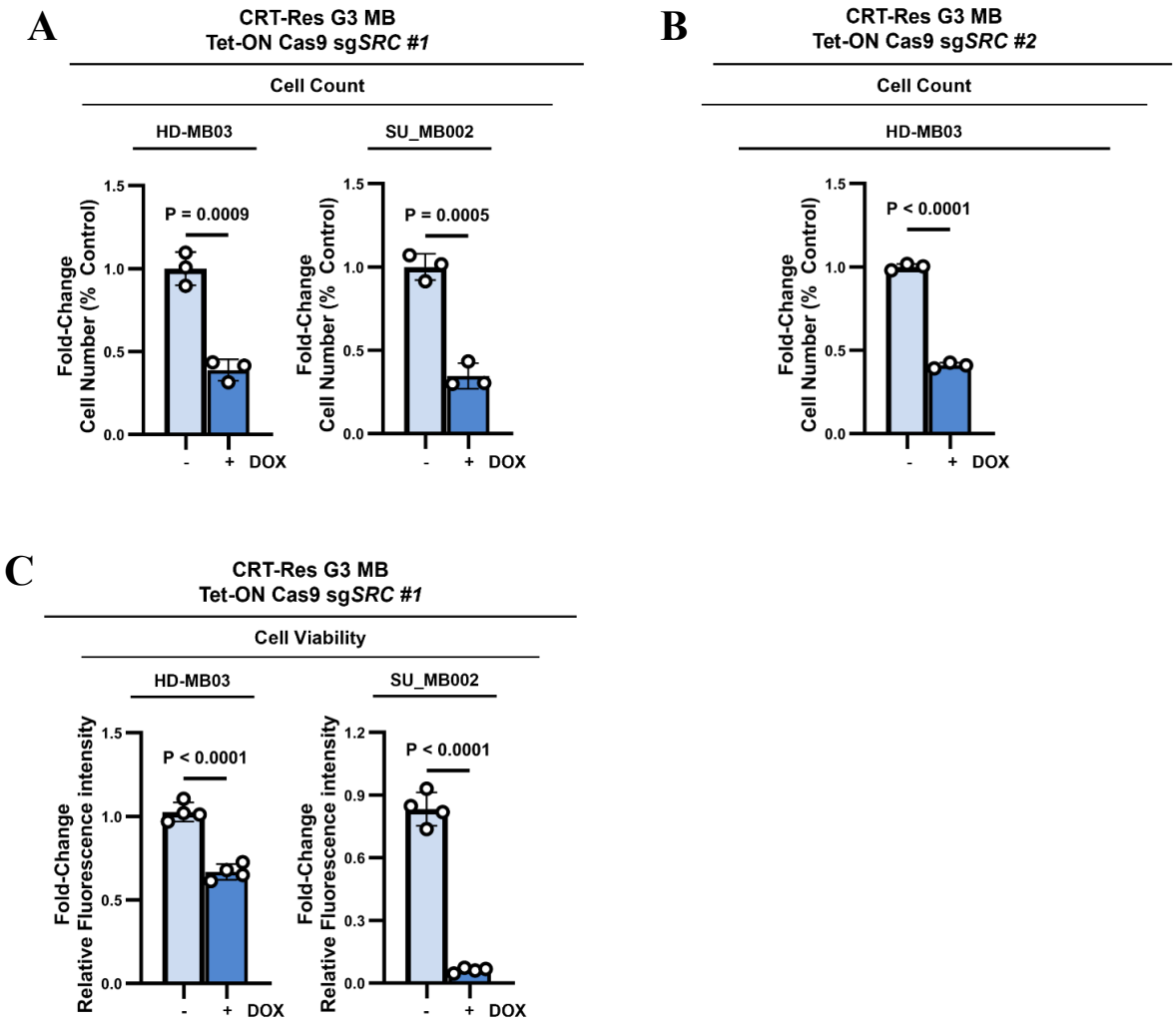

Figure 22: Impaired growth and viability following SRC KO in CRT-Resistant G3 MB cells.
A-B Cell count analysis of **(A)** CRT-Res HD-MB03 and SU_MB002 cells expressing Tet-ON Cas9 sg*SRC #1* and **(B)** CRT-Res HD-MB03 cells expressing Tet-ON Cas9 sg*SRC #2* treated with DOX to induce *SRC* KO. Graph represents fold-change in cell number of *SRC* KO cells (+DOX) compared to controls (-DOX). Data presented as mean ± s.e.m; from $n = 3$ experimental replicates; unpaired two-tailed t-test. **(C)** PrestoBlue viability analysis of CRT-Res HD-MB03 and SU_MB002 cells expressing Tet-ON Cas9 sg*SRC* #1 treated with DOX to induce *SRC* KO. Graphs represent fluorescent PrestoBlue signal in *SRC* KO cells (+DOX) compared to controls (-DOX). Data presented as mean ± s.e.m. from $n = 4$ experimental replicates; unpaired two-tailed t-test.

To gain further insight into the mechanism underlying SRC-depletion-mediated cell death, we evaluated activation of both the apoptosis and necroptosis pathways. CRT-Res HD-MB03 and SU_MB002 cells expressing Tet-ON Cas9 sg*SRC #1* and *#2* were treated with DOX. In western blot, we found evidence of apoptosis, as demonstrated by the activation of cleaved caspase-3 **(Figure 23A-B)**, a primary executioner caspase responsible for dismantling cellular architecture

during programmed cell death. This activation of caspase-3 was accompanied by cleavage of poly (ADP-ribose) polymerase-1 (PARP-1), a nuclear enzyme involved in DNA repair; cleavage of PARP-1 serves as a biochemical marker of apoptosis **(Figure 23A-B)**. Simultaneously, necroptosis was also triggered as indicated by increased expression of receptor-interacting protein kinase 3 (RIP3K) **(Figure 24A-B)**, a signaling kinase that is part of the necrosome complex. This complex leads to necroptotic cell death when caspase activity is deficient or inhibited. The coordinated induction of cleaved caspase-3 and PARP-1 alongside RIP3K demonstrates that the loss of SRC activates both the apoptosis and necroptosis programmed cell death pathways simultaneously.

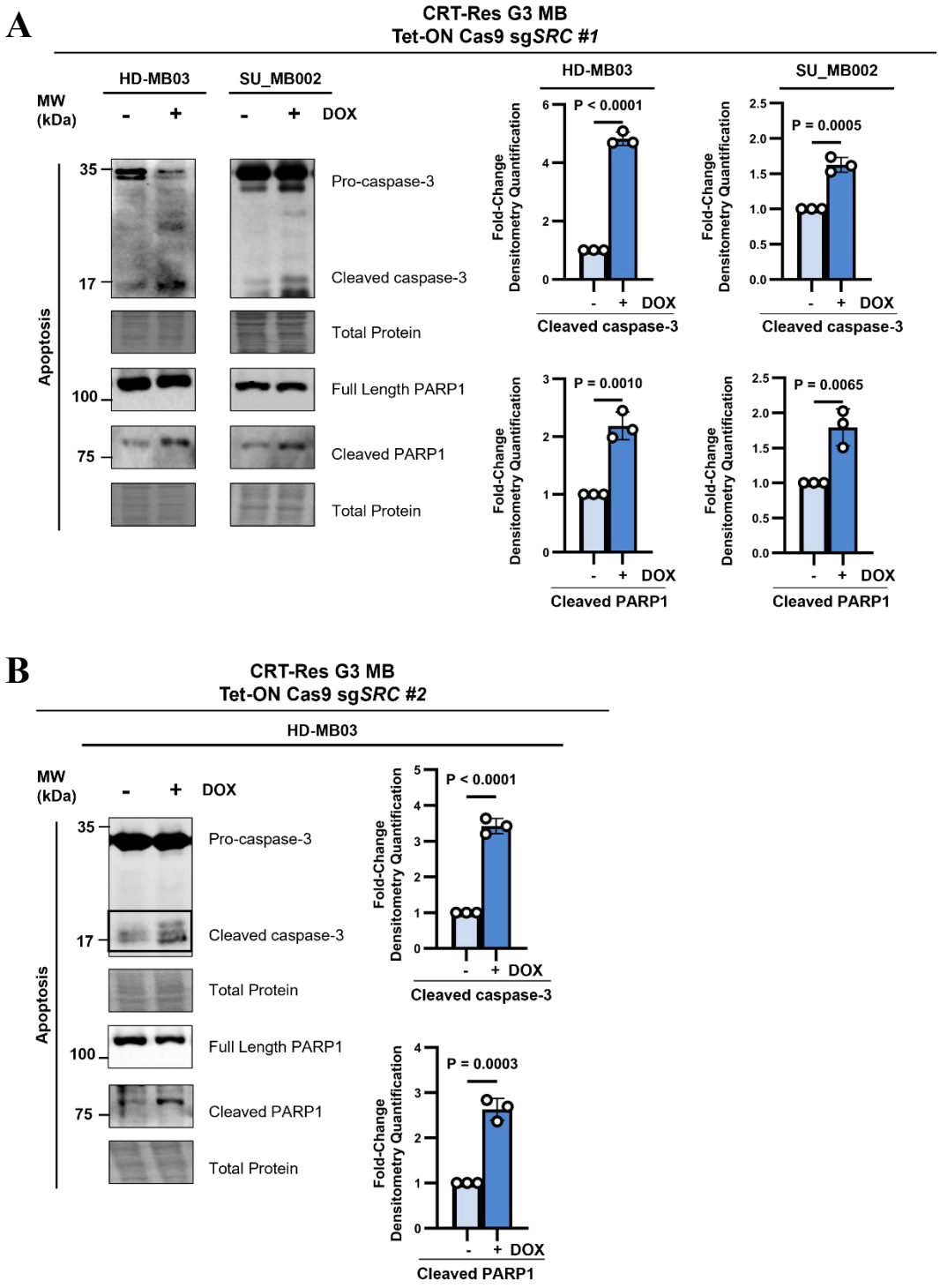

Figure 23: SRC depletion drives programmed cell death via apoptosis in CRT-Resistant G3 MB cells.
A-B Immunoblot of Cas9, p-SRC (Y419), total SRC, pro-caspase-3, cleaved caspase-3, full-length PARP1, and cleaved PARP1 in **(A)** CRT-Res HD-MB03 and SU_MB002 cells expressing Tet-ON Cas9 sg*SRC #1* and **(B)** CRT-Res HD-MB03 cells expressing Tet-ON Cas9 sg*SRC #2* treated with DOX. Graphs represent densitometry quantification measurement of cleaved caspase-3, and cleaved PARP1 normalized to the total protein stain levels from $n = 3$ experimental replicates, presented as mean ± s.e.m; unpaired two-tailed t-test.

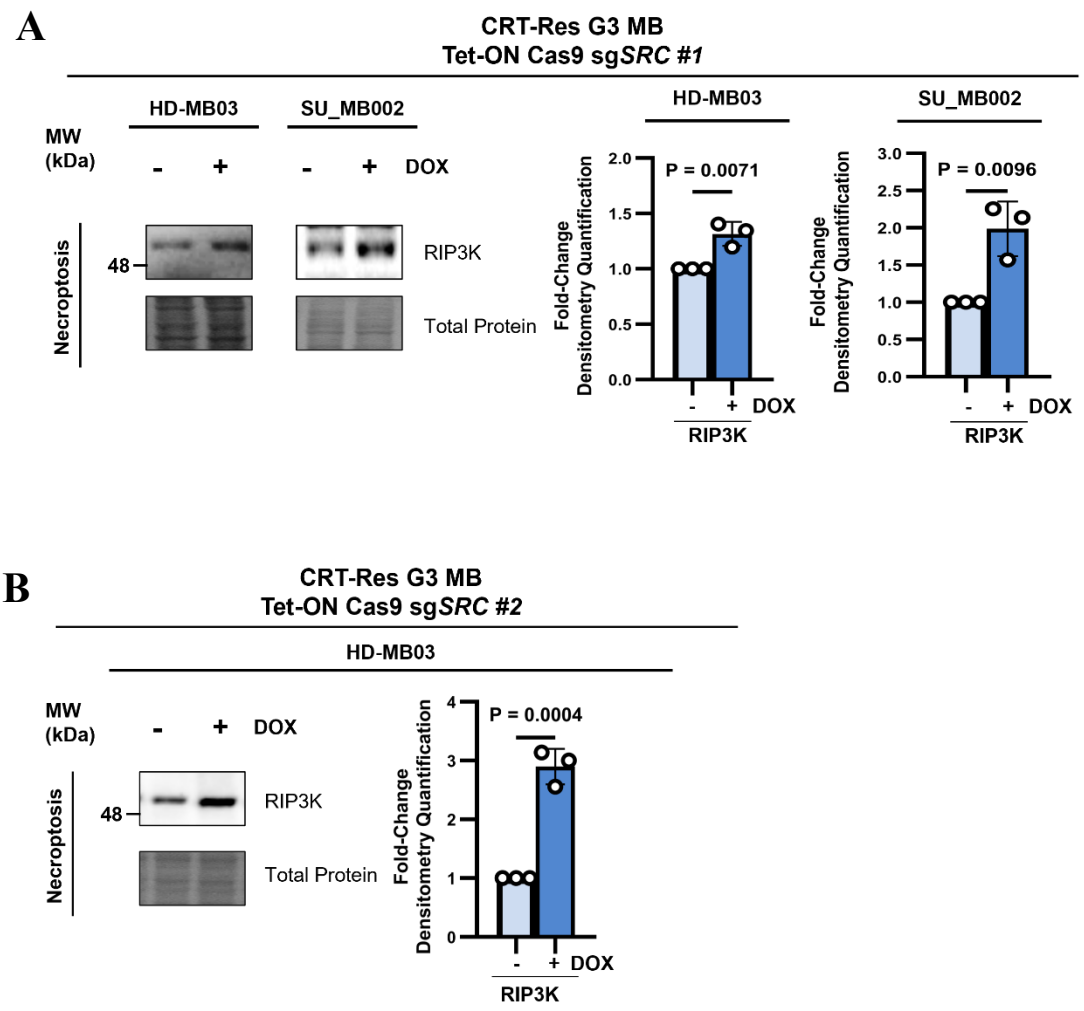

Figure 24: SRC Depletion Drives Programmed Cell Death via Necroptosis in CRT-Resistant G3 MB Cells. **A-B** Immunoblot of Cas9, p-SRC (Y419), total SRC, and RIP3K in **(A)** CRT-Res HD-MB03 and SU_MB002 cells expressing Tet-ON Cas9 sg*SRC #1* and **(B)** CRT-Res HD-MB03 cells expressing Tet-ON Cas9 sg*SRC* #2 treated with DOX. Graphs represent densitometry quantification measurement of RIP3K normalized to the total protein stain levels from $n = 3$ experimental replicates, presented as mean ± s.e.m; unpaired two-tailed t-test.

To further validate these findings, we pharmacologically inhibited the apoptotic and necroptotic pathways in *SRC*-depleted cells. CRT-Res HD-MB03 and SU_MB002 expressing Tet-ON Cas9 sg*SRC* #1 cells were treated with DOX to induce *SRC* KO and co-administered with either the pan-caspase inhibitor Z-VAD-FMK or Necrostatin-1 (Nec-1), a necroptosis inhibitor. Western blot analysis confirmed that Z-VAD-FMK successfully abrogated caspase-3 activation

and subsequent PARP-1 cleavage, while Nec-1 treatment effectively reduced RIP3K expression **(Figure 25)**. To assess the functional impact on cell survival, we performed trypan blue exclusion assays. Consistent with our western blot data, pharmacological blockade of either apoptotic or necroptotic signaling significantly rescued the viability of *SRC* KO cells **(Figure 26A-B)**, suggesting that SRC depletion induces cell death through both pathways.

The functional necessity of SRC was further validated by re-expressing the active SRC in *SRC* KO CRT-Res G3 MB cells. The restoration abrogated the induction of pro-apoptotic and necroptotic markers while effectively restoring cell viability **(Figure 27A-B)**. These rescue data underscore that the activation of these programmed cell death pathways is a direct consequence of SRC depletion, identifying SRC as a critical survival factor in therapy-resistant G3 MB.

Overall, these data demonstrate that SRC is essential for the survival of CRT-Res G3 MB cells by actively suppressing programmed cell death. In the absence of SRC, cells undergo both apoptosis, mediated by Caspase-3 and PARP-1, and necroptosis, driven by RIP3K signaling. The activation of these dual mechanisms upon SRC loss underscores a lack of functional redundancy, identifying SRC as a targetable vulnerability in recurrent G3 MB.

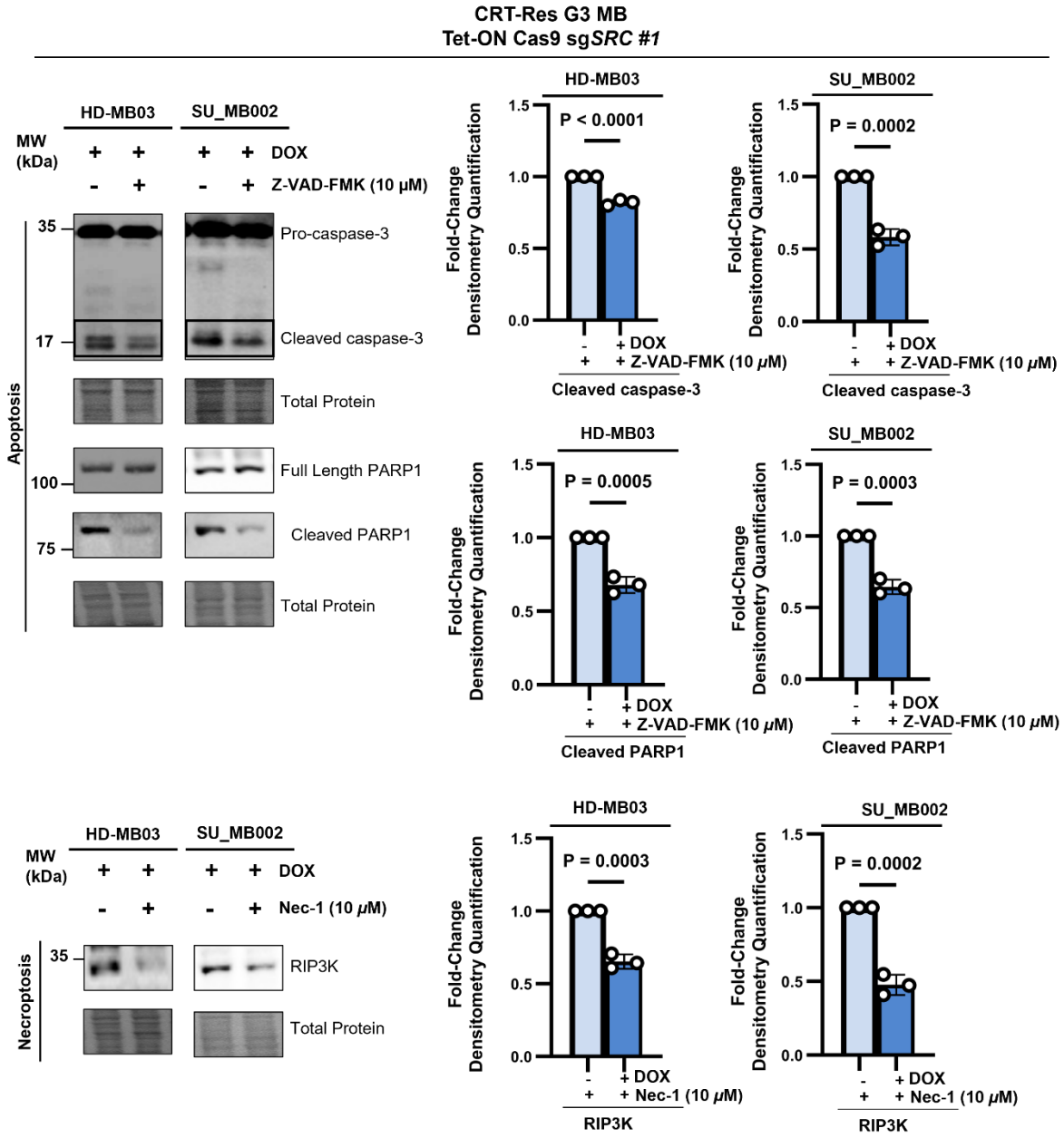

Figure 25: Pharmacological inhibition of apoptosis and necroptosis reverses cell death markers in SRC KO CRT-Resistant G3 MB cells.

Immunoblot of pro-caspase-3, cleaved caspase-3, full length PARP1, cleaved PARP1, and RIP3K in CRT-Res HD-MB03 and SU_MB002 cells expressing Tet-ON Cas9 sg*SRC #1* following DOX-induced *SRC* KO treated with Z-VAD-FMK (10 μM) or Nec-1 (10 μM) treatment. Graphs represent densitometry quantification measurements of cleaved caspase-3, cleaved PARP1, and RIP3K, normalized to total protein levels in CRT-Res HDMB03 and SU_MB002 cells from $n = 3$ experimental replicates, presented as mean ± s.e.m; unpaired two-tailed t-test.

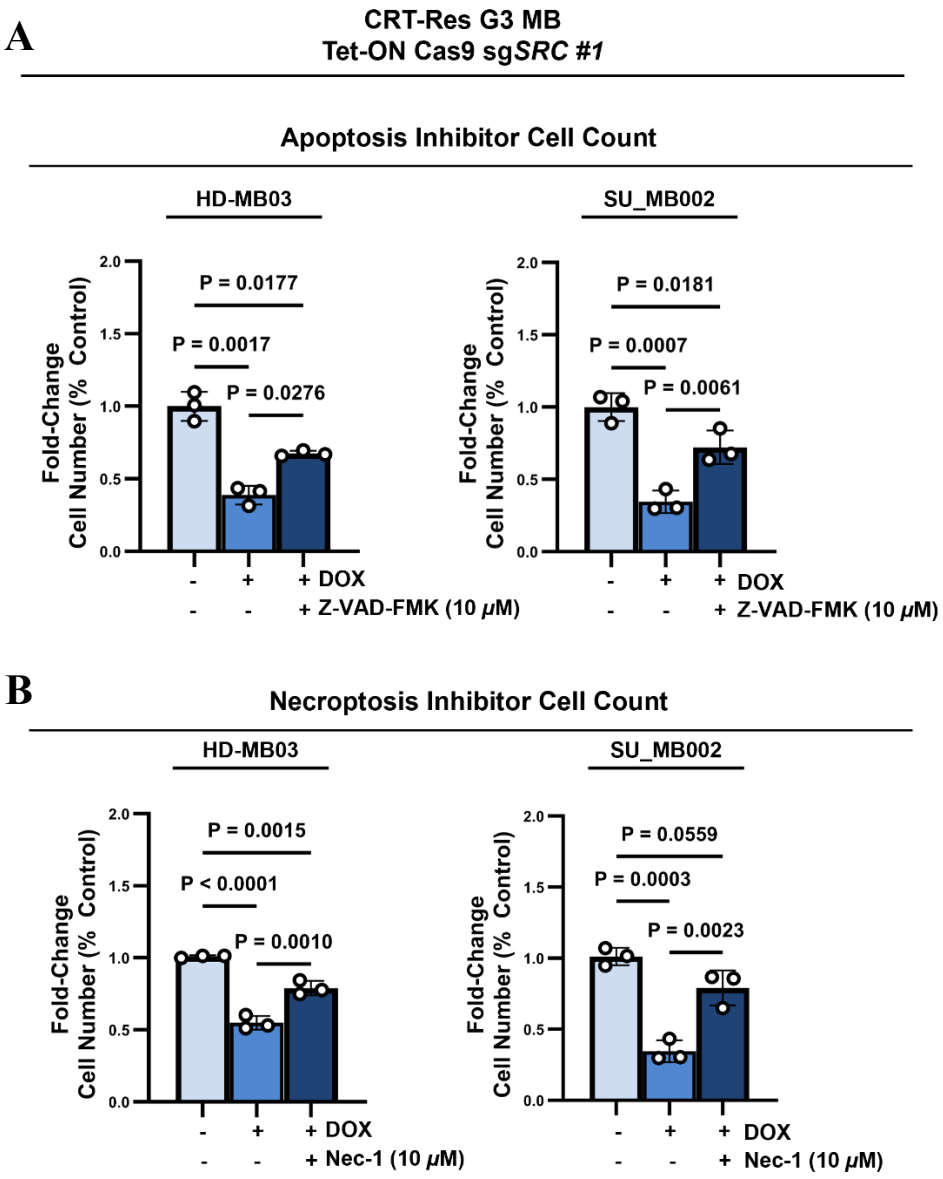

Figure 26: Pharmacological blockade of apoptosis and necroptosis restores cell survival in SRC KO cells.
A-B Cell count analysis of CRT-Res HD-MB03 and SU_MB002 cells expressing Tet-ON Cas9 sg*SRC #1* treated with DOX and **(A)** Z-VAD-FMK (10 μM) and **(B)** Nec-1 (10μM) treatment. Graphs represent fold-change in cell number compared to CRT-Res controls from $n = 3$ experimental replicates, presented as mean ± s.e.m; two-way ANOVA with Tukey's test.

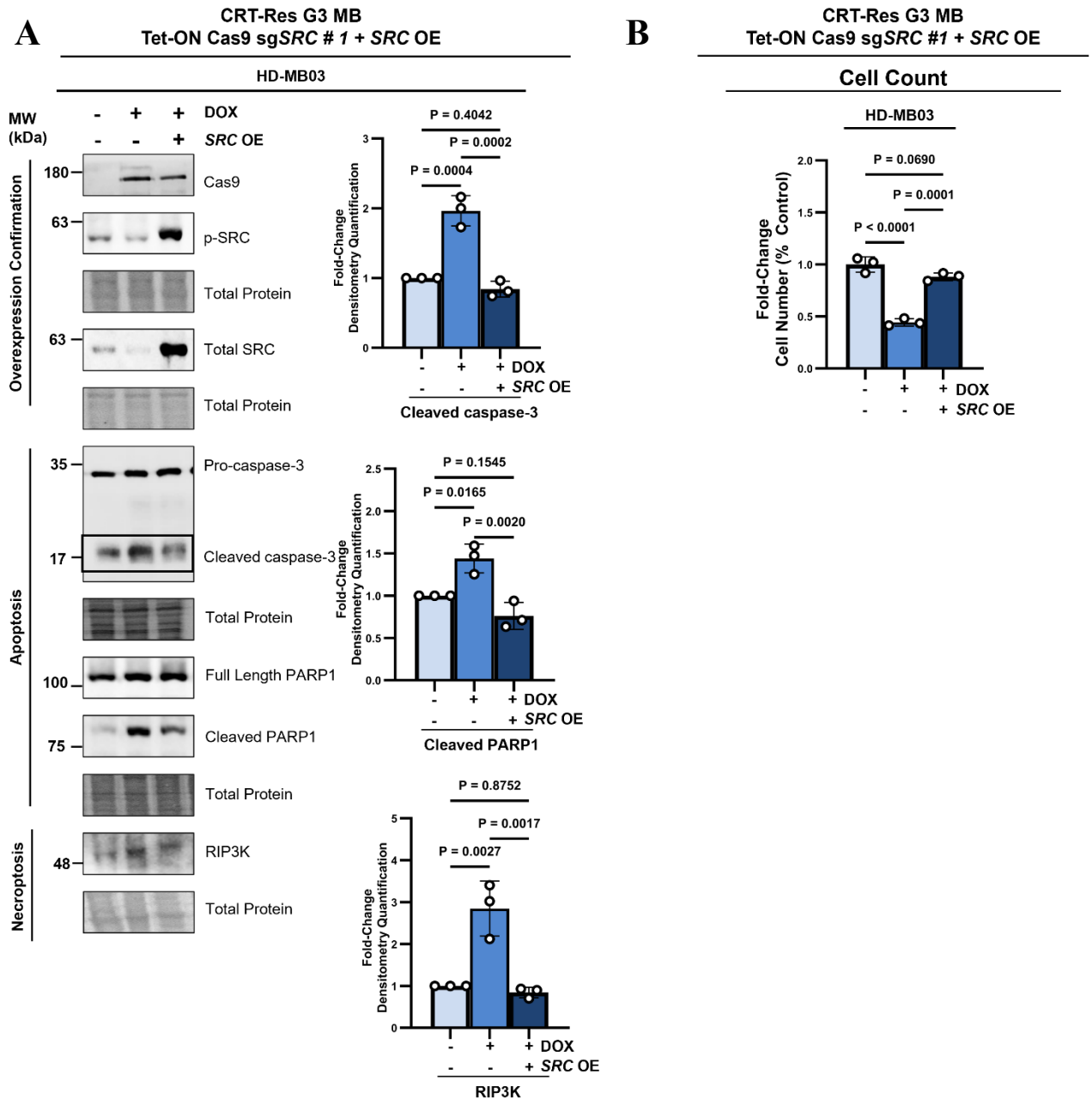

Figure 27: SRC restoration reverses programmed cell death in CRT-Resistant G3 MB cells.
(A) Immunoblot of Cas9, p-SRC (Y419), total SRC, pro-caspase-3, cleaved caspase-3, full length PARP1, cleaved PARP1, and RIP3K in CRT-Res HD-MB03 cells expressing Tet-ON Cas9 sg*SRC* #1 treated with DOX and Transfected with *SRC* OE. Graphs represent densitometry quantification measurement of cleaved caspase-3, cleaved PARP1, and RIP3K normalized to the total protein levels from $n = 3$ experimental replicates, presented as mean ± s.e.m; unpaired two-tailed t-test. **(B)** Cell count analysis of CRT-Res HD-MB03 and SU_MB002 cells expressing Tet-ON Cas9 sg*SRC* #1 treated with DOX and transfected with *SRC* OE. Graphs represent fold change against CRT treatment alone from $n = 3$ experimental, presented as mean ± s.e.m; two-way ANOVA with Tukey's test.

3.6. Pharmacological blockade of SRC promotes differentiation and cell death in therapy-resistant G3 MB cells

Our findings establish SRC as a central orchestrator of therapy resistance and recurrence in G3 MB. By dismantling the tumor's core maintenance programs, SRC inhibition does more than just stop growth; it forces a shift from a primitive, aggressive state toward differentiation and programmed cell death. This dual action, targeting both survival and stemness in resistant cells, offers a compelling translational pathway, especially through the repurposing of existing clinical agents.

To move these insights toward a clinical reality, we systematically evaluated three SRC inhibitors with unique pharmacological profiles. We prioritized bosutinib and saracatinib for their critical ability to penetrate the blood-brain barrier (BBB), a prerequisite for effective neuro-oncology treatment. While bosutinib is already FDA-approved for leukemia and saracatinib is in advanced clinical trials for other fibrotic diseases (NCT04598919)[115, 116], their transition to pediatric brain tumor therapy represents a promising new frontier. Complementing these, we also employed SU6656[117], a potent and highly selective compound, to precisely isolate and validate the mechanistic role of SRC signaling, free from the confounding effects of broader kinase inhibition.

A dose-response assessment of the CRT-Res G3 MB lines, HD-MB03 and SU_MB002, demonstrated significant sensitivity to all three SRC inhibitors **(Figure 28)**. From these data, we derived the optimal inhibitory concentrations for use in subsequent functional assays. Immunoblotting validated that these concentrations effectively suppressed SRC phosphorylation in CRT-Res HD-MB03 cells **(Figure 29)**.

We next assessed the efficacy of these optimized doses in combination with CRT using both G3 MB lines and non-malignant controls (human astrocytes and NSCs). The SRC inhibitors

significantly reduced the survival of CRT-Res cells without inducing significant toxicity in the non-malignant models **(Figure 30)**. This selective sensitivity underscores a potential therapeutic window for SRC inhibition in the treatment of recurrent G3 MB.

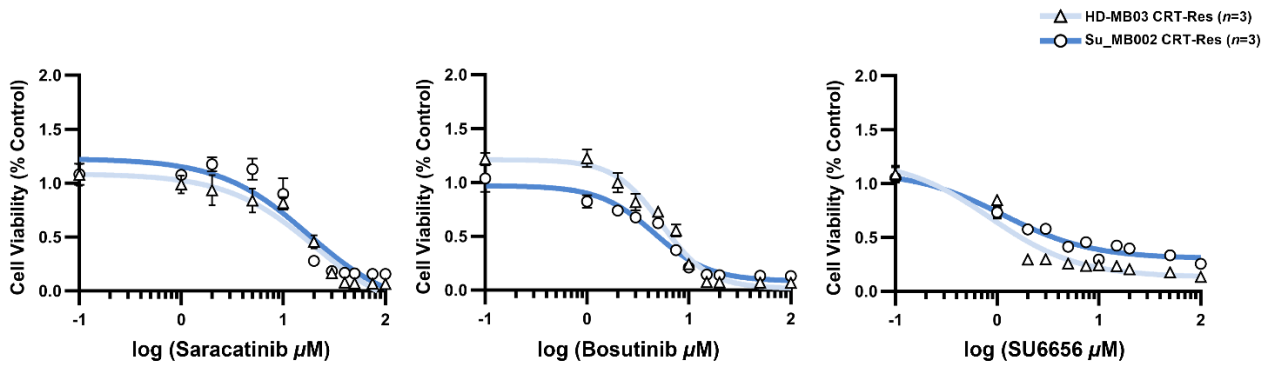

Figure 28: Dose–response curves of CRT-Resistant G3 MB cells treated with SRC inhibitors.
Dose-response curves of cell viability measured using PrestoBlue in CRT-Res HD-MB03 and SU_MB002 cells treated with increasing concentrations of saracatinib, bosutinib, or SU6656. Values plotted as mean % of vehicle-treated CRT-Res controls ± s.e.m.

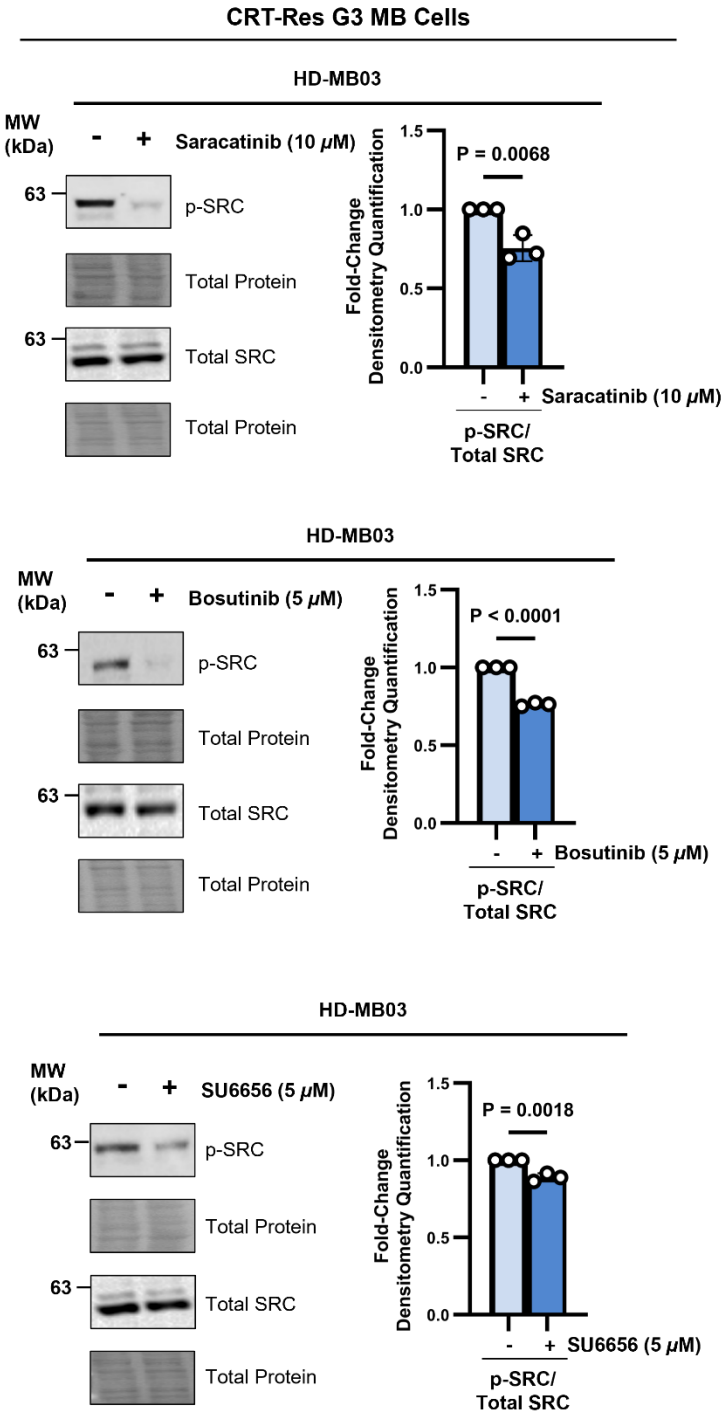

Figure 29: SRC inhibitors suppress p-SRC in CRT-Resistant G3 MB cells.
Immunoblot of p-SRC (Y419) and total SRC in CRT-Res HD-MB03 cells treated with SRC inhibitors: saracatinib (top panel), bosutinib (middle panel), and SU6656 (bottom panel). Graphs represent densitometry quantification measurement of p-SRC/total SRC normalized to the total protein stain from $n = 3$ experiments, presented as mean ± s.e.m.; unpaired two-tailed t-tests.

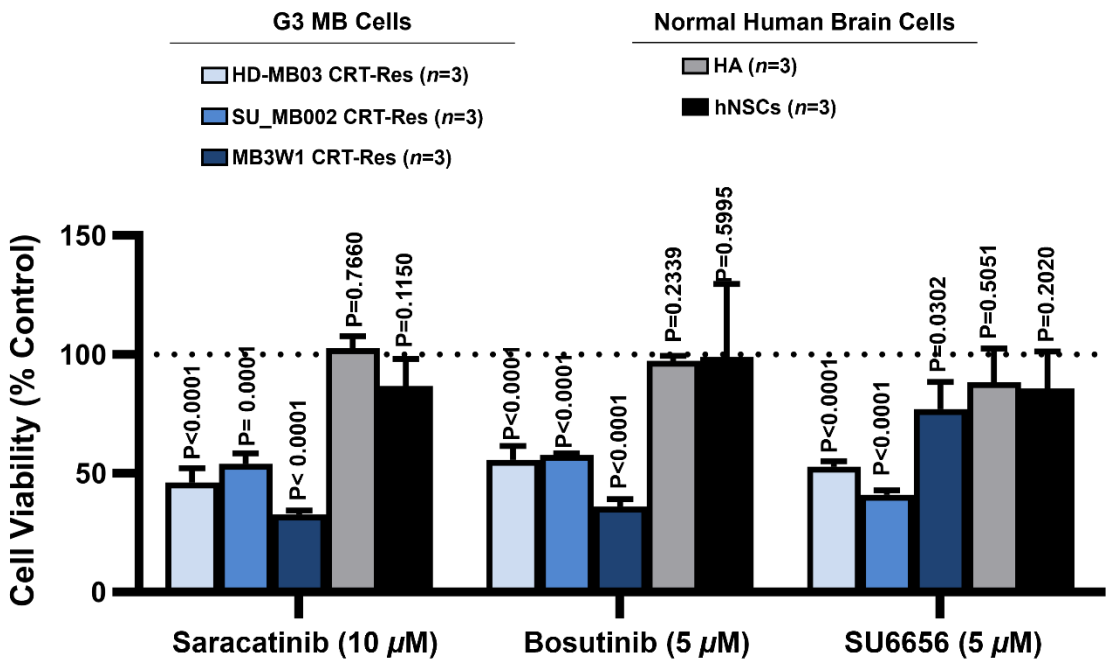

Figure 30: Selective cytotoxicity of SRC inhibitors in CRT-Resistant cells, sparing Human Astrocytes and NSCs Cell viability measured using PrestoBlue in CRT-Res G3 MB cells (HD-MB03, SU_MB002, and MB3W1) and normal human brain cells (human astrocytes and human NSCs) treated with saracatinib (10 μM), bosutinib (5 μM), or SU6656 (5 μM). Fluorescent PrestoBlue signal calculated as % of vehicle-treated controls from $n = 3$ experimental replicates plotted as mean ± s.e.m; using unpaired two-tailed t-tests.

Consistent with results from *SRC* KO models, pharmacological inhibition of SRC using Saracatinib in CRT-Res HD-MB03 cells leads to both apoptotic and necroptotic cell death. This is evidenced by the cleavage of caspase-3 and PARP-1, along with the accumulation of RIP3K, as shown by western blot, indicating the activation of both apoptosis and necroptosis **(Figure 31)**. In addition to cell death, SRC inhibition also alters the molecular pathways that regulate stemness and differentiation. Treating CRT-Res cells with Saracatinib downregulated SOX2 and NOTCH1, which are critical regulators of stemness **(Figure 32)**. Meanwhile, there was an observed increase in the expression of TUBB3, a neuronal differentiation marker **(Figure 32)**.

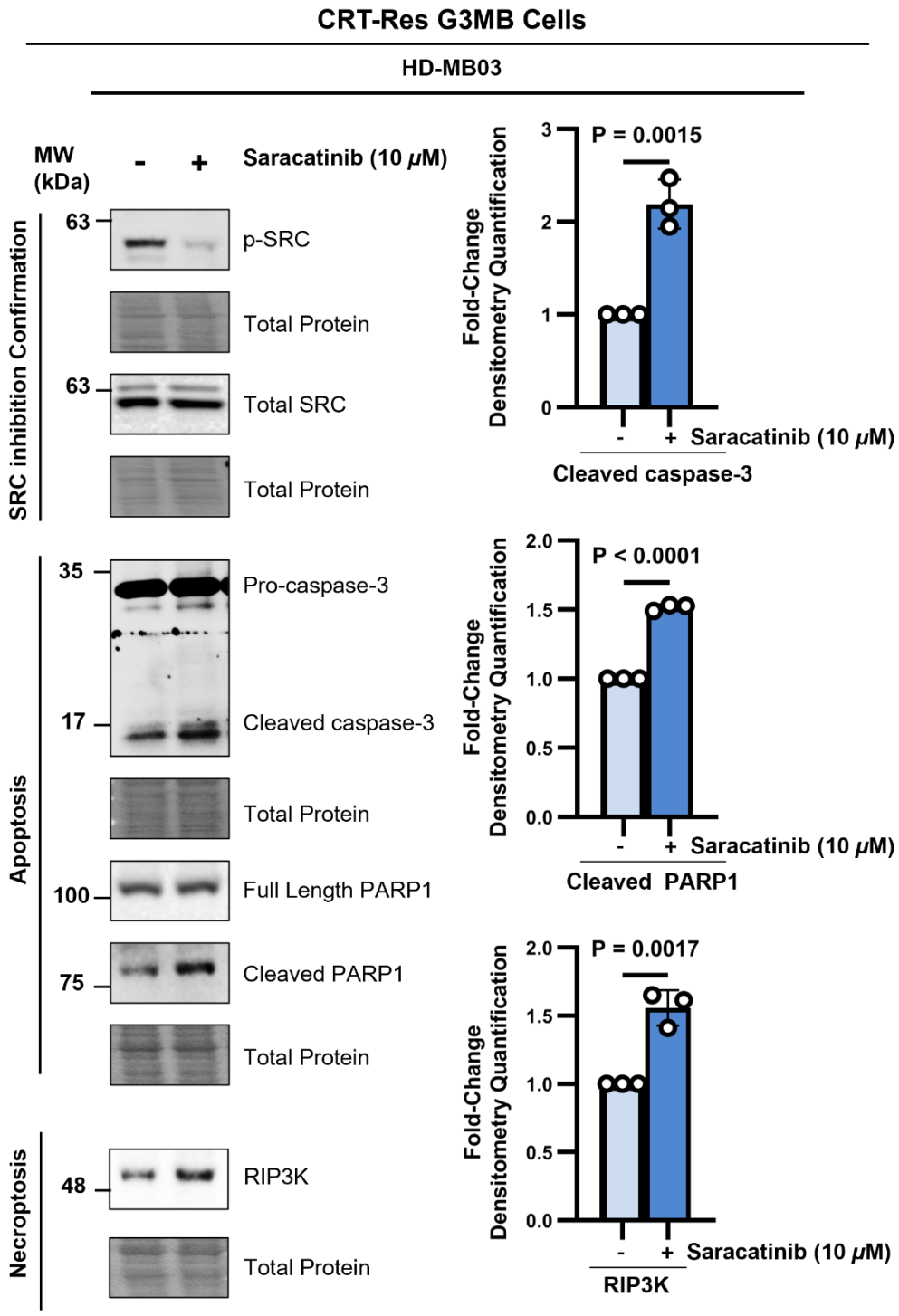

Figure 31: Saracatinib induces apoptosis and necroptosis in CRT-Resistant G3 MB cells
Immunoblot of p-SRC (Y419), total SRC, pro-caspase-3, cleaved caspase-3, full length PARP1, cleaved PARP1, and RIP3K in CRT-Res HD-MB03 and SU_MB002 cells treated with saracatinib (10 μM). Graphs represent densitometry quantification measurement normalized of cleaved caspase-3, cleaved PARP1, and RIP3K to the total protein stain levels from $n = 3$ experimental replicates, presented as mean ± s.e.m; unpaired two-tailed t-test.

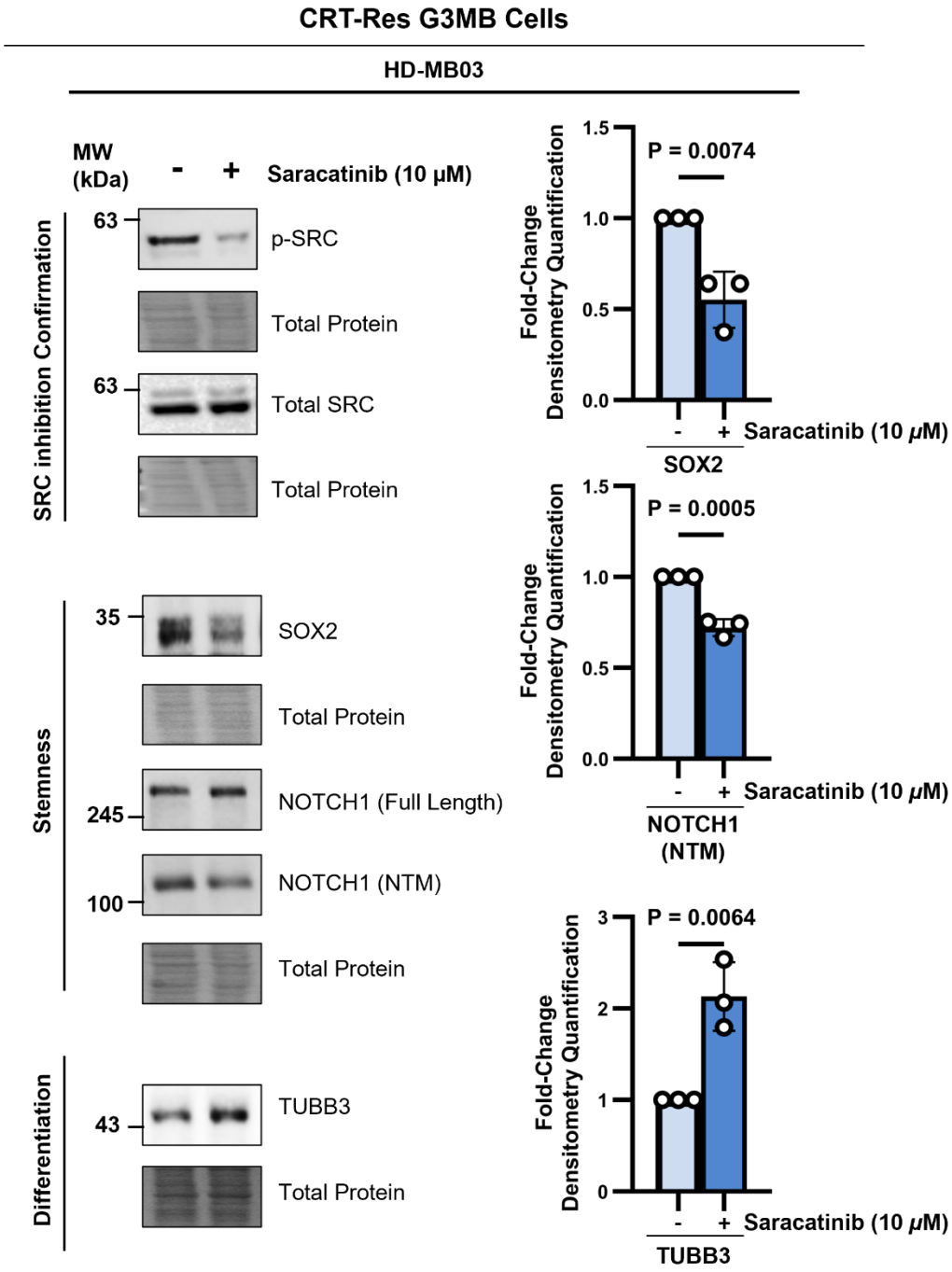

Figure 32: Saracatinib reduces stemness and restores differentiation in CRT-Resistant G3 MB cells
Protein blots of p-SRC (Y419), total SRC, SOX2, NOTCH1 (full length and NTM), and TUBB3 in CRT-Res HD-MB03 cells treated with saracatinib (10 µM). Graphs represent densitometry quantification measurement of SOX2, NOTCH1 (NTM), and TUBB3 normalized to the total protein stain levels from n = 3 experimental replicates, presented as mean ± s.e.m; unpaired two-tailed t-test.

Moreover, the SRC inhibitor Saracatinib diminished the capacity of CRT-Res HD-MB03 cells to form both primary and secondary tumorspheres, indicating a defect in their self-renewal

potential **(Figure 33A)**. Most importantly, the stem-like properties of human NSCs remained unaffected by all three SRC inhibitor treatments, suggesting that SRC dependence for self-renewal is a vulnerability specific to G3 MB cells **(Figure 33B)**. This unique SRC-related vulnerability has significant clinical implications, as it indicates a lower risk of developmental side effects when targeting pediatric tumors.

Given the decisive impact of metastasis on patient prognosis[48, 58], we investigated whether the SRC inhibitor impairs the migratory behavior of therapy-resistant cells. CRT-Res HD-MB03 cells expressing GFP were subjected to transwell migration assays. Fluorescence microscopy revealed that all three inhibitors significantly abrogated the migratory capacity of these cells **(Figure 34)**, indicating that SRC signaling is essential for maintaining their invasive potential. Consequently, pharmacological targeting of SRC represents a multi-modal therapeutic strategy as it not only compromises tumor survival and stemness but also suppresses the migratory mechanisms that drive distant metastasis, a primary driver of poor outcomes in recurrent G3 MB.

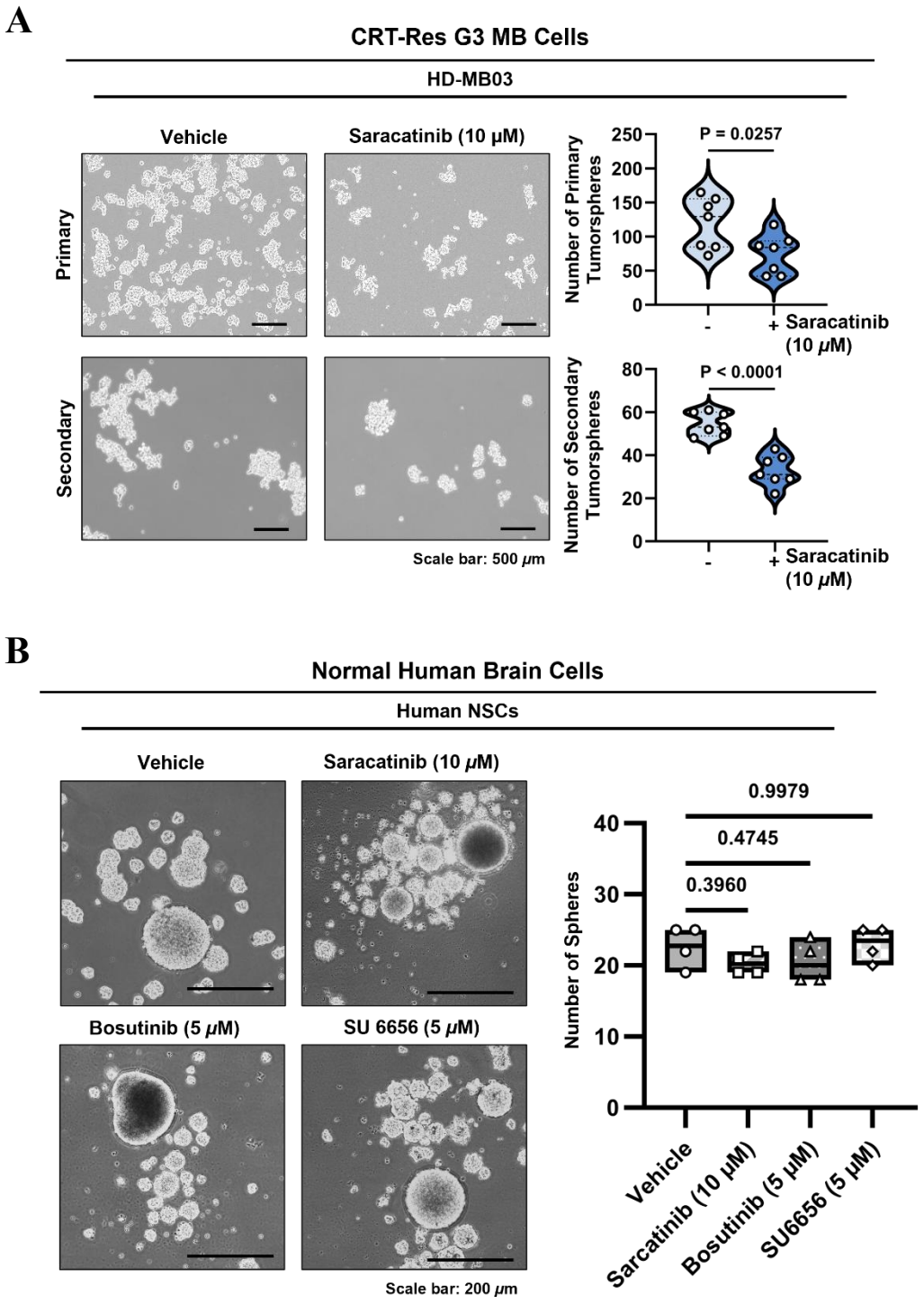

Figure 33: SRC inhibition impairs self-renewal in CRT-Resistant G3 MB cells but not in Human NSCs
(A) Primary and secondary tumorsphere formation assay of CRT-Res HD-MB03 cells treated with Saracatinib (10 μM). Violin plot represents quantification of total sphere number from n =7 replicates, with dashed lines at the mean and quartiles; unpaired two-tailed t-test. **(B)** Sphere formation analysis of human NSCs treated with Saracatinib (10 μM), Bosutinib (5 μM), or SU6656 (5 μM). Box plot graphs represent quantification of the total sphere number from n = 4 replicates; one-way ANOVA with Dunnett's test.

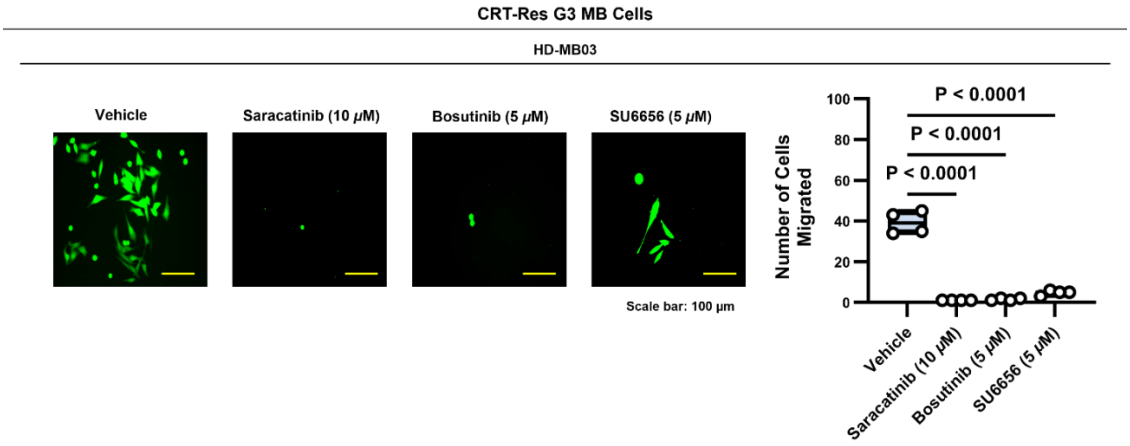

Figure 34: SRC inhibitors impair the migration of CRT-Resistant G3 MB cells.
Representative images and quantification of migration assays in HD-MB03 cells treated with Saracatinib (10 μM), Bosutinib (5 μM), or SU6656 (5 μM). Box plot graphs represent quantification from n = 4 experimental replicates, with solid line at mean; two-way ANOVA with Tukey's test.

Collectively, these findings establish a compelling rationale for SRC inhibition as a transformative therapeutic strategy for therapy-resistant G3 MB. By acting as a central node in the tumor's signaling network, SRC allows these cells to evade death and maintain their primitive state. Our data demonstrate that blocking SRC effectively collapses this network, simultaneously triggering a dual-mode of cell death, apoptosis and necroptosis, while forcing stem-like cells toward neuronal differentiation and halting their invasive spread.

Beyond the bench, the clinical potential of this approach is particularly promising. Because several of these inhibitors are already navigating clinical development or are FDA-approved for other diseases, they offer a feasible pathway for rapid translation into pediatric neuro-oncology. Ultimately, this strategy moves us closer to a treatment model that not only improves survival for children with recurrent disease but does so with a precision that minimizes the devastating neurodevelopmental toxicities often associated with traditional, more aggressive therapies.

3.6. *In vivo* suppression of p-SRC prolongs survival in recurrent G3 MB

To evaluate the therapeutic potential of SRC inhibition in a setting that closely mimics the clinical reality of patient care, we utilized a PDOX model of HD-MB03. This allowed us to test a novel combination regimen: our standard CRT protocol integrated with the BBB-permeable SRC inhibitor, Saracatinib.

These orthotopic tumors were established by intracerebral injection of HD-MB03 cells. Initially, all animals received a primary course of RT to simulate standard clinical care for newly diagnosed diseases. After this initial RT treatment, the mice were randomized into groups to receive either 40mg/kg Saracatinib or methylcellulose suspension placebo control every other day via oral gavage. **(Figure 6).**

MRI imaging revealed a striking difference in therapeutic response. While animals receiving only conventional CRT showed aggressive tumor recurrence, mirroring the clinical challenges seen in G3 MB patients, the addition of saracatinib significantly attenuated tumor burden **(Figure 35)**, suggesting that SRC inhibition effectively sensitizes resistant cells to standard multimodal therapy.

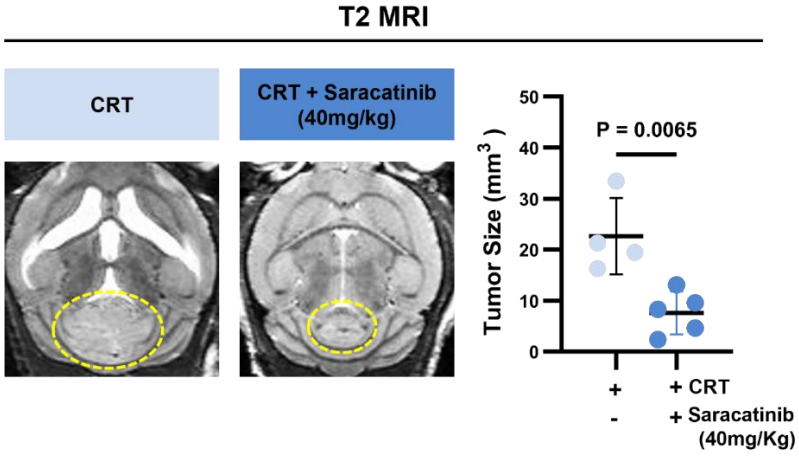

Figure 35: SRC inhibitor in combination with CRT reduces tumor burden in the G3 MB animal model. Representative T2-weighted MRI images acquired 22 days post-transplant, with tumor margins outlined. Quantification of tumor volumes across treatment groups ($n = 4$ for CRT alone, $n = 5$ for CRT +Saracatinib); unpaired two-tailed t-test.

Survival analysis further demonstrated the therapeutic advantage of targeting SRC. In this highly aggressive *in vivo* G3 MB model, animals receiving CRT alone showed only a marginal improvement in median survival (5.5 days) compared to placebo controls **(Figure 36)**. In striking contrast, the combination of CRT and saracatinib significantly extended median survival by approximately 8 days relative to the placebo control group.

This CRT + saracatinib combination regimen resulted in an overall survival rate of 47% compared with placebo controls, while representing about 15% improvement over CRT alone. Statistical analysis revealed a hazard ratio of 3.070, further validating the efficacy of the dual-treatment approach. Collectively, these data indicate that pharmacological inhibition of SRC, when integrated with standard-of-care radiotherapy, provides a superior survival benefit compared to conventional therapy alone

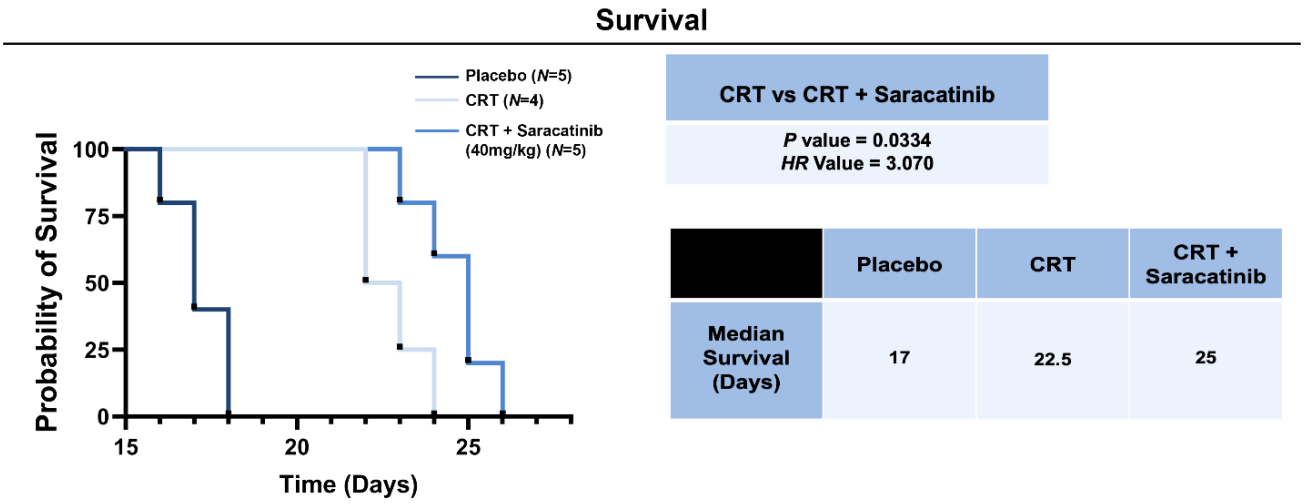

Figure 36: Saracatinib prolongs survival in combination with CRT in G3 MB PDOX Mode.
Kaplan-Meier survival curves of mice treated with CRT alone or CRT + saracatinib. *P* and *HR* values reflect the statistical comparison between the CRT-alone and CRT + saracatinib groups, calculated using the logrank method. The table shows the median survival in days for the Placebo, CRT, and CRT + saracatinib groups.

Recurrent tumors from both the CRT-only and CRT + saracatinib cohorts were surgically excised and paraffin-embedded for histological evaluation. A mechanistic assessment of these tissues confirmed that the systemic administration of saracatinib successfully reached the tumor site and inhibited its target. IF analysis revealed a marked reduction in p-SRC levels in the combination treatment group, validating the *in vivo* pharmacological blockade of SRC signaling **(Figure 37A).** To understand the biological drivers of the observed survival benefit, we evaluated markers of programmed cell death. The combination of saracatinib and CRT triggered a robust induction of both apoptotic and necroptotic pathways, as evidenced by significantly increased levels of cleaved Caspase-3 and RIPK3 **(Figure 37B)**.

Beyond promoting cell death, SRC inhibition actively redirected the fate of the surviving tumor population. IF profiling demonstrated a significant loss of the stemness marker SOX2, coupled with a compensatory increase in the neuronal differentiation marker TUBB3 **(Figure 37C)**. These findings suggest that the clinical efficacy of this combination therapy stems from a dual-pronged mechanism: it directly eliminates resistant cells through multiple death pathways while simultaneously forcing the remaining population toward a more differentiated, less aggressive state. This effectively exhausts the tumor's self-renewal potential and halts disease progression.

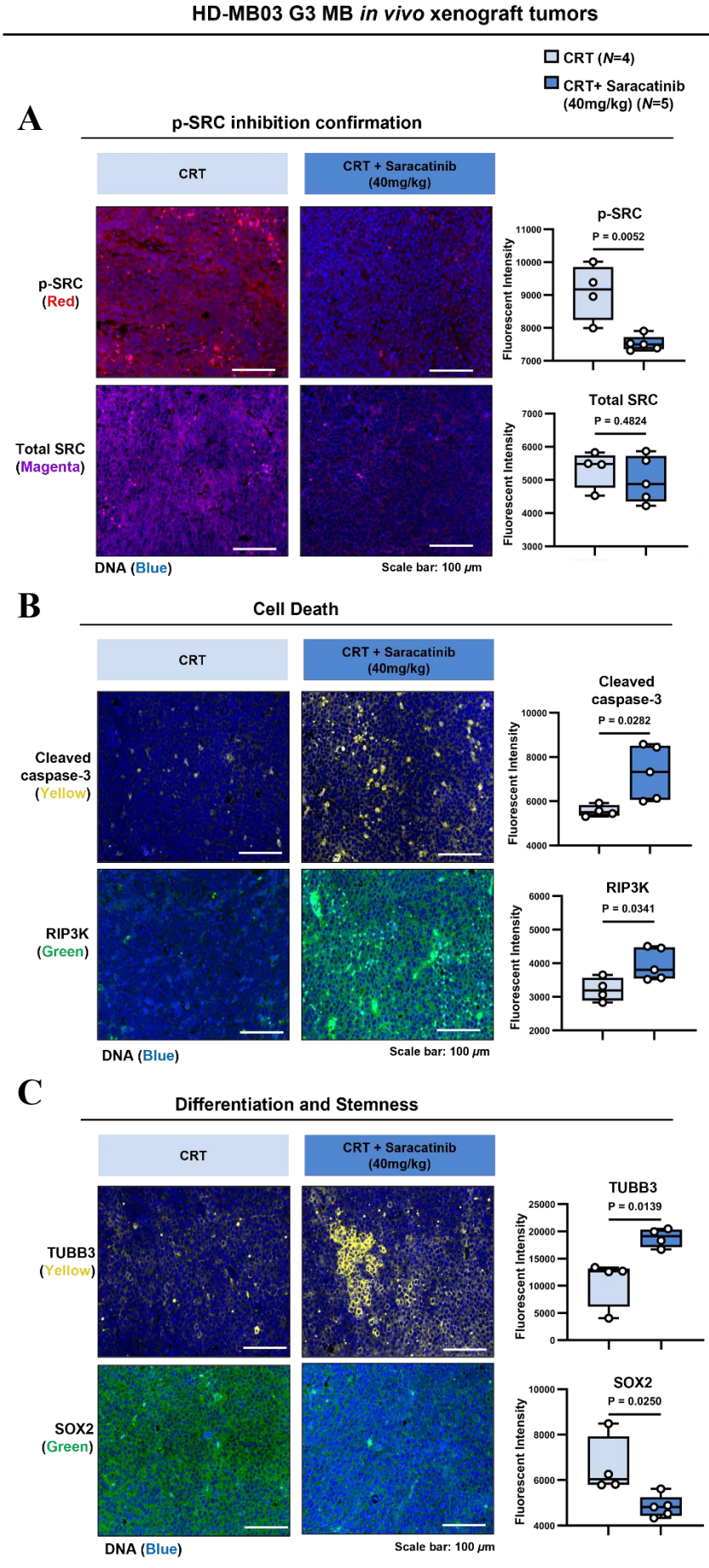
HD-MB03 G3 MB *in vivo* xenograft tumors
CRT (N=4)
CRT+ Saracatinib (40mg/kg) (N=5)
A
p-SRC inhibition confirmation
CRT
CRT + Saracatinib (40mg/kg)
p-SRC (Red)
Total SRC (Magenta)
DNA (Blue)
Scale bar: 100 μm
p-SRC
P = 0.0052
Total SRC
P = 0.4824
Fluorescent Intensity
B
Cell Death
Cleaved caspase-3 (Yellow)
RIP3K (Green)
Cleaved caspase-3
P = 0.0282
RIP3K
P = 0.0341
C
Differentiation and Stemness
TUBB3 (Yellow)
SOX2 (Green)
TUBB3
P = 0.0139
SOX2
P = 0.0250

Figure 37: Saracatinib enhances cell death, restores differentiation while suppressing stemness in G3 MB PDOX Mode.
A-C IF images of xenograft tumors from CRT-treated and CRT + saracatinib-treated recurrent tumors labeled with **(A)** p-SRC (red), total SRC (magenta), **(B)** cleaved caspase-3 (yellow), RIP3K (green), **(C)** TUBB3 (yellow), SOX2 (green), and DAPI (blue). Graphs show quantification of fluorescence intensity from $n = 4$ (CRT alone) and $n = 5$ (CRT + saracatinib) animals per group, with solid lines at the mean; unpaired two-tailed t-test.

Lastly, to ensure that the therapeutic efficacy of our combination regimen did not come at the cost of healthy brain tissue, we rigorously evaluated potential neurotoxicity. We used IBA1 IF as a sensitive marker of microglial activation and neuronal inflammation and performed Bielschowsky silver staining to assess the structural integrity and morphological health of neighboring neurons.

Our IBA1 IF analysis revealed that while CRT alone was associated with a mild decrease in active microglia compared to Placebo, the addition of saracatinib did not further exacerbate this inflammatory profile **(Figure 38)**. Moreover, Silver staining revealed no significant alterations in optical density or neuronal fiber morphology across treatment groups. The delicate architecture of axons and dendrites in both the CRT and combinatorial cohorts remained indistinguishable from that of placebo **(Figure 39)**.

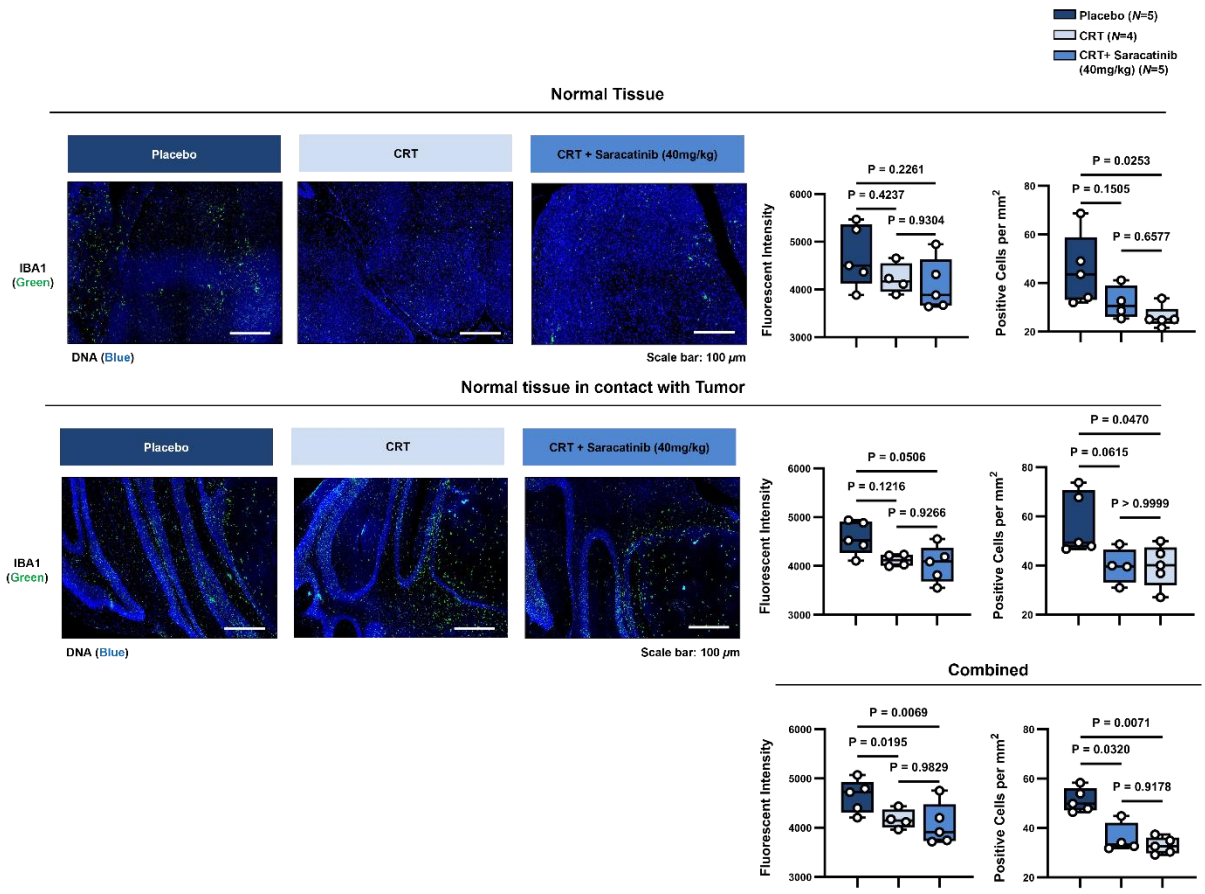

Figure 38: Saracatinib in combination with CRT preserves microglial activation.
Representative IF images of IBA1 (Green) and DAPI-ed DNA (blue) in HD-MB03 therapy-naïve control tumors, CRT-treated, and CRT + saracatinib-treated recurrent tumors. Box-and-whisker plots represent quantification of fluorescence intensity from $n = 5$ (therapy-naïve), $n = 4$ (CRT alone), and $n = 5$ (CRT + saracatinib) animals per group, with solid lines at the mean; mean ± s.e.m. two-way ANOVA with Tukey's test

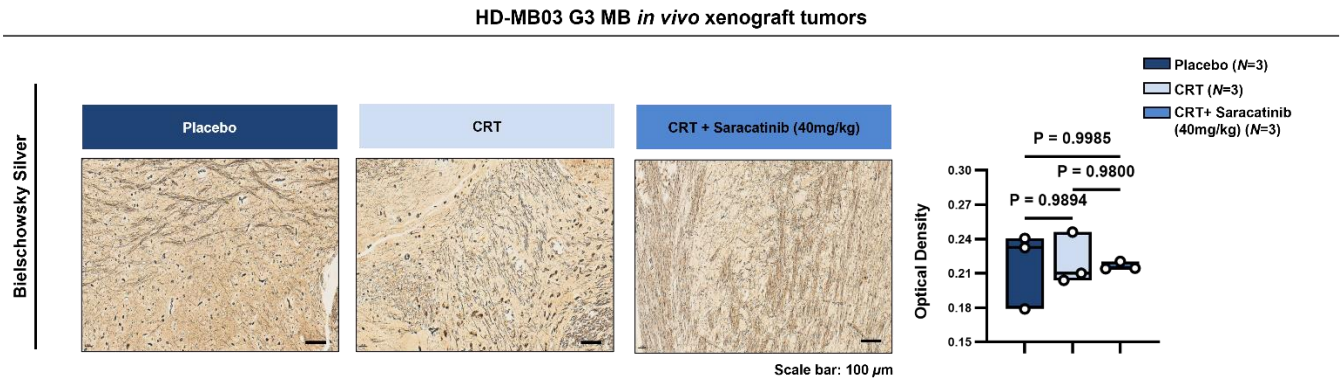

Figure 39: Assessment of neuronal integrity via silver staining.
Representative Bielschowsky Silver images in HD-MB03 therapy-naïve control tumors, CRT-treated, and CRT + saracatinib-treated recurrent tumors. Graph represents quantification of optical density from $n = 3$ tumor samples per group, with a solid line at the mean, mean ± s.e.m., two-way ANOVA with Tukey's test.

Collectively, our findings establish p-SRC upregulation as a pivotal driver of G3 MB recurrence, acting as a central signaling hub that sustains stemness and aids therapy resistance. We demonstrate that both the genetic ablation of *SRC* and its pharmacological blockade with saracatinib, when integrated with standard-of-care CRT, effectively dismantle this oncogenic survival network. This combinatorial strategy does more than merely arrest tumor growth; it fundamentally reshapes the cellular landscape. By forcing primitive, undifferentiated cells toward a mature neuronal lineage while simultaneously triggering a dual mode of programmed cell death via both apoptotic and necroptotic pathways, this approach strikes at the core of tumor persistence.

By successfully extending survival in aggressive orthotopic models without inducing neurotoxicity, these results underscore SRC as a high-priority, actionable target. Ultimately, this research provides a robust scientific and clinical rationale for repurposing SRC inhibitors as a targeted, neuro-sparing treatment strategy, offering a much-needed new frontier in the effort to improve outcomes for children facing recurrent brain tumors **(Figure 40)**.

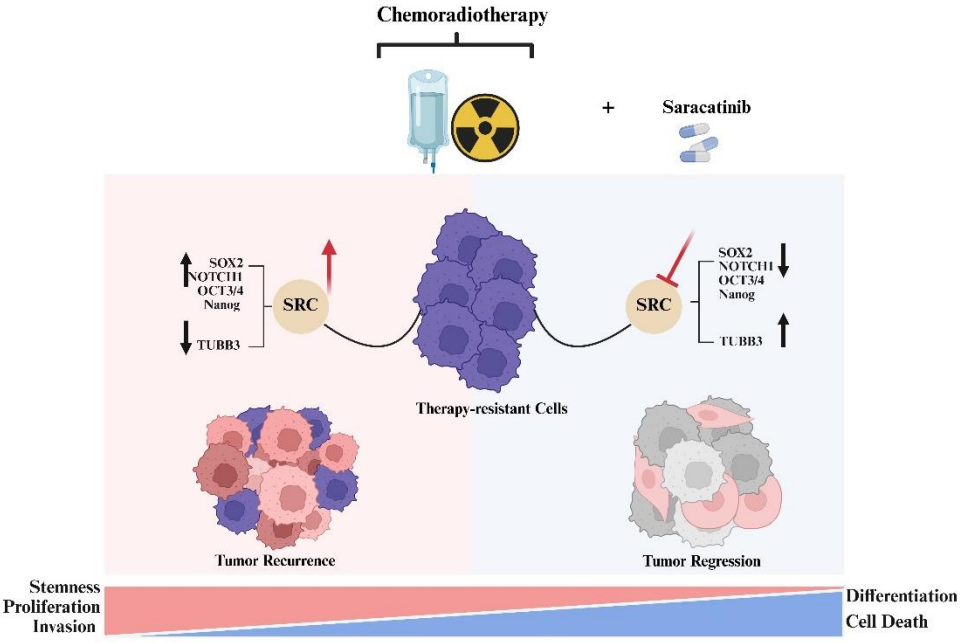

Figure 40: Summary diagram illustrating the effect of CRT with or without saracatinib.
Generated using Biorender.

CHAPTER 4. DISCUSSION

4.1. SRC Landmark that Redefined Oncology

The discovery of the nRTK SRC marks the beginning of modern oncology, transforming our understanding of cancer from an external invasion to a biological betrayal from within. The journey began in the early 1900s, when Peyton Rous observed that a cell-free filtrate from a chicken tumor could induce new sarcomas in healthy birds[118]. This virus, known as the Rous Sarcoma Virus, remained a biological mystery for decades until 1976, when J. Michael Bishop and Harold Varmus used molecular probes to isolate the specific genetic material responsible for this transformation. To their surprise, they discovered that the gene responsible for causing cancer in the virus, *v-SRC*, had a nearly identical counterpart in the DNA of normal, healthy animal cells: its cellular version, *c-SRC*, was not a foreign invader but a vital gene involved in normal cell signaling. For demonstrating that viruses can hijack normal cellular genes and turn them into oncogenes, Bishop and Varmus were awarded the 1989 Nobel Prize in Physiology or Medicine. This landmark recognition established the foundational concept of the proto-oncogene[119].

Despite its historical significance, SRC remains a biological enigma because it challenges the conventional mutation-centric model of cancer development. In modern genomics, we often search for driver mutations, such as those in *KRAS* or *TP53*, to explain how malignancies arise. However, SRC is rarely mutated in human clinical samples[120]. This lack of genetic alteration initially obscured its importance, creating a paradox: how can a gene so central to cancer biology remain genetically normal? The answer lies in the structural differences between the viral and cellular forms of SRC. While the viral *v-SRC* is a truncated, constitutively active on-switch due to loss of its inhibitory C-terminal tail, the cellular *c-SRC* is regulated by a complex auto-inhibitory mechanism involving phosphorylation of its Y530 residue. As a result, simply overexpressing wild-type *c-SRC* is often insufficient to drive complete cellular transformation. Rather than acting

as a solitary initiator or commander that dictates tumor onset, SRC functions as a sophisticated force multiplier. It exists within the signaling framework, waiting to be hijacked not through mutation but by the dysregulation of surrounding pathways[120].

This role as a force multiplier is realized through SRC's unique position as a central switchboard just beneath the cell membrane. Rather than relying on internal mutations for activation, SRC is typically recruited by upstream mediators such as RTKs (e.g., EGF or MET), GPCRs, and integrins[64, 65]. When these receptors are activated, SRC undergoes a conformational change that exposes its kinase domain, allowing SRC to link extracellular signals to a wide range of intracellular pathways[81, 82].

SRC does not merely relay signals; it amplifies and diversifies them. By phosphorylating multiple substrates, SRC coordinates mechanisms essential for cell survival, proliferation, and metabolic reprogramming. Importantly, SRC plays a critical role in the epithelial-to-mesenchymal transition (EMT) by regulating FAK and E-cadherin[82, 85, 86]. This regulation confers the motility that enables cancer cells to invade and metastasize.

In this way, SRC acts as a master coordinator of the malignant phenotype, ensuring that once a cell begins its transformation toward cancer, the internal signaling environment is optimized for aggressive growth and adaptation to changing conditions.

4.2. The Landscape of SRC in Solid Malignancies

The theoretical framework of SRC as a signaling hub is well established, but its clinical relevance is especially evident in the diverse landscape of solid tumors, where SFKs are often exploited to support tumor survival. In healthy tissues, SFK activity is tightly regulated[82]; however, malignant cells frequently display chronic hyperactivation and protein overexpression. This molecular change enables SFKs to function as critical processing centers, integrating signals from

cell-surface growth factor receptors, adhesion signals from the extracellular matrix via integrins, and chemical stressors in the increasingly hostile tumor microenvironment.[121] By connecting these external signals to internal growth programs, SFKs effectively convert a chaotic extracellular environment into a coordinated strategy for malignant expansion. The following discussion synthesizes specific evidence of SRC's involvement in several representative solid tumors, highlighting how its molecular interactions create unique clinical challenges and shape our current therapeutic strategies.

4.2.1. *Breast Cancer*

In breast cancer research, SRC has become a critical signaling hub that integrates the PI3K/AKT and MAPK/ERK survival pathways. It is particularly associated with poor prognosis, especially in HER2+ breast cancer and cases of therapy resistance. In triple-negative breast cancer (TNBC), the SRC-AKT-ERK2 axis stabilizes the EMT transcription factors Slug and Snail, enhances TGFβ2 signaling, and promotes chemoresistance and negative outcomes[122].

Pharmacological inhibition of SRC using Dasatinib has been shown to reduce tumor growth and improve responsiveness to epirubicin in preclinical TNBC models. Additionally, the Hippo-pathway transducers YAP1 and TEAD drive transcriptional programs that support cell proliferation and resistance to Trastuzumab in HER2+ breast cancer. This aligns with a cooperative SRC-YAP/TEAD resistance network[123, 124].

A specific nuclear complex driven by SRC, involving YAP1, TFAP2A, and TEAD, which directly upregulates HER2 and EGFR, has not been fully characterized. Metabolic research has identified a CDCP1-mitochondrial SRC axis in TNBC. In this axis, the cell-surface protein CDCP1 recruits and activates SRC in the mitochondria, leading to increased Complex I activity and oxidative phosphorylation (OXPHOS)[125]. This enhancement boosts respiratory capacity,

migration, and metastasis. Disrupting this axis lowers OXPHOS and metastatic potential, whereas restoring Complex I can rescue these traits[126, 127].

Independent studies have found that OXPHOS-high and chemotherapy-resistant TNBC relies on mitochondrial respiration and can be re-sensitized by OXPHOS inhibitors[128]. This highlights metabolic plasticity as a crucial factor in SRC-linked survival, even though a precise FAO-AMPK-SRC axis has not yet been formally defined in breast cancer. In addition to its kinase activity, SRC also acts as a scaffold. Repurposing studies have shown that the antivirals Ledipasvir and Daclatasvir destabilize the SRC-EPHA2 complex, downregulate the SRC-EPHA2-AKT pathway, and reduce proliferation and invasion in colorectal and TNBC cells[126]. Notably, this occurs without broadly inhibiting SRC's catalytic activity, illustrating how scaffolding can sustain signaling even when kinase activity is only partially inhibited. Therapeutically, Dasatinib and related ATP-competitive SRC inhibitors bind to SRC in its open, active conformation and have demonstrated preclinical chemo-sensitizing effects in TNBC. However, they may not completely eliminate non-catalytic SRC functions[123].

Next-generation agents, such as NXP900, are conformation-selective SRC family inhibitors that lock SRC in a closed, inactive state. This inhibits both catalytic and kinase-independent functions. NXP900 has shown potent anti-tumor activity in squamous cell carcinomas and exhibits high selectivity for SRC family kinases. Early preclinical evidence also suggests its effectiveness in SRC-dependent and endocrine-resistant tumors, including ER+ breast cancer. Nevertheless, detailed datasets for luminal breast cancer are still emerging[129].

Additionally, researchers are exploring the use of repurposed antivirals that target SRC-EPHA2 scaffolding, metabolic interventions that take advantage of OXPHOS dependence, and rational multi-target strategies. These include the conceptual dual inhibition of SRC and BRD4,

along with pathway-modulating natural products like Arctigenin and EGCG[130, 131]. These high-precision combinations aim to block EMT, survival signaling, and metabolic adaptation, positioning SRC as a master integrator of resistance across hormone receptor-positive, HER2+, and TNBC subtypes[132].

4.2.2. *Brain Cancer*

In Glioblastoma (GBM), SRC is often activated and plays a crucial role as an integrator of oncogenic signaling and metabolic reprogramming, promoting tumor growth in the nutrient-limited environment of the brain. Recent studies have shown that SRC directly regulates lipid and acetate metabolism by phosphorylating ACSS2 at the tyrosine residues Y530 and Y562, which stimulates the production of acetate-derived acetyl-CoA. At the same time, SRC phosphorylates ACLY at Y682, inhibiting its enzymatic activity and redirecting citrate toward *IDH1*-mediated NADPH production[133]. This coordinated metabolic remodeling meets the dual requirements of GBM cells for acetyl-CoA and NADPH, both of which are essential for de novo fatty acid synthesis and maintaining redox balance. Importantly, the SRC-unresponsive double mutant of ACSS2 and ACLY significantly reduces fatty acid synthesis and impedes GBM progression *in vivo*, highlighting SRC's role as a driver of metabolic adaptation in the brain[133].

SRC is a crucial effector downstream of EGFR gene alterations, particularly the oncogenic variant *EGFRvIII*, which is common and clinically aggressive in GBM. *EGFRvIII* predominantly signals through STAT5, and experimental studies indicate that the invasion and survival induced by *EGFRvIII* rely on an *EGFRvIII*-SRC-STAT5 pathway[134]. This pathway upregulates the *Fn14* receptor. Inhibition of SRC using the SRC family kinase inhibitor saracatinib reduces STAT5 activation, decreases *Fn14* expression, and impairs the migration and survival of GBM cells. These findings connect receptor mutations like *EGFRvIII* to nuclear transcriptional programs via SRC-

STAT5 signaling, suggesting that SRC promotes aggressive and invasive behavior and influences chemotherapy sensitivity in *EGFRvIII*-positive GBM[135]. Additionally, preclinical studies of anti-VEGF therapy have shown that Bevacizumab can lead to a more invasive growth pattern at the tumor's edge. SRC kinase activity is upregulated in this invasive front. In model systems, Dasatinib effectively blocks the invasion induced by Bevacizumab, underscoring the role of SRC in adaptive resistance to anti-angiogenic therapy through invasion[136].

Recent studies have identified SRC as a key regulator of redox defense and resistance to ferroptosis in GBM through its interaction with the transcription factor NRF2. When SRC signaling is hyperactive, it stabilizes and activates NRF2, leading to increased expression of NRF2 target genes and suppression of ferroptosis induced by ionizing radiation[137]. In contrast, the use of pharmacological SRC inhibitors, such as Dasatinib, decreases NRF2 activity and sensitizes GBM cells and patient-derived neurospheres to cell death caused by radiation-induced ferroptosis. These findings highlight SRC as a significant factor in radio resistance. However, the assertion that SRC promotes the repair of DNA double-strand breaks (DSBs) via the EGFR/PI3K/AKT pathway in GBM is not fully substantiated. Current data primarily emphasize SRC's role in ferroptosis and antioxidant defenses rather than a clearly defined SRC-centered DSB repair pathway[138]. Nevertheless, combining SRC inhibition with radiation enhances radiation-induced damage and increases the lethality of GBM cells in preclinical models, suggesting that targeting SRC could be a promising strategy for radio-sensitization.

The relationship between SRC and chemotherapy is becoming clearer. In GBM models that express *EGFRvIII, EGFRvIII* primarily signals through STAT5. Inhibition of either STAT5 or SRC can make tumor cells more sensitive to temozolomide and promote apoptosis. This suggests that the *EGFRvIII*-SRC-STAT5 pathway contributes to the chemo-resistant characteristics of these

tumors. A recent study demonstrated that *EGFRvIII* expression leads to greater reliance on SRC-STAT5 signaling, which in turn results in increased sensitivity to saracatinib[135, 139]. By contrast, GBM models with wild-type EGFR show less responsiveness, highlighting that the effectiveness of SRC inhibition is highly dependent on the context and the status of *EGFRvIII*[135]. These findings support the idea that SRC/SFK inhibitors like saracatinib can enhance the sensitivity of *EGFRvIII+* tumors to temozolomide. However, there is currently no definitive clinical evidence that combined treatments may have adverse outcomes in EGFR-wild-type GBM. This potential concern should be viewed as a theoretical issue arising from differing pathway dependencies rather than as a confirmed clinical negative impact.

Despite robust preclinical biology, the broad clinical success of SRC inhibitors in unselected GBM populations has been limited. In the phase II NCCTG N0877 (Alliance) trial, adding dasatinib to standard chemoradiation with temozolomide did not improve outcomes in newly diagnosed GBM, and the phase II NCCTG N0872 trial combining bevacizumab with dasatinib in recurrent GBM similarly failed to show a consistent survival benefit[136]. These results, together with molecular data showing that only certain GBM subsets (for example, those with *EGFRvIII* or strong SRC-STAT5 or SRC-NRF2 dependence) are highly SRC-addicted, have led to a consensus that SRC-targeted therapy will likely require careful biomarker-based patient selection rather than a one-size-fits-all approach[135]. Other SRC family kinase inhibitors, including bosutinib and KX2-391 (also known as Tirbanibulin), continue to be evaluated in early-phase or exploratory settings[140]. Still, the dominant view is that future success will depend on rational, combination regimens such as pairing SRC inhibition with radiation, ferroptosis inducers, or *EGFRvIII*- and STAT5-directed therapies, in molecularly defined GBM subgroups to prevent metabolic, invasive, and redox-based adaptive resistance.

4.2.3. *Prostate Cancer*

SRC acts as a key signaling hub in the progression of prostate cancer from an androgen-dependent state to castration-resistant disease. In experimental models, SRC and related SRC family kinases directly phosphorylate the androgen receptor (AR) on tyrosine residues, enhancing AR transcriptional activity and enabling ligand-independent or low-androgen signaling that supports tumor growth after androgen deprivation. This creates a functional feedback loop in which upstream growth factor and cytokine pathways activate SRC. At the same time, SRC-driven AR signaling sustains transcriptional programs that favor proliferation, survival, and metastatic spread, thereby undermining conventional hormone therapies[141].

A key structural feature of SRC is its N-terminal myristoylation. In prostate cancer models, either genetic or pharmacological disruption of SRC myristoylation leads to a reduction in SRC autophosphorylation and downstream signaling. This decrease in activity suppresses tumor cell growth and limits the cooperative effect of SRC and the AR on tumor progression[142]. These findings highlight that myristoylation is not just a signal for localization; it is a critical factor in SRC's oncogenic potential. This presents an attractive, structurally specific therapeutic target distinct from conventional ATP-competitive kinase inhibition.

SRC not only directly modulates AR but also integrates signals that shape the invasive and physical characteristics of prostate cancer. By interacting with FAK and downstream components of the MAPK pathway, such as ERK and SRC itself, SRC promotes focal adhesion turnover, cytoskeletal reorganization, and cell migration[143, 144]. These processes collectively enhance local invasion and metastasis. Additionally, SRC plays a role in regulating cell-cycle progression by controlling proteins like p27 and other critical checkpoints[145]. This regulation supports rapid cell proliferation and contributes to resistance against therapy. While SRC’s influence on the

cytoskeleton and mitosis is well established, the specific claim that SRC phosphorylation of TUBB3 is a primary factor in taxane resistance in prostate cancer is more speculative than definitive[146]. Current evidence suggests a broader relationship between SRC activity, cytoskeletal dynamics, and response to taxane therapies, rather than pinpointing a single TUBB3 substrate as the determining factor.

SRC additionally cooperates with canonical survival pathways. In various tumor systems, including prostate cancer, SRC can activate or amplify JAK/STAT signaling, particularly STAT3, driving expression of genes that promote proliferation, inhibit apoptosis, and modulate immune interactions in the tumor microenvironment[147]. SRC-AR signaling is also connected to DNA damage responses: AR can participate in transcription-coupled DNA breakage and rearrangements, and SRC-modulated phosphorylation events influence AR's chromatin behavior, with implications for genomic instability and therapeutic vulnerability[148]. These links have prompted interest in combining SRC-pathway inhibition with DNA-damage-targeted agents such as PARP inhibitors, especially in tumors that harbor pre-existing defects in homologous recombination repair, although this approach is still under active investigation rather than standard of care.

Targeting SRC has been a promising strategy for treating prostate cancer; however, translating the successes seen in preclinical studies into improved survival rates has proven difficult. Multi-kinase inhibitors targeting SRC, such as dasatinib and saracatinib, have shown significant efficacy *in vitro* and in animal models. These inhibitors reduce AR tyrosine phosphorylation, decrease AR-driven transcription, inhibit cell proliferation and invasion, and can delay or reduce the onset of castration-resistant growth[149].

Despite this potential, large-scale trials involving unselected populations with metastatic castration-resistant prostate cancer (CRPC) have not demonstrated any meaningful improvements in overall survival when these agents are used alone or in simple combinations. This lack of success appears to be related to factors like pathway redundancy, poor patient selection, and dose-limiting toxicity.

Consequently, the focus in this field is shifting away from using SRC inhibition as a monotherapy. Instead, researchers are exploring biomarker-guided combination therapies. For instance, pairing SRC-pathway blockades with next-generation androgen receptor-targeted therapies or PARP inhibitors in specific genomic subsets may enable SRC inhibition to serve as a strategy to modify resistance rather than a standalone treatment[149].

The key points are that SRC collaborates with AR to promote growth that resists castration, and that SRC myristoylation is crucial for its full oncogenic function in prostate cancer. Additionally, SRC plays a role in integrating signals related to adhesion, motility, survival, and DNA damage, thereby contributing to metastasis and therapy resistance[150]. The main therapeutic implication is that targeting the SRC pathway is likely to be most effective when used in carefully selected patients and in rational combinations, especially with AR-directed agents and therapies focused on DNA damage, rather than as a broad, untargeted monotherapy.

4.3. From Solid Architectures to Fluid Malignancies

While the above discussion highlights SRC's role in the physical architecture and metabolic flexibility of solid tumors, its influence also extends deeply into the hematological system. In a fluid environment, SRC is not merely a passenger; instead, it plays a vital role in regulating the entire hematopoietic hierarchy. SRC helps maintain the delicate balance between blood cell growth, lineage differentiation, and functional activation[151]. Under normal physiological

conditions, this kinase acts as a reliable switch, ensuring proper blood development and immune responses. However, in the context of leukemia, this regulatory mechanism is fundamentally disrupted[152]. The finely tuned switches within the hematopoietic hierarchy become locked in an active state, leading to uncontrolled cell proliferation and a systematic evasion of programmed cell death. SRC integrates signals from various growth factors and cytokine receptors, functioning as a potent biological amplifier that transforms normal physiological signals into abnormal oncogenic ones. This central role makes SRC a significant therapeutic target for various blood cancers[84]. The following discussion summarizes the evidence of SRC's involvement in different types of leukemia, outlining the molecular short circuits that drive disease progression and the strategies developed to counteract them.

4.3.1. *Chronic Myeloid Leukemia*

In chronic myeloid leukemia (CML), the disease is primarily driven by the BCR-ABL1 fusion protein. Unlike relying solely on one SRC protein as an independent oncogenic partner, BCR-ABL1 engages multiple SFKs. It phosphorylates and activates various SFKs, including LYN, HCK, and FYN[153]. This activation enhances downstream signaling pathways that promote cell proliferation, survival, and changes in cell adhesion. However, there is insufficient evidence to support the idea of a simple bidirectional loop in which SRC stabilizes BCR-ABL1 and serves as the sole driver of the disease. SFKs play a crucial role in the phosphorylation of proteins involved in cytoskeletal and adhesion signaling, such as FAK and paxillin[153]. These processes affect cell motility and interactions with the microenvironment. Ultimately, these functions are part of a wider BCR-ABL1 signaling network, rather than being focused exclusively on SRC.

The canonical BCR-ABL1 pathways provide the most comprehensive explanation for the survival and proliferation characteristics of CML. These pathways include RAS/RAF/MEK/ERK,

PI3K/AKT/mTOR, and particularly the JAK/STAT5 pathway[153]. In contrast, the SRC-YAP-Survivin/Cyclin D1 axis is not as well-established. These well-characterized signaling cascades increase the levels of anti-apoptotic proteins such as BCL-xL and MCL-1, while also inducing cell cycle regulators like cyclin D1. Additionally, the stabilization of *β-catenin* promotes cell proliferation and enhances stem cell-like properties. Although YAP and Hippo signaling pathways are being investigated in myeloid diseases, the SRC-YAP-Survivin/Cyclin D1 pathway lacks strong clinical validation in the context of CML compared to the prominent STAT5 and *β-catenin*-driven pathways[154].

BCR-ABL1 influences interactions with the bone marrow niche by altering leukemic cell adhesion to stromal components, such as fibronectin. This altered adhesion can protect leukemic cells and contribute to the development of minimal residual disease. The dependence on this niche involves cooperative signaling through BCR-ABL1, SFKs, and other pathways, rather than relying solely on SRC as an environmental architect. While tyrosine kinase inhibitors (TKIs) can modify adhesion and partially dislodge cells from protective niches, their primary clinical impact in CML stems from the direct inhibition of survival signals driven by BCR-ABL1[155].

Dasatinib, a second-generation TKI, effectively inhibits both BCR-ABL1 and multiple SFKs[155]. This dual activity is likely to enhance its efficacy, especially in certain resistant cases, although the benefits are not primarily due to the disruption of fibronectin anchoring.

Later-generation TKIs have more complex target profiles such as bosutinib inhibits BCR-ABL1 and several SFKs but shows relatively weak activity against KIT and PDGFR compared to Dasatinib. However, its toxicity profile cannot be fully explained by its selective sparing of these kinases[156]. Ponatinib was specifically designed to inhibit the T315I-mutant BCR-ABL1 and exhibits broad off-target activity, including against some SFKs. Clinically, its main value lies in its

potent, mutation-tolerant blockade of BCR-ABL1 rather than in a defined dual BCR-ABL1/SRC mechanism[157]. Newer STAMP inhibitors, such as asciminib, are being developed to target the myristoyl pocket of ABL, aiming for deeper molecular responses and more treatment-free remissions[158]. Additionally, combinations of site-selective ABL inhibitors with broader TKIs are under investigation. However, the routine combination of dual SRC/ABL inhibitors and achieving reliable cures for refractory disease remain goals of ongoing research rather than established realities as of early 2026.

4.3.2. *Acute Myeloid Leukemia*

In acute myeloid leukemia (AML), SFKs, particularly SRC, Lyn, Hck, and Fgr, act as key signaling intermediaries downstream of aberrant RTKs, with a prominent role in FLT3-ITD-mutated cases, which occur in ~25-30% of AML and confer poor prognosis. SRC selectively binds FLT3-ITD (but not TKD point mutations) via its SH2 domain to phosphorylated tyrosines in the juxtamembrane region (including Y589/591), enabling full STAT5 activation, which is essential for proliferation and survival; this ITD-specific dependence highlights SFK vulnerability unique to this mutation. High SFK expression correlates with inferior survival across AML cohorts, even in FLT3 wild-type disease, where SFKs amplify PI3K/AKT, MAPK/ERK, and adhesion signals (e.g., via FAK, PYK2, p130Cas) to sustain anti-apoptotic proteins like MCL-1 and promote microenvironmental protection[159].

In preclinical models of AML, inhibiting SRC significantly disrupts various signaling pathways. This disruption leads to the dephosphorylation of adhesion and cytoskeletal effectors, as well as a downregulation of MCL-1[159]. Collectively, these changes halt cell proliferation and sensitize the cells to apoptosis, irrespective of FLT3 status in many primary samples. Multi-kinase inhibitors, such as Dasatinib, which target SRC, ABL, and Lyn, have shown effectiveness against

AML cells that overexpress SFKs. These inhibitors reduce the phosphorylation of STAT5 and ERK while enhancing the effects of chemotherapy[160]. However, outcomes can vary by AML subtype, with the most significant results observed in FLT3-ITD-positive cases. Bosutinib, another inhibitor of SRC and ABL, has shown modest activity as a single agent in trials for relapsed or refractory AML. It reduces dependence on MCL-1 and works synergistically with venetoclax and hypomethylating agents (HMAs) to target progenitor cells by suppressing STAT3 and c-Myc. However, it does not specifically promote MCL-1 ubiquitination[161].

As of early 2026, SRC/SFK targeting remains investigational in AML, with a focus on biomarker-driven combinations (e.g., high SFK expression, FLT3-ITD) to overcome redundancy and resistance in aggressive subtypes, such as secondary AML or those that have failed venetoclax. Dasatinib and Bosutinib are repurposed in trials with hypomethylating agents or FLT3 inhibitors, aiming to deepen responses, but no SRC-specific agent like SAR103168 has reached pivotal clinical validation; efforts prioritize patient selection via SFK activity signatures to neutralize survival networks in therapy-resistant disease[162].

4.4. SRC as the Architect of Cancer Recurrence

SRC as an architect of cancer recurrence is best understood as part of a broader adaptive signaling network rather than a solitary master regulator. Oncogenic drivers such as *EGFR, HER2*, *KRAS*, or *BRAF* typically initiate tumorigenesis and remain dominant targets, but treatment pressure frequently reshapes signaling, allowing alternative pathways to emerge[120]. SRC and other SFKs are often upregulated or activated in drug-resistant tumors and function as central hubs that integrate microenvironmental inputs, including growth factors, integrin engagement, cytokines, and mechanical cues, to sustain survival and proliferation despite targeted therapies. In several models (for example, *BRAF*-mutant melanoma or *EGFR*-mutant lung cancer), resistant cells show

increased EGFR-SFK-STAT3 or integrin-SFK-FAK activity[163], indicating that SRC contributes importantly to the second wave of signaling that supports relapse, though it is one key node among many rather than a universal, standalone driver.

4.4.1. *Bypass Signaling: The Redundant Route Strategy*

A well-documented role of SRC in recurrence is its role in bypass signaling. When a primary oncogenic receptor such as *EGFR* or *HER2* is inhibited, tumors can recruit alternative RTKs, such as MET, AXL, or IGF1R, which converge on SRC and downstream PI3K/AKT and MAPK cascades[121, 164]. SRC thereby helps route survival and proliferation signals around the blocked target, contributing to kinome reprogramming and reduced dependence on the original oncogenic driver. However, most studies describe SRC as part of a broader web of RTKs and nRTKs adaptors rather than as the sole master coordinator of this reprogramming, and the degree of SRC dependence varies considerably by tumor type and resistance mechanism[121, 165]. Similarly, the idea that stress from therapy always triggers a generalized compensatory rise in SRC and that this alone guarantees multidrug resistance is too strong; SRC activation is common in resistance, but not universal, and acts alongside many other adaptive changes.

4.4.2. *EMT and the Invasive Escape*

SRC is also strongly implicated in EMT, invasion, and dissemination, which are central to spatial patterns of recurrence. SRC/FAK signaling regulates E-cadherin function and cell–cell junctions, and elevated SRC/FAK activity can promote E-cadherin internalization or mislocalization, contributing to EMT-like phenotypes and enhanced motility. Through phosphorylation and activation of partners such as FAK and p130CAS, SRC reorganizes the actin cytoskeleton and focal adhesions, enabling cancer cells to detach, migrate, and invade, thereby facilitating spread to sanctuary sites where drug penetration is poor[166, 167]. The reversible nature of

EMT and EMT-likely supports recurrence from disseminated cells, but it is more accurate to state that SRC is an important contributor to EMT and invasion in multiple tumor types, rather than the single key EMT regulator across cancers.

4.4.3. *Metabolic Plasticity and the Persister State*

Drug-tolerant persister (DTP) cells and metabolic plasticity are recognized as major components of recurrence, and many DTPs exhibit shifts towards OXPHOS, altered fatty acid oxidation, and reprogrammed redox and biosynthetic pathways[168]. SRC has been linked to mitochondrial function and metabolic control in some models, and SRC-dependent signaling can intersect with pathways that regulate OXPHOS and ROS handling[132]; however, the literature does not yet support a universal, SRC-centered model in which SRC is the primary coordinator of DTP metabolic reprogramming in all cancers[84]. Research studies instead highlights a heterogeneous set of metabolic adaptations, including changes in OXPHOS, pentose phosphate pathway, and antioxidant systems as key DTP features, with SRC acting as one of several kinases that can modulate these states in a context-dependent manner[169].

The ability of SRC to maintain cellular survival even in the presence of primary oncogenic drivers is what defines its role as a major contributor to tumor recurrence. SRC turns the tumor into a resilient and adaptable target by controlling alternative signaling pathways, altering metabolic processes, and enabling invasive plasticity[121]. This concept of molecular resilience is particularly critical in the context of the most aggressive pediatric brain tumors. In G3 MB, where the primary driver is often an elusive transcriptional program rather than a single, targetable mutation, SRC's role in orchestrating therapy resistance and recurrence post-treatment becomes uniquely significant.

4.5. SRC in Group 3 Medulloblastoma

In primary G3 MB, SRC functions as an important signaling hub rather than merely an on-off switch. It integrates signals from RTKs and neurodevelopmental programs that drive growth and dissemination. Multiple RTKs, including PDGFR and members of the ERBB family, can signal through SRC or SRC-family kinases to promote cell migration and survival. Signaling through the PDGFR-SRC-FAK pathway has been implicated in MB cell motility in experimental models[110].

A recent study focusing on neurodevelopment and multi-omics has identified a SMARCD3 (BAF60C)-Reelin/DAB1-SRC axis that connects abnormal epigenetic regulation to metastatic spread in medulloblastoma. This research shows that increased SMARCD3 expression activates Reelin/DAB1-mediated SRC signaling and that inhibiting SRC reduces both migration and metastasis in preclinical models. Once activated, SRC engages downstream pathways, including STAT3, as well as cytoskeletal adaptors such as p130CAS and FAK[170]. This engagement remodels the cytoskeleton and supports cell survival, making SRC a significant contributor but not the sole master regulator of the invasive characteristics of G3 MB at diagnosis.

Pharmacological inhibition of SRC in MB has shown promising early-stage results. Non-ATP-competitive SRC signaling inhibitors, such as KX2-391 (tirbanibulin), which inhibit tubulin polymerization, along with multi-kinase SRC/ABL inhibitors like dasatinib, have demonstrated significant anti-tumor effects in both MB cell lines and mouse models. These effects include reduced tumor cell migration and metastasis[170]. At low nanomolar concentrations, dasatinib works synergistically with cisplatin to suppress colony formation, migration, and the activation of STAT3 and ERK in human MB cells. Additionally, when dasatinib is combined with the aurora kinase inhibitor AT9283, it further impairs tumor growth and disrupts cell-cycle progression *in vivo*[171].

However, it is important to note that these kinases inhibitors are still in the preclinical stage. There are significant challenges to overcome before these results can be translated into effective and tolerable treatment regimens for children. Therefore, SRC-targeted strategies for G3 MB remain investigational and are not yet part of standard care.

Although the SRC roles in primary MB have been established[110, 172], its behavior during the crucial transition to recurrence remains poorly understood. Relapses are the main obstacle to survival in G3 MB, with approximately 30% of patients experiencing a recurrence that is resistant to current therapy, making it universally fatal[47]. At this stage, the tumor is no longer a predictable target but rather a battle-hardened survivor. Current evidence presents a compelling paradox: paired *in vitro* studies show that recurrent G3 MB cell lines exhibit significantly greater sensitivity to inhibitors such as Dasatinib than their treatment-naïve counterparts[170]. This suggests a potential dependency shift, indicating a dramatic molecular rewiring that occurs after therapy. However, these findings do not yet provide a direct quantification of SRC's enzymatic activity in the clinical context of a patient's recurring tumor.

This lack of head-to-head comparison between primary and recurrent clinical specimens represents a dangerous blind spot in pediatric neuro-oncology. Despite the mechanistic plausibility of the Reelin/DAB1-SRC axis and various RTKs-driven developmental programs[170], we cannot yet state a general rule for how SRC activity evolves from the moment of diagnosis to the point of lethal relapse. We understand how SRC helps a primary tumor move and grow, but we have yet to fully decode how it helps a tumor survive the onslaught of chemotherapy and radiation. It is within this unmapped territory, where the biology of the primary tumor ends and the resilience of the fatal recurrence begins, that the proper role of SRC in therapy resistance must be uncovered.

4.6. Summary of the findings

Our research establishes a new understanding and treatment approach for G3 MB by identifying SRC as a key factor in therapy resistance and disease relapses. We established a clinically relevant experimental model in which patient-derived G3 MB cells were subjected to a rigorous treatment regimen comprising craniospinal irradiation and chemotherapy (cisplatin and vincristine). This framework effectively simulates the molecular crucible that patients encounter during standard care. Through this approach, we isolated a highly resilient population of CRT-treated cells that reflects the aggressive nature of clinical relapses. Our analysis of the kinome revealed a significant and consistent increase in p-SRC (Y419). This signaling adaptation is not just a temporary stress response; it is a persistent characteristic of resistance observed across multiple independent G3 MB models. We also validated these findings in both orthotopic PDOX recurrent tumors and matched primary-recurrent patient samples.

Importantly, the increase in SRC signaling observed is a unique vulnerability specific to a particular subgroup. In G3 MB cells, SRC was recruited to help them survive treatment-related stress; however, this adaptation was not seen in the SHH and Group 4 subgroups, where treatment actually reduced SRC activity. Most significantly for pediatric care, this signaling shift was absent in healthy human astrocytes and NSCs. This tumor-specific activation offers a rare therapeutic opportunity: the chance to target the cancer directly while avoiding damage to the delicate, developing structure of the healthy brain.

Our data shows that SRC functions as a master regulator of the undifferentiated state in G3 MB recurrent tumors. When we genetically KO *SRC* or inhibited it pharmacologically, we effectively dismantled the tumor's maintenance programs. This led to a significant reduction in stemness markers, specifically SOX2, OCT4, and NANOG, as well as impaired tumor sphere formation and migration. By blocking SRC, we did more than halt tumor growth; we induced a

fate switch in surviving cells, shifting them from a primitive, flexible state to terminal neuronal differentiation, as indicated by TUBB3 expression.

Once the stem-like characteristics were eliminated, the cells became susceptible to a dual mechanism of cell death, undergoing both apoptosis and necroptosis. This lack of functional redundancy highlights SRC as a crucial survival factor that tumors cannot easily bypass, making it a high-priority target for clinical treatment.

The potential of this discovery was most clearly demonstrated in our *in vivo* PDOX models. The combination of the BBB-permeable SRC inhibitor Saracatinib with standard CRT resulted in a significant reduction in tumor burden and prolonged overall survival. Mechanistically, this combination therapy accomplished what conventional treatment could not: it effectively evicted the tumor from its stem-like niche and initiated widespread programmed cell death. Importantly, this survival benefit was achieved without causing neuroinflammation or damaging neuronal integrity, as indicated by stable microglial activity and preserved axonal structure. Collectively, these findings provide a strong scientific and clinical rationale for repurposing SRC inhibitors. By targeting the root cause of G3 MB recurrence, we move closer to a treatment model that offers hope for the most at-risk children while safeguarding their neurodevelopmental future[173].

4.7. Implication of the findings

The implications of our research extend far beyond the laboratory, offering a transformative perspective on the management of G3 MB, the most lethal pediatric brain tumors. By uncovering the role of SRC as an inducible survival anchor, this study identifies a novel mechanism of recurrence that has remained hidden within the complex signaling landscape of G3 MB. For the first time, we demonstrate that the transition to a refractory state is not random, but rather a programmed signaling adaptation that can be strategically dismantled. The successful integration

of Saracatinib, a drug already established in clinical pipelines, provides an immediate and viable pathway for therapeutic repurposing. This approach bypasses the decade-long challenges of traditional drug development, allowing us to reach at-risk children more quickly. Furthermore, because the recruitment of SRC as a central resistance hub likely represents a fundamental survival strategy shared by diverse malignancies, these findings offer a broader template for targeting the molecular resilience of recurring tumors far beyond the scope of pediatric neuro-oncology. Ultimately, this work lays the scientific foundation for a new frontier in oncology that aims to be neuro-sparing. Instead of relying on the blunt force of broad-spectrum toxins, it promotes the use of a targeted resistance-breaker, which could significantly improve the prognosis for the 30% of children for whom modern medicine currently has no effective treatment.

4.8. Limitations

The findings of this study provide strong mechanistic and preclinical evidence that SRC is a key driver of therapy resistance in G3 MB. However, several limitations need to be addressed to guide future research efforts.

4.8.1. *Sex Representation in Patient-Derived Models*

All the patient-derived cell lines used in this study were obtained exclusively from male patients. It is important to recognize that biological differences between sexes, including hormonal environments, immune responses, and transcriptional regulation, can significantly impact tumor biology and treatment efficacy. Therefore, the applicability of our findings to female patients has yet to be confirmed. Although G3 MB primarily affects males, it also occurs in females. The absence of female-derived G3 MB specimens in this study was not a deliberate choice, but rather a reflection of their limited availability. To address this critical issue, future research should focus on collecting and banking samples from female G3 MB patients. In the meantime, a practical

approach would be to treat male patient-derived cells or animal models with female sex hormones, particularly estrogen and progesterone. This would help replicate the hormonal environment of female patients and investigate whether sex hormone signaling influences SRC activity, kinome adaptation, or therapeutic response.

4.8.2. *Limited Kinome Prolife*

The kinase activity profiling conducted in this study utilized a targeted phospho-kinase array capable of simultaneously detecting 37 kinases. While this method effectively identified p-SRC and its downstream proteins as a consistently elevated and functionally significant component, it captures only a small portion of the broader kinome. Consequently, compensatory or cooperative kinase networks that may function alongside SRC or that may arise following SRC inhibition remain largely unexplored. This limitation is particularly important in the context of resistance mechanisms, as kinome plasticity is a well-documented survival strategy employed by tumor cells.

4.8.3. *Residual Lethality Following Saracatinib Combination Therapy*

The combination of saracatinib with CRT significantly extended overall survival in PDOX models compared to CRT alone. However, the animals ultimately succumbed to the disease. This indicates that while SRC inhibition is highly effective at dismantling the resistance mechanism, it does not completely eliminate the tumor's ability to adapt. The continued presence of lethality aligns with the concept of kinome rewiring[96], in which selective pressure from targeted therapy drives the emergence of alternative survival kinases that bypass SRC dependency. Identifying these escape mechanisms is crucial for the rational design of next-generation combination strategies.

4.9. Future Directions

The limitations mentioned above highlight several critical areas for future research. First and foremost, it is essential to conduct unbiased global phosphoproteomic profiling in both therapy-naïve and CRT-Res G3 MB cells, as well as in CRT + saracatinib-treated cells. Comprehensive mapping of the kinome landscape will not only validate and expand upon our kinase array findings but will also uncover the full range of signaling adaptations associated with resistance. This could help identify potential co-targets for combinatorial treatments. Additionally, further investigation is needed into the mechanisms downstream of SRC that influence the transition from stem cells to neuronal differentiation. Understanding the specific transcriptional and epigenetic pathways through which SRC maintains the undifferentiated state and how its inhibition facilitates terminal differentiation could reveal new therapeutic vulnerabilities and potential biomarkers for treatment response.

To strengthen the clinical translatability of our findings, we plan to expand validation efforts to include a larger cohort of patient-derived samples, possibly including matched samples from both primary and recurrent patients. This should ideally encompass diverse patient demographics, including specimens derived from females. By correlating baseline SRC activity with clinical outcomes, including time to relapse and overall survival, we can establish SRC's prognostic utility as a predictive biomarker. Additionally, given the emerging evidence that the tumor microenvironment, comprising microglia, infiltrating immune cells, and the extracellular matrix, can significantly influence kinome dynamics and drug penetration, future studies should utilize immune-competent models[174]. This will help assess how the immunological context of the developing brain affects both SRC-mediated resistance and saracatinib efficacy.

Finally, while saracatinib's BBB permeability is a significant advantage, further optimization of pharmacokinetics and refinement of the dosing schedule will be essential to

maximize intratumoral drug exposure while preserving the neurodevelopmental safety profile we have documented. Together, these future directions leverage a strong mechanistic foundation and outline a clear path toward clinical translation, offering genuine hope for children who currently lack effective treatment options at relapse.

CHAPTER 5. CONCLUSION

This study identifies SRC kinase as a pivotal, inducible anchor of therapy resistance and recurrence in G3 MB. By moving beyond the static genetic landscape of the primary tumor, we have demonstrated that the molecular resilience of G3 MB is a dynamic process, one in which therapeutic pressure drives a fundamental signaling shift toward a primitive, stem-like state. Our findings reveal that the surge in SRC phosphorylation following conventional treatment is not a generalized stress response, but a subgroup-specific adaptation that sustains the tumor's self-renewal and invasive potential. By dismantling this survival hub through genetic ablation or pharmacological blockade with Saracatinib, we successfully collapsed the tumor's defense mechanisms, triggering a dual mode of programmed cell death and forcing resistant cells toward terminal neuronal differentiation.

Ultimately, these results provide a compelling scientific and clinical rationale for a new frontier in pediatric neuro-oncology. The successful extension of survival in aggressive PDOX models achieved without inducing neurotoxicity or inflammatory damage to the developing brain highlights the transformative potential of repurposing BBB-permeable SRC inhibitors. This strategy moves us away from the era of non-specific, blunt-force toxins and toward a model of precision medicine that strikes specifically at the engines of relapse. By offering a targeted solution to the lethal paradox of recurrence, this work provides a much-needed roadmap for improving the long-term outcomes of children facing the most aggressive forms of brain cancer, turning a previously fatal 30% relapse rate into an actionable therapeutic opportunity.

APPENDIX

Proteome Profiler Phospho-Kinase Array

Membrane layout and blot coordinates

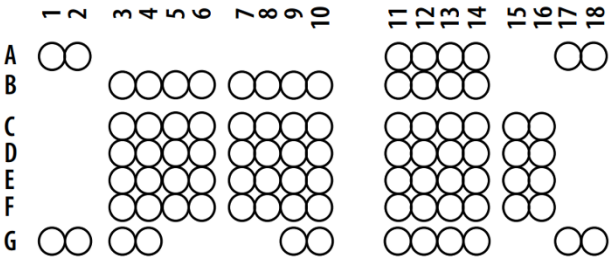

Coordinates	Target/Control	Phosphorylation Site
A1,A2	Reference Spot	_____
A11,A12	Akt 1/2/3	T308
A13, A14	Akt 1/2/3	S473
A17, A18	Reference Spot	_____
B3, B4	CREB	S133
B5, B6	EGF R	Y1086
B7, B8	eNOS	S1177
B9,B10	ERK1/2	T202/Y204, T185/Y187
B11, B12	Chk-2	T68
B13,B14	c-Jun	S63
C3,C4	Fgr	Y412
C5,C6	GSK-3α/β	S21/S9
C7,C8	GSK-3β	S9
C9, C10	HSP27	S78/S82
C11,C12	p53	S15
C13, C14	p53	S46
C15, C16	p53	S392
D3, D4	JNK 1/2/3	T183/Y185, T221/T223
D5, D6	Lck	Y394
D7, D8	Lyn	Y397
D9, D10	MSK1/2	S376/S360
D11, D12	P70 S6 Kinase	T389
D13, D14	P70 S6 Kinase	T421/S424
D15, D16	PRAS40	T246

Coordinates	Target/Control	Phosphorylation Site
E3, E4	p38α	T180/Y182
E5, E6	PDGF Rβ	Y7751
E7, E8	PLC-γ1	Y783
E9, E10	SRC	Y419
E11, E12	PYK2	Y402
E13, E14	RSK1/2	S221/S227
E15, E16	RSK1/2/3	S380/S386/S377
F3, F4	STAT2	(Py690)
F5, F6	STAT5a/b	Y694/y699
F7, F8	WNK1	T60
F9, F10	Yes	Y426
F11, F12	STAT1	Y701
F13, F14	STAT3	Y705
F15, F16	STAT3	S727
G1, G2	Reference Spot	_____
G3, G4	B-Catenin	_____
G9, G10	PBS (Negative Control)	_____
G11, G12	STAT6	
G13, G14	HSP60	_____
G17, G18	PBS (Negative Control)	_____

Appendix Figure A1. Membrane layout and blot coordinates of proteome profile phospho-kinase array.

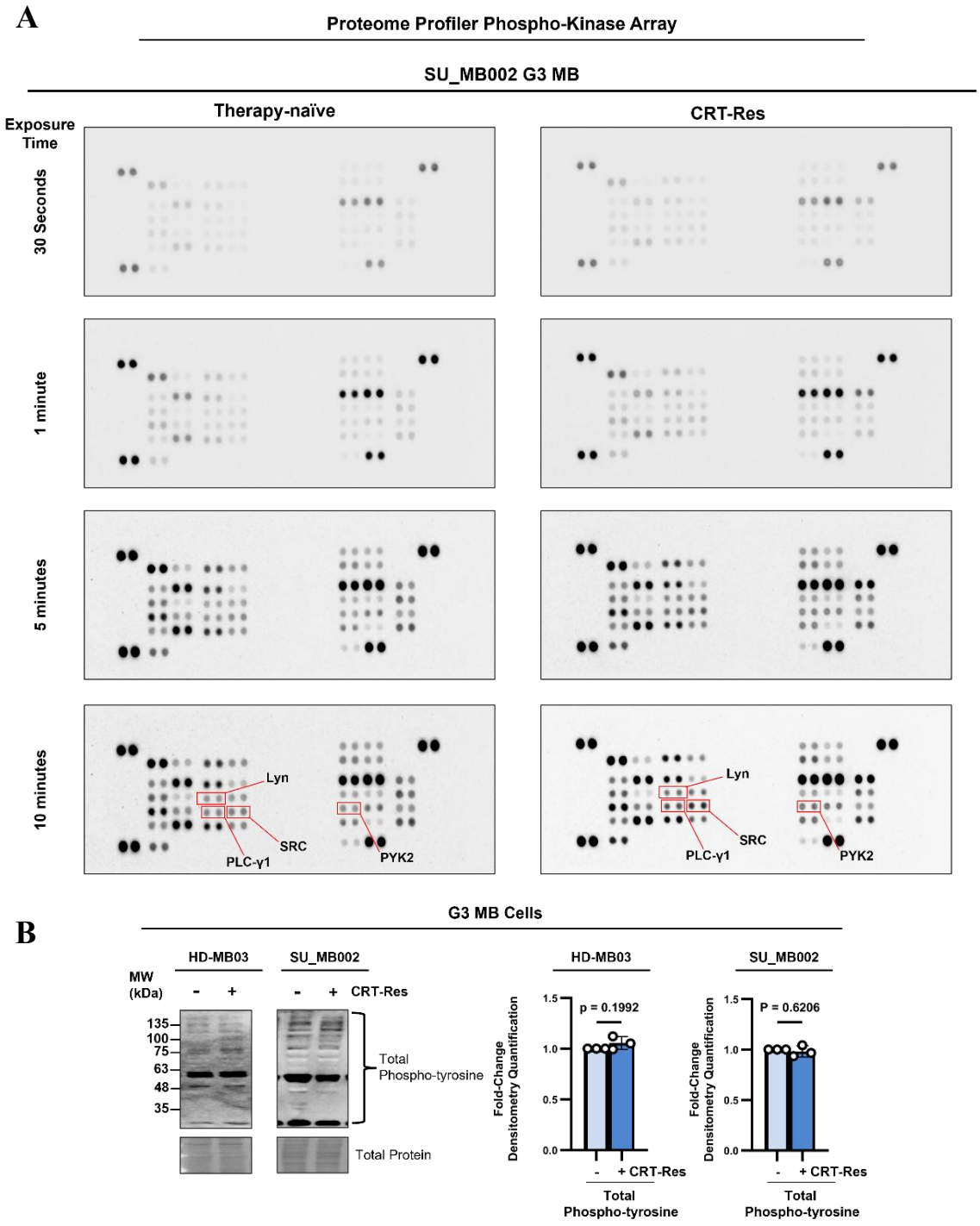

Appendix Figure 2. (A) Uncut Phospho-kinase array blots of therapy naïve and CRT-Res SU_MB002 samples. Array blots imaged at multiple exposure times (30 seconds, 1 minute, 5 minutes, and 10 minutes). Red boxes highlight the locations of the kinases of interest presented in Figure 1D (p-SRC, p-Lyn, p-PYK2, p-PLC-γ1, p-AKT, p-ERK, and p-JNK). **(B)** Anti-Phospho tyrosine levels in CRT-Res HD-MB03 and SU_MB002 cells. Graphs represent densitometry quantification measurement of Anti-Phospho Tyrosine normalized to the total protein from n = 3 experimental replicates, presented as mean ± s.e.m; unpaired two-tailed t-test.

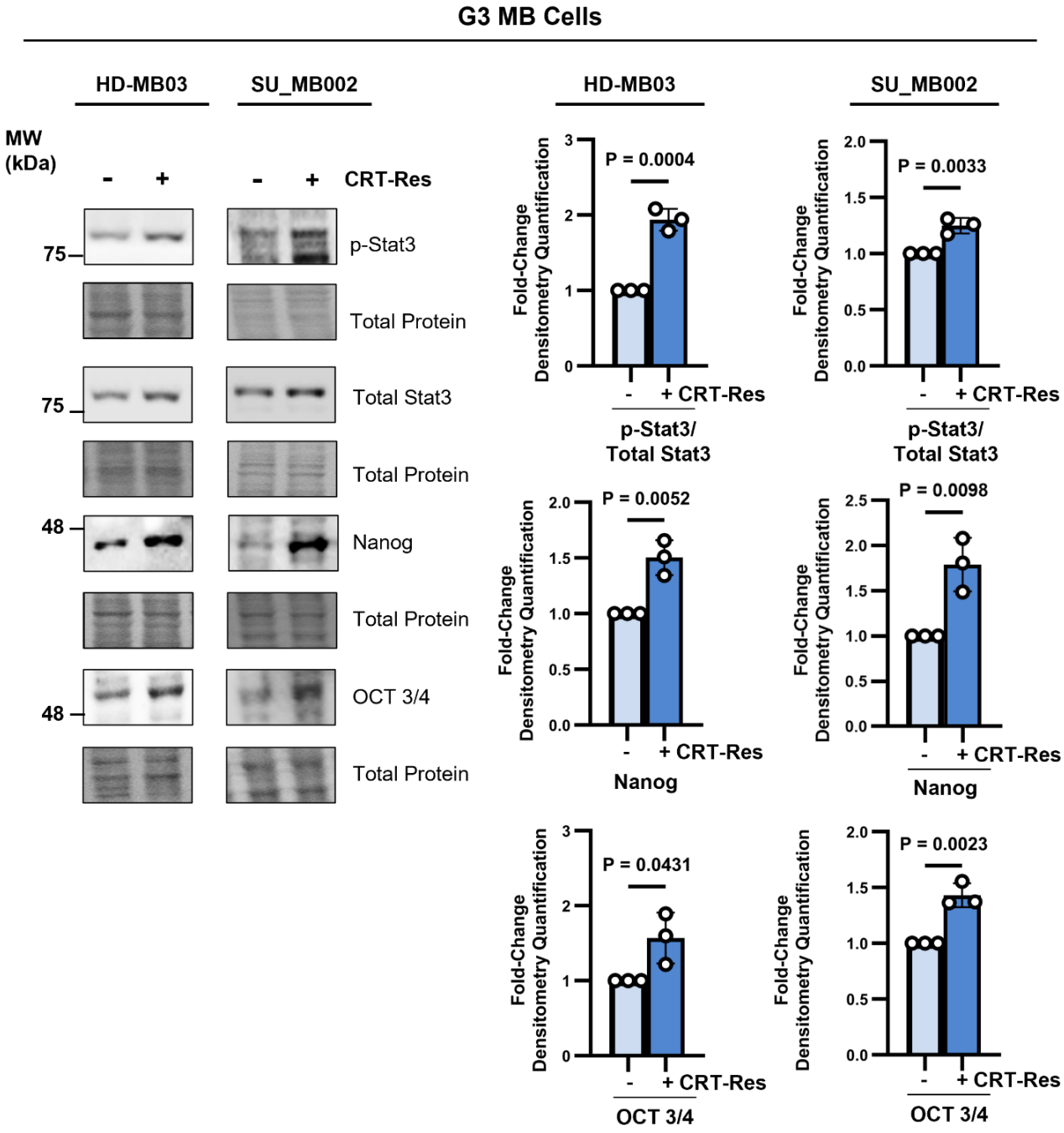

Appendix Figure 3: Immunoblot of p-Stat3, total Stat3, Nanog, and OCT3/4 expression in CRT-Res HD-MB03 and SU_MB002 cells. Graphs represent densitometry quantification measurement normalized to the total protein of p-Stat3/total Stat3, Nanog, and OCT3/4 in therapy naïve and CRT-Res HD-MB03 and SU_MB002 cells from $n = 3$ experimental replicates, presented as mean ± s.e.m; unpaired two-tailed t-test.

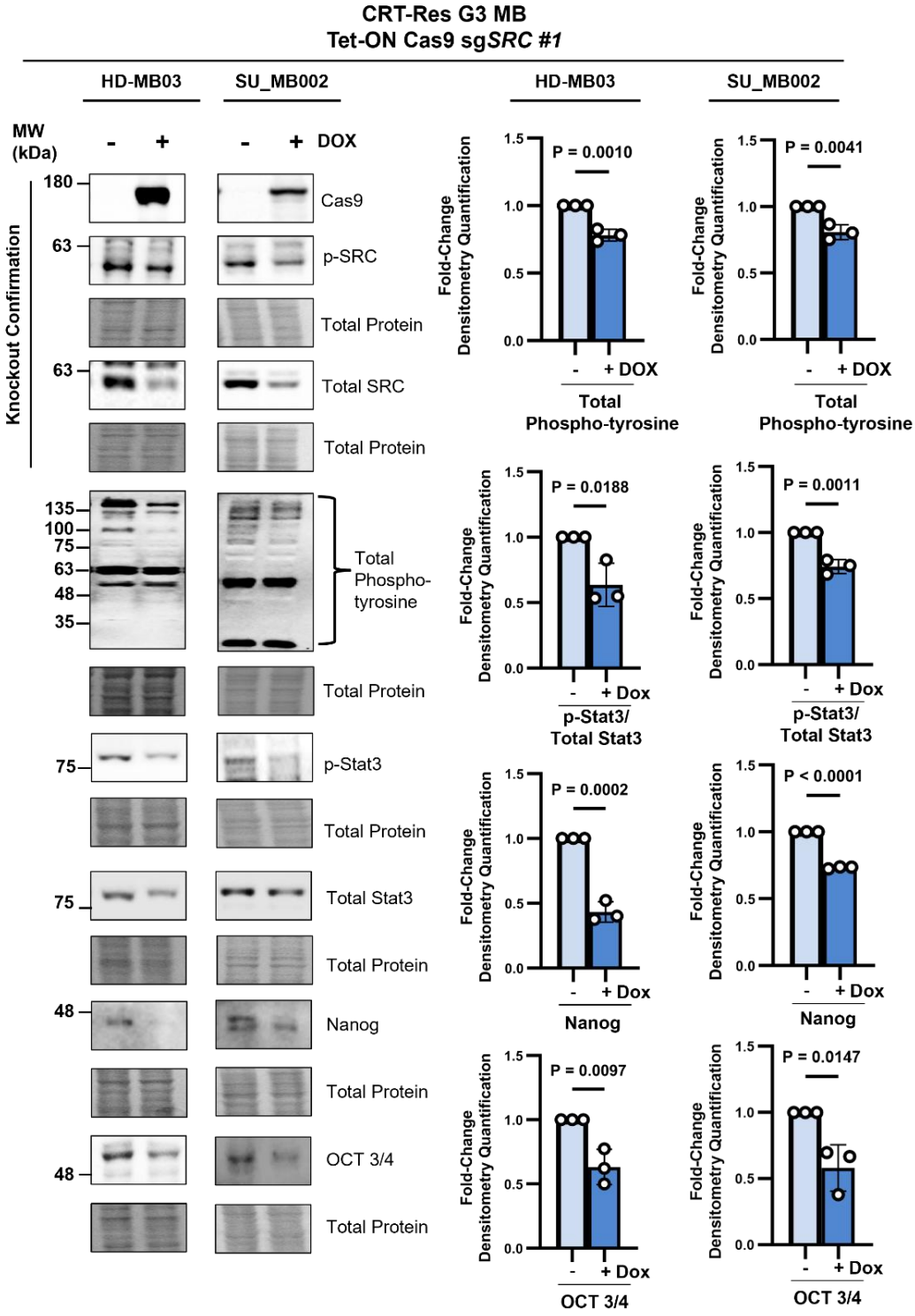

Appendix Figure S4. **(A)** Immunoblot of Cas9, p-SRC (Y419), total SRC, Anti-Phospho tyrosine, p-Stat3, total Stat3, Nanog, and OCT3/4 expression in CRT-Res HD-MB03 and SU_MB002 cells expressing Tet-ON Cas9 sg*SRC* #1 treated with DOX. Graphs represent densitometry quantification measurement normalized to the total protein of p-Stat3/total Stat3, Nanog, and OCT3/4 in therapy naïve and CRT-Res HD-MB03 and SU_MB002 cells from $n = 3$ experimental replicates, presented as mean ± s.e.m; unpaired two-tailed t-test**.**

CHAPTER 6. REFERENCES

1. Canadian Cancer Statistics Advisory Committee in collaboration with the Canadian Cancer Society SCatPHAoC. Canadian Cancer Statistics 2023. 2023.

2. Public Health Agency of Canada. Childhood Cancer Counts in Canada Ottawa, ON: Government of Canada; 2022 [Available from: https://www.canada.ca/en/public-health/services/publications/diseases-conditions/childhood-cancer-counts-canada.html.

3. Terry Fox Research Institute. Pediatric & Young Adult Cancers Vancouver, BC: The Terry Fox Research Institute; 2019 [Available from: https://www.tfri.ca/about-cancer/cancer-types/cancer-type/pediatric-and-young-adult.

4. McKenzie K, Xie L, Khafagy R, Ricci C, Grywacheski V. Prevalence of childhood cancer in Canada: an analysis using 5-year, 18-year and 25-year limited-duration prevalence from the CYP-C data tool. Health Promot Chronic Dis Prev Can. 2025;45(10):418-23.

5. Public Health Agency of Canada. Cancer in Young People in Canada: A Report from the Enhanced Childhood Cancer Surveillance System. 2017.

6. Central Brain Tumor Registry of the United States. CBTRUS Fact Sheet: Mid-2022 Pediatric Brain and Other Central Nervous System Tumors. Hinsdale, IL; 2022.

7. Gateway for Cancer Research. Brain Cancer Surpasses Leukemia as Deadliest Childhood Cancer Chicago, IL: Gateway for Cancer Research; 2021 [Available from: https://gatewaycr.org/about/in-the-news/brain-cancer-surpasses-leukemia-as-deadliest-childhood-cancer/.

8. Li JW, Yingxue; Dong, Chunli; Luo, Lifu. Advancements in leukemia management: Bridging diagnosis, prognosis and nanotechnology (Review). International Journal of Oncology. 2024;65(6):112.

9. Onyije FM, Dolatkhah R, Olsson A, Bouaoun L, Deltour I, Erdmann F, et al. Risk factors for childhood brain tumours: A systematic review and meta-analysis of observational studies from 1976 to 2022. Cancer Epidemiol. 2024;88:102510.

10. Ostrowski RP, Acewicz A, He Z, Pucko EB, Godlewski J. Environmental Hazards and Glial Brain Tumors: Association or Causation? International Journal of Molecular Sciences. 2025;26(15):7425.

11. Caffo MC, Gerardo; La Fata, Giuseppe; Barresi, Valeria; Visalli, Maria; Venza, Mario; Venza, Isabella. Heavy Metals and Epigenetic Alterations in Brain Tumors. Current Genomics. 2014;15(6):457-63.

12. Baker SJE, David W; Gutmann, David H. Pediatric Gliomas as Neurodevelopmental Disorders. Glia. 2016;64(6):879-95.

13. Bruschi M, Grill J, Guerrini-Rousseau L. Pediatric brain tumors as a developmental disease. Curr Opin Oncol. 2021;33(6):608-14.

14. Hemmati HD, Nakano I, Lazareff JA, Masterman-Smith M, Geschwind DH, Bronner-Fraser M, et al. Cancerous stem cells can arise from pediatric brain tumors. Proceedings of the National Academy of Sciences. 2003;100(25):15178-83.

15. Zhang S, Xiao X, Yi Y, Wang X, Zhu L, Shen Y, et al. Tumor initiation and early tumorigenesis: molecular mechanisms and interventional targets. Signal Transduction and Targeted Therapy. 2024;9(1).

16. Hardwick LJA, Ali FR, Azzarelli R, Philpott A. Cell cycle regulation of proliferation versus differentiation in the central nervous system. Cell and Tissue Research. 2015;359(1):187-200.

17. D'Amati A, Bargiacchi L, Rossi S, Carai A, Bertero L, Barresi V, et al. Pediatric CNS tumors and 2021 WHO classification: what do oncologists need from pathologists? Frontiers in Molecular Neuroscience. 2024;17.

18. Louis DNP, Arie; Wesseling, Pieter; Brat, Daniel J; Cree, Ian A; Figarella-Branger, Dominique; Hawkins, Cynthia; Ng, H K; Pfister, Stefan M; Reifenberger, Guido; Soffietti, Riccardo; Deimling, Andreas von; Ellison, David W. The 2021 WHO Classification of Tumors of the Central Nervous System: a summary. Neuro-Oncology. 2021;23(8):1231-51.

19. Ahrendsen HSJT. What's new in neuropathology 2024: CNS WHO 5th edition updates. Journal of Pathology and Translational Medicine. 2024;58(6):346-9.

20. National Cancer Institute. Childhood medulloblastoma and other central nervous system embryonal tumors treatment (PDQ®): Treatment – health professional information: PeaceHealth Health Information Library; 2025 [Available from: https://www.peacehealth.org/medical-topics/id/ncicdr0000548358.

21. Kumar L, Deepa SFA, Moinca I, Suresh P, Naidu KVJR. Medulloblastoma: A common pediatric tumor: Prognostic factors and predictors of outcome. Asian Journal of Neurosurgery. 2015;10(01):50-.

22. Cocito CM, Brice; Giantini-Larsen, Alexandra M.; Valcarce-Aspegren, Marcus; Souweidane, Mark M.; Szalontay, Luca; Dahmane, Nadia; Greenfield, Jeffrey P. Leptomeningeal dissemination in pediatric brain tumors. Neoplasia. 2023;39.

23. Tenório RB, Vieira AA, Franklin GL, Della Coletta MV, Teive HAG, Camargo CHF. The cognitive cerebellum: a hub for motor, emotional, and executive control. Arquivos de Neuro-Psiquiatria. 2025;83(12):001-12.

24. Leto K, Arancillo M, Becker EBE, Buffo A, Chiang C, Ding B, et al. Consensus Paper: Cerebellar Development. The Cerebellum. 2016;15(6):789-828.

25. Sepp ML, K.; Murat, F.; Okonechnikov, K.; Joshi, P.; Leushkin, E.; Spänig, L.; Mbengue, N.; Schneider, C.; Schmidt, J.; Trost, N.; Schauer, M.; Khaitovich, P.; Lisgo, S.; Palkovits, M.; Giere, P.; Kutscher, L. M.; Anders, S.; Cardoso-Moreira, M.; Sarropoulos, I.; Pfister, S. M.; Kaessmann, H. 2024. Nature.625:788-96.

26. Haldipur PA, Kimberly A.; Bernardo, Silvia; Deng, Mei; Timms, Andrew E.; Overman, Lynne M.; Winter, Conrad; Lisgo, Steven N.; Razavi, Ferechte; Silvestri, Evelina; Manganaro, Lucia; Adle-Biassette, Homa; Guimiot, Fabien; Russo, Rosa; Kidron, Debora; Hof, Patrick R.; Gerrelli, Dianne; Lindsay, Susan J.; Dobyns, William B.; Glass, Ian A.; Alexandre, Paula; Millen, Kathleen J. Spatiotemporal expansion of primary progenitor zones in the developing human cerebellum. Science. 2019;366:454-60.

27. Aldinger KAT, Zachary; Phelps, Ian G.; Haldipur, Parthiv; Deng, Mei; Timms, Andrew E.; Hirano, Matthew; Santpere, Gabriel; Roco, Charles; Rosenberg, Alexander B.; Lorente-Galdos, Belen; Gulden, Forrest O.; O'Day, Diana; Overman, Lynne M.; Lisgo, Steven N.; Alexandre, Paula; Sestan, Nenad; Doherty, Dan; Dobyns, William B.; Seelig, Georg; Glass, Ian A.; Millen, Kathleen J. Spatial and cell type transcriptional landscape of human cerebellar development. Nature Neuroscience. 2021;24:1163-75.

28. Selvadurai HJ, Luis E, Desai K, Lan X, Vladoiu MC, Whitley O, et al. Medulloblastoma Arises from the Persistence of a Rare and Transient Sox2+ Granule Neuron Precursor. Cell Reports. 2020;31(2):107511.

29. Schwalbe EC, Lindsey JC, Nakjang S, Crosier S, Smith AJ, Hicks D, et al. Novel molecular subgroups for clinical classification and outcome prediction in childhood medulloblastoma: a cohort study. The Lancet Oncology. 2017;18(7):958-71.

30. Northcott PA, Korshunov A, Witt H, Hielscher T, Eberhart CG, Mack S, et al. Medulloblastoma comprises four distinct molecular variants. J Clin Oncol. 2011;29(11):1408-14.

31. Gibson P, Tong Y, Robinson G, Thompson MC, Currle DS, Eden C, et al. Subtypes of medulloblastoma have distinct developmental origins. Nature. 2010;468(7327):1095-9.

32. Wang JW-R, R. J. . The role of stem cells and progenitors in the genesis of medulloblastoma. Experimental Neurology. 2014;260:69-73.

33. Helgager J, Pytel P, Vasudevaraja V, Lee EQ, Snuderl M, Iorgulescu JB, et al. WNT-Activated Medulloblastomas With Hybrid Molecular Subtypes. JCO Precis Oncol. 2020;4.

34. Mikkelsen MK, Pinto SN, Chiang J, Shimony N, Gajjar A. Evolving Biology and Therapy of WNT-Activated Medulloblastoma. Journal of the National Comprehensive Cancer Network. 2025;23(10):1-7.

35. Menyhárt O, Győrffy B. Principles of tumorigenesis and emerging molecular drivers of activated medulloblastomas. Annals of Clinical and Translational Neurology. 2019;6(5):990-1005.

36. Smit MJ, Martini TEI, Armandari I, Bočkaj I, Zomerman WW, De Camargo Magalhães ES, et al. The developmental stage of the medulloblastoma cell-of-origin restricts Sonic hedgehog pathway usage and drug sensitivity. Journal of Cell Science. 2022;135(11).

37. Hendrikse LD, Haldipur P, Saulnier O, Millman J, Sjoboen AH, Erickson AW, et al. Failure of human rhombic lip differentiation underlies medulloblastoma formation. Nature. 2022;609(7929):1021-8.

38. Vladoiu MC, El-Hamamy I, Donovan LK, Farooq H, Holgado BL, Sundaravadanam Y, et al. Childhood cerebellar tumours mirror conserved fetal transcriptional programs. Nature. 2019;572(7767):67-73.

39. Kool M, Jones DT, Jäger N, Northcott PA, Pugh TJ, Hovestadt V, et al. Genome sequencing of SHH medulloblastoma predicts genotype-related response to smoothened inhibition. Cancer Cell. 2014;25(3):393-405.

40. Pereira V, Torrejon J, Kariyawasam D, Berlanga P, Guerrini-Rousseau L, Ayrault O, et al. Clinical and molecular analysis of smoothened inhibitors in Sonic Hedgehog medulloblastoma. Neurooncol Adv. 2021;3(1):vdab097.

41. Zhukova N, Ramaswamy V, Remke M, Pfaff E, Shih DJ, Martin DC, et al. Subgroup-specific prognostic implications of TP53 mutation in medulloblastoma. J Clin Oncol. 2013;31(23):2927-35.

42. Williamson D, Schwalbe EC, Hicks D, Aldinger KA, Lindsey JC, Crosier S, et al. Medulloblastoma group 3 and 4 tumors comprise a clinically and biologically significant expression continuum reflecting human cerebellar development. Cell Reports. 2022;40(5):111162.

43. Smith KS, Bihannic L, Gudenas BL, Haldipur P, Tao R, Gao Q, et al. Unified rhombic lip origins of group 3 and group 4 medulloblastoma. Nature. 2022;609(7929):1012-20.

44. Taylor MD, Northcott PA, Korshunov A, Remke M, Cho YJ, Clifford SC, et al. Molecular subgroups of medulloblastoma: the current consensus. Acta Neuropathol. 2012;123(4):465-72.

45. Northcott PA, Shih DJ, Peacock J, Garzia L, Morrissy AS, Zichner T, et al. Subgroup-specific structural variation across 1,000 medulloblastoma genomes. Nature. 2012;488(7409):49-56.

46. Bagchi A, Dhanda SK, Dunphy P, Sioson E, Robinson GW. Molecular Classification Improves Therapeutic Options for Infants and Young Children With Medulloblastoma. Journal of the National Comprehensive Cancer Network. 2023;21(10):1097-105.

47. Doss D, Kanchan R, Perumal N, Batra S, Mahapatra S. MDB-40. Transcriptome-based Drug Repurposing in Group 3 Medulloblastoma Neuro-Oncology. 2023

48. Ramaswamy V, Remke M, Bouffet E, Bailey S, Clifford SC, Doz F, et al. Risk stratification of childhood medulloblastoma in the molecular era: the current consensus. Acta Neuropathol. 2016;131(6):821-31.

49. Stromecki M, Tatari N, Morrison LC, Kaur R, Zagozewski J, Palidwor G, et al. Characterization of a novel OTX2-driven stem cell program in Group 3 and Group 4 medulloblastoma. Mol Oncol. 2018;12(4):495-513.

50. Christin Schmidt SH, Annika Carlson , Sarah Cohen , Samantha Westelman , Linyu Wang , William Weiss , Bjoern Schwer. MODL-32. Impact of PRDM6 on Chromatin Accessibitly, Gene Expression, and Medullolastoma Formation Neuro-Oncology. 2022;24(7):vii297-vii8.

51. Ramaswamy V, Remke M, Bouffet E, Faria CC, Perreault S, Cho YJ, et al. Recurrence patterns across medulloblastoma subgroups: an integrated clinical and molecular analysis. Lancet Oncol. 2013;14(12):1200-7.

52. Gajjar A, Robinson GW, Smith KS, Lin T, Merchant TE, Chintagumpala M, et al. Outcomes by Clinical and Molecular Features in Children With Medulloblastoma Treated With Risk-Adapted Therapy: Results of an International Phase III Trial (SJMB03). J Clin Oncol. 2021;39(7):822-35.

53. Robinson GW, Rudneva VA, Buchhalter I, Billups CA, Waszak SM, Smith KS, et al. Risk-adapted therapy for young children with medulloblastoma (SJYC07): therapeutic and molecular outcomes from a multicentre, phase 2 trial. Lancet Oncol. 2018;19(6):768-84.

54. Huybrechts S, Le Teuff G, Tauziède-Espariat A, Rossoni C, Chivet A, Indersie É, et al. Prognostic Clinical and Biologic Features for Overall Survival after Relapse in Childhood Medulloblastoma. Cancers (Basel). 2020;13(1).

55. Lee H, Kim B, Park J, Park S, Yoo G, Yum S, et al. Cancer stem cells: landscape, challenges and emerging therapeutic innovations. Signal Transduction and Targeted Therapy. 2025;10(1).

56. Morrissy AS, Cavalli FMG, Remke M, Ramaswamy V, Shih DJH, Holgado BL, et al. Spatial heterogeneity in medulloblastoma. Nat Genet. 2017;49(5):780-8.

57. Marzagalli M, Fontana F, Raimondi M, Limonta P. Cancer Stem Cells—Key Players in Tumor Relapse. Cancers. 2021;13(3):376.

58. Hill RM, Richardson S, Schwalbe EC, Hicks D, Lindsey JC, Crosier S, et al. Time, pattern, and outcome of medulloblastoma relapse and their association with tumour biology at diagnosis and therapy: a multicentre cohort study. The Lancet Child & Adolescent Health. 2020;4(12):865-74.

59. Bonnans C, Chou J, Werb Z. Remodelling the extracellular matrix in development and disease. Nat Rev Mol Cell Biol. 2014;15(12):786-801.

60. Singer SJ. Intercellular communication and cell-cell adhesion. Science. 1992;255(5052):1671-7.

61. Rouault H, Hakim V. Different Cell Fates from Cell-Cell Interactions: Core Architectures of Two-Cell Bistable Networks. Biophysical Journal. 2012;102(3):417-26.

62. Ramilowski JA, Goldberg T, Harshbarger J, Kloppmann E, Lizio M, Satagopam VP, et al. A draft network of ligand-receptor-mediated multicellular signalling in human. Nat Commun. 2015;6:7866.

63. Sonnen KF, Janda CY. Signalling dynamics in embryonic development. Biochem J. 2021;478(23):4045-70.

64. Mapstone TB. Cell surface receptors. An introduction. Pediatr Neurosurg. 1997;27(2):57-62.

65. Bruce MC, McAllister D, Murphy LC. The kinome associated with estrogen receptor-positive status in human breast cancer. Endocrine Related Cancer. 2014;21(5):R357-R70.

66. Schillace RV, Scott JD. Organization of kinases, phosphatases, and receptor signaling complexes. Journal of Clinical Investigation. 1999;103(6):761-5.

67. Gilmour KC, Reich NC. Signal transduction and activation of gene transcription by interferons. Gene Expr. 1995;5(1):1-18.

68. Cairns RA, Harris IS, Mak TW. Regulation of cancer cell metabolism. Nature Reviews Cancer. 2011;11(2):85-95.

69. Duong-Ly KC, Peterson JR. The Human Kinome and Kinase Inhibition. Current Protocols in Pharmacology. 2013;60(1).

70. Lahiry P, Torkamani A, Schork NJ, Hegele RA. Kinase mutations in human disease: interpreting genotype-phenotype relationships. Nat Rev Genet. 2010;11(1):60-74.

71. Johnson GL, Lapadat R. Mitogen-activated protein kinase pathways mediated by ERK, JNK, and p38 protein kinases. Science. 2002;298(5600):1911-2.

72. Pawson T. Regulation and targets of receptor tyrosine kinases. Eur J Cancer. 2002;38 Suppl 5:S3-10.

73. Bagnato G, Leopizzi M, Urciuoli E, Peruzzi B. Nuclear Functions of the Tyrosine Kinase Src. International Journal of Molecular Sciences. 2020;21(8):2675.

74. Eshaq AM, Flanagan TW, Hassan S-Y, Al Asheikh SA, Al-Amoudi WA, Santourlidis S, et al. Non-Receptor Tyrosine Kinases: Their Structure and Mechanistic Role in Tumor Progression and Resistance. Cancers. 2024;16(15):2754.

75. Lemmon MA, Schlessinger J. Cell Signaling by Receptor Tyrosine Kinases. Cell. 2010;141(7):1117-34.

76. Mendoza MC, Er EE, Blenis J. The Ras-ERK and PI3K-mTOR pathways: cross-talk and compensation. Trends in Biochemical Sciences. 2011;36(6):320-8.

77. Parsons SJ, Parsons JT. Src family kinases, key regulators of signal transduction. Oncogene. 2004;23(48):7906-9.

78. Sen B, Johnson FM. Regulation of Src Family Kinases in Human Cancers. Journal of Signal Transduction. 2011;2011:1-14.

79. Lee J, Wang Z, Luoh SM, Wood WI, Scadden DT. Cloning of FRK, a novel human intracellular SRC-like tyrosine kinase-encoding gene. Gene. 1994;138(1-2):247-51.

80. Oberg-Welsh C, Welsh M. Cloning of BSK, a murine FRK homologue with a specific pattern of tissue distribution. Gene. 1995;152(2):239-42.

81. Boggon TJ, Eck MJ. Structure and regulation of Src family kinases. Oncogene. 2004;23(48):7918-27.

82. Martin GS. Rous sarcoma virus: a function required for the maintenance of the transformed state. Nature. 1970;227(5262):1021-3.

83. Tanaka A, Gibbs CP, Arthur RR, Anderson SK, Kung HJ, Fujita DJ. DNA sequence encoding the amino-terminal region of the human c-src protein: implications of sequence divergence among src-type kinase oncogenes. Mol Cell Biol. 1987;7(5):1978-83.

84. Pelaz SG, Tabernero A. Src: coordinating metabolism in cancer. Oncogene. 2022;41(45):4917-28.

85. Hecker TP, Grammer JR, Gillespie GY, Stewart J, Jr., Gladson CL. Focal adhesion kinase enhances signaling through the Shc/extracellular signal-regulated kinase pathway in anaplastic astrocytoma tumor biopsy samples. Cancer Res. 2002;62(9):2699-707.

86. Reynolds AB, Kanner SB, Bouton AH, Schaller MD, Weed SA, Flynn DC, et al. SRChing for the substrates of Src. Oncogene. 2014;33(37):4537-47.

87. Arcaro A, Aubert M, Espinosa del Hierro ME, Khanzada UK, Angelidou S, Tetley TD, et al. Critical role for lipid raft-associated Src kinases in activation of PI3K-Akt signalling. Cell Signal. 2007;19(5):1081-92.

88. Kirsch DG, Doseff A, Chau BN, Lim D-S, De Souza-Pinto NC, Hansford R, et al. Caspase-3-dependent Cleavage of Bcl-2 Promotes Release of Cytochrome c. Journal of Biological Chemistry. 1999;274(30):21155-61.

89. Sun Q, Wang Y, Desgrosellier JS. Combined Bcl-2/Src inhibition synergize to deplete stem-like breast cancer cells. Cancer Lett. 2019;457:40-6.

90. Chakraborty G, Patail NK, Hirani R, Nandakumar S, Mazzu YZ, Yoshikawa Y, et al. Attenuation of SRC Kinase Activity Augments PARP Inhibitor-mediated Synthetic Lethality in BRCA2-altered Prostate Tumors. Clin Cancer Res. 2021;27(6):1792-806.

91. Anerillas C, Herman AB, Rossi M, Munk R, Lehrmann E, Martindale JL, et al. Early SRC activation skews cell fate from apoptosis to senescence. Sci Adv. 2022;8(14):eabm0756.

92. Huang X, Xiao F, Li Y, Qian W, Ding W, Ye X. Bypassing drug resistance by triggering necroptosis: recent advances in mechanisms and its therapeutic exploitation in leukemia. Journal of Experimental & Clinical Cancer Research. 2018;37(1).

93. Seo EJ, Kim DK, Jang IH, Choi EJ, Shin SH, Lee SI, et al. Hypoxia-NOTCH1-SOX2 signaling is important for maintaining cancer stem cells in ovarian cancer. Oncotarget. 2016;7(34):55624-38.

94. Lee JH, Suk J, Park J, Kim SB, Kwak SS, Kim JW, et al. Notch Signal Activates Hypoxia Pathway through HES1-Dependent SRC/Signal Transducers and Activators of Transcription 3 Pathway. Molecular Cancer Research. 2009;7(10):1663-71.

95. Zou H, Luo J, Guo Y, Tong T, Liu Y, Chen Y, et al. Tyrosine kinase SRC-induced YAP1-KLF5 module regulates cancer stemness and metastasis in triple-negative breast cancer. Cellular and Molecular Life Sciences. 2023;80(2).

96. Hanahan D, Weinberg RA. The Hallmarks of Cancer. Cell. 2000;100(1):57-70.

97. Das S, Bhattacharya B, Das B, Sinha B, Jamatia T, Paul K. Etiologic Role of Kinases in the Progression of Human Cancers and Its Targeting Strategies. Indian Journal of Surgical Oncology. 2021;12(S1):34-45.

98. Brognard J, Hunter T. Protein kinase signaling networks in cancer. Curr Opin Genet Dev. 2011;21(1):4-11.

99. Cicenas J, Zalyte E, Bairoch A, Gaudet P. Kinases and Cancer. Cancers. 2018;10(3):63.

100. Milde T, Lodrini M, Savelyeva L, Korshunov A, Kool M, Brueckner LM, et al. HD-MB03 is a novel Group 3 medulloblastoma model demonstrating sensitivity to histone deacetylase inhibitor treatment. J Neurooncol. 2012;110(3):335-48.

101. Bandopadhayay P, Bergthold G, Nguyen B, Schubert S, Gholamin S, Tang Y, et al. BET bromodomain inhibition of MYC-amplified medulloblastoma. Clin Cancer Res. 2014;20(4):912-25.

102. Dietl S, Schwinn S, Dietl S, Riedel S, Deinlein F, Rutkowski S, et al. MB3W1 is an orthotopic xenograft model for anaplastic medulloblastoma displaying cancer stem cell- and Group 3-properties. BMC Cancer. 2016;16:115.

103. Ivanov DP, Coyle B, Walker DA, Grabowska AM. In vitro models of medulloblastoma: Choosing the right tool for the job. J Biotechnol. 2016;236:10-25.

104. Trojanowski JQ, Friedman HS, Burger PC, Bigner DD. A rapidly dividing human medulloblastoma cell line (D283 MED) expresses all three neurofilament subunits. Am J Pathol. 1987;126(2):358-63.

105. Manoranjan B, Venugopal C, Bakhshinyan D, Adile AA, Richards L, Kameda-Smith MM, et al. Wnt activation as a therapeutic strategy in medulloblastoma. Nat Commun. 2020;11(1):4323.

106. Klementová J, Jarošová Š, Danilová I, Farníková M, Novotný J, Davídková M, et al. Comparative analysis of pediatric SHH medulloblastoma DAOY spheres and adherent monolayers: implications for medulloblastoma research. Cancer Cell Int. 2025;25(1):22.

107. Okonechnikov K, Federico A, Schrimpf D, Sievers P, Sahm F, Koster J, et al. Comparison of transcriptome profiles between medulloblastoma primary and recurrent tumors uncovers novel variance effects in relapses. Acta Neuropathol Commun. 2023;11(1):7.

108. Suk Y, Kieliszek A, Mobilio D, Venugopal C, Singh SK. Derivation and culturing of neural stem cells from human embryonic brain tissue. STAR Protoc. 2022;3(3):101628.

109. Wagner EF, Nebreda AR. Signal integration by JNK and p38 MAPK pathways in cancer development. Nat Rev Cancer. 2009;9(8):537-49.

110. Forget A, Martignetti L, Puget S, Calzone L, Brabetz S, Picard D, et al. Aberrant ERBB4-SRC Signaling as a Hallmark of Group 4 Medulloblastoma Revealed by Integrative Phosphoproteomic Profiling. Cancer Cell. 2018;34(3):379-95.e7.

111. Prados MD. Current Strategies for Management of Medulloblastoma. Diagnostics. 2023;13(16):2622.

112. Wu JF, Ji J, Dong SY, Li BB, Yu ML, Wu DD, et al. Gefitinib enhances oxaliplatin-induced apoptosis mediated by Src and PKC-modulated gap junction function. Oncol Rep. 2016;36(6):3251-8.

113. Wang H, Han S, Xie J, Zhao R, Li S, Li J. IL-17A exacerbates caspase-12-dependent neuronal apoptosis following ischemia through the Src-PLCγ-calpain pathway. Exp Neurol. 2024;379:114863.

114. Fu Y, Yang G, Zhu F, Peng C, Li W, Li H, et al. Antioxidants decrease the apoptotic effect of 5-Fu in colon cancer by regulating Src-dependent caspase-7 phosphorylation. Cell Death Dis. 2014;5(1):e983.

115. García-Gutiérrez V, Hernández-Boluda JC. Tyrosine Kinase Inhibitors Available for Chronic Myeloid Leukemia: Efficacy and Safety. Front Oncol. 2019;9:603.

116. Ramos R, Vale N. Dual Drug Repurposing: The Example of Saracatinib. Int J Mol Sci. 2024;25(8).

117. Blake RA, Broome MA, Liu X, Wu J, Gishizky M, Sun L, et al. SU6656, a selective src family kinase inhibitor, used to probe growth factor signaling. Mol Cell Biol. 2000;20(23):9018-27.

118. Kumar P, Murphy FA. Francis Peyton Rous. Emerging Infectious Diseases. 2013;19(4):660-3.

119. Varmus H. Of oncogenes and open science: an interview with Harold Varmus. Disease Models & Mechanisms. 2019;12(3):dmm038919.

120. Irby RB, Yeatman TJ. Role of Src expression and activation in human cancer. Oncogene. 2000;19(49):5636-42.

121. Wheeler DL, Iida M, Dunn EF. The Role of Src in Solid Tumors. The Oncologist. 2009;14(7):667-78.

122. Angel CZ, Beattie S, Hanif EAM, Ryan MP, Guerra Liberal FDC, Zhang SD, et al. A SRC-slug-TGFβ2 signaling axis drives poor outcomes in triple-negative breast cancers. Cell Commun Signal. 2024;22(1):454.

123. Gaule P, Mukherjee N, Corkery B, Eustace A, Gately K, Roche S, et al. Dasatinib Treatment Increases Sensitivity to c-Met Inhibition in Triple-Negative Breast Cancer Cells. Cancers. 2019;11(4):548.

124. Peiró G, Ortiz-Martínez F, Gallardo A, Pérez-Balaguer A, Sánchez-Payá J, Ponce JJ, et al. Src, a potential target for overcoming trastuzumab resistance in HER2-positive breast carcinoma. British Journal of Cancer. 2014;111(4):689-95.

125. Woytash JA, Lefebvre AEYT, Zhang Z, Xu B, Harchenko SA, Le HT, et al. CDCP1/mitochondrial Src axis increases electron transport chain function to promote metastasis in triple-negative breast cancer. British Journal of Cancer. 2025;133(9):1265-77.

126. Mezquita B, Reyes-Farias M, Pons M. FDA-approved antivirals ledipasvir and daclatasvir downregulate the Src-EPHA2-Akt oncogenic pathway in colorectal and triple-negative breast cancer cells. Biomed Pharmacother. 2024;179:117325.

127. González-Alonso P, Zazo S, Martín-Aparicio E, Luque M, Chamizo C, Sanz-Álvarez M, et al. The Hippo Pathway Transducers YAP1/TEAD Induce Acquired Resistance to Trastuzumab in HER2-Positive Breast Cancer. Cancers. 2020;12(5):1108.

128. Cemile Uslu EK, Alex Lyakhovich,. OXPHOS inhibition overcomes chemoresistance in triple negative breast cancer. Redox Biology. 2025;83.

129. Dash S, Hanson S, King B, Nyswaner K, Foss K, Tesi N, et al. The SRC family kinase inhibitor NXP900 demonstrates potent antitumor activity in squamous cell carcinomas. Journal of Biological Chemistry. 2024;300(9):107615.

130. Liu H, Li Z, Xu X, Xu B, Li Z. Network pharmacology and in vitro analyses reveal EGCG inhibits breast cancer progression via suppression of the EGFR/Src pathway. Biochem Biophys Res Commun. 2025;769:151942.

131. Baggio C, Udompholkul P, Gambini L, Pellecchia M. Targefrin: A Potent Agent Targeting the Ligand Binding Domain of EphA2. J Med Chem. 2022;65(22):15443-56.

132. Wang Y, Huang A, Chen L, Sun F, Zhao M, Zhang M, et al. Design and synthesis of dual BRD4/Src inhibitors for treatment of triple-negative breast cancer. Eur J Med Chem. 2024;264:116009.

133. Zhao W, Ouyang C, Zhang L, Wang J, Zhang J, Zhang Y, et al. The proto-oncogene tyrosine kinase c-SRC facilitates glioblastoma progression by remodeling fatty acid synthesis. Nature Communications. 2024;15(1).

134. Álvarez-Vázquez A, San-Segundo, L., Cerveró-García, P., Flores-Hernández, R., Ollauri-Ibáñez, C., Segura-Collar, B., Hubert, C. G., Morrison, G., Pollard, S. M., Lathia, J. D., Sánchez-Gómez, P., & Tabernero, A.. EGFR amplification and EGFRvIII predict and participate in TAT-Cx43266–283 antitumor response in preclinical glioblastoma models. Neuro-oncology. 2024;26(7):1230–46.

135. Roos A, Dhruv HD, Peng S, Inge LJ, Tuncali S, Pineda M, et al. EGFRvIII–Stat5 Signaling Enhances Glioblastoma Cell Migration and Survival. Molecular Cancer Research. 2018;16(7):1185-95.

136. Galanis E, Anderson SK, Twohy EL, Carrero XW, Dixon JG, Tran DD, et al. A phase 1 and randomized, placebo-controlled phase 2 trial of bevacizumab plus dasatinib in patients with recurrent glioblastoma: Alliance/North Central Cancer Treatment Group N0872. Cancer. 2019;125(21):3790-800.

137. Li L, Liu X, Si Z, Wang X. Epigenetic Mechanisms Governing Nrf2 Expression and Its Role in Ferroptosis. Biomedicines. 2025;13(8):1913.

138. Cirotti C, Taddei I, Contadini C, Di Girolamo C, Pepe G, De Bardi M, et al. NRF2 connects Src tyrosine kinase to ferroptosis resistance in glioblastoma. Life Science Alliance. 2024;7(1):e202302205.

139. Blomquist MR, Eghlimi R, Beniwal A, Grief D, Nascari DG, Inge L, et al. EGFRvIII Confers Sensitivity to Saracatinib in a STAT5-Dependent Manner in Glioblastoma. International Journal of Molecular Sciences. 2024;25(11):6279.

140. Koc D, Ibis K, Besarat P, Banoglu E, Kiris E. Tirbanibulin (KX2-391) analog KX2-361 inhibits botulinum neurotoxin serotype A mediated SNAP-25 cleavage in pre- and post-intoxication models in cells. Drug Development Research. 2024;85(6).

141. Chattopadhyay I, Wang J, Qin M, Gao L, Holtz R, Vessella RL, et al. Src promotes castration-recurrent prostate cancer through androgen receptor-dependent canonical and non-canonical transcriptional signatures. Oncotarget. 2017;8(6):10324-47.

142. Kim S, Alsaidan OA, Goodwin O, Li Q, Sulejmani E, Han Z, et al. Blocking Myristoylation of Src Inhibits Its Kinase Activity and Suppresses Prostate Cancer Progression. Cancer Research. 2017;77(24):6950-62.

143. Cai H, Babic I, Wei X, Huang J, Witte ON. Invasive Prostate Carcinoma Driven by c-Src and Androgen Receptor Synergy. Cancer Research. 2011;71(3):862-72.

144. Tatarov O, Mitchell TJ, Seywright M, Leung HY, Brunton VG, Edwards J. Src Family Kinase Activity Is Up-Regulated in Hormone-Refractory Prostate Cancer. Clinical Cancer Research. 2009;15(10):3540-9.

145. Gao L, Han B, Dong X. The Androgen Receptor and Its Crosstalk With the Src Kinase During Castrate-Resistant Prostate Cancer Progression. Frontiers in Oncology. 2022;12.

146. Alfano A, Xu J, Yang X, Deshmukh D, Qiu Y. SRC Kinase-Mediated Tyrosine Phosphorylation of TUBB3 Regulates Its Stability and Mitotic Spindle Dynamics in Prostate Cancer Cells. Pharmaceutics. 2022;14(5):932.

147. Uivarosi V, Miricescu D, Vacaroiu IA, Spinu DA, Stefani C, Stanciu S, et al. Prostate Cancer, JAK/STAT3 Dysregulation, and Flavonoids: Is There a Possible Link? International Journal of Molecular Sciences. 2026;27(2):885.

148. Sands M, Adams S, Lee J, Li M, Wang M, Walsh TJ, et al. The interconnection between androgen receptor and DNA damage response pathways in prostate cancer. Current Urology. 2025;19(6):376-87.

149. Martellucci S, Clementi L, Sabetta S, Mattei V, Botta L, Angelucci A. Src Family Kinases as Therapeutic Targets in Advanced Solid Tumors: What We Have Learned So Far. Cancers. 2020;12(6):1448.

150. Fizazi K. The role of Src in prostate cancer. Annals of Oncology. 2007;18(11):1765-73.

151. Hu M, Zeng H, Chen S, Xu Y, Wang S, Tang Y, et al. SRC-3 is involved in maintaining hematopoietic stem cell quiescence by regulation of mitochondrial metabolism in mice. Blood. 2018;132(9):911-23.

152. Chen E, Louis, Anthony. Janus Kinase Deregulation in Leukemia and Lymphoma. Immunity. 2012;36(4):529-41.

153. Quintás-Cardama A, Cortes J. Molecular biology of bcr-abl1–positive chronic myeloid leukemia. Blood. 2009;113(8):1619-30.

154. Li H, Huang Z, Gao M, Huang N, Luo Z, Shen H, et al. Inhibition of YAP suppresses CML cell proliferation and enhances efficacy of imatinib in vitro and in vivo. Journal of Experimental & Clinical Cancer Research. 2016;35(1).

155. Sun J, Hu R, Han M, Tan Y, Xie M, Gao S, et al. Mechanisms underlying therapeutic resistance of tyrosine kinase inhibitors in chronic myeloid leukemia. International Journal of Biological Sciences. 2024;20(1):175-81.

156. Shyam Sunder S, Sharma UC, Pokharel S. Adverse effects of tyrosine kinase inhibitors in cancer therapy: pathophysiology, mechanisms and clinical management. Signal Transduction and Targeted Therapy. 2023;8(1).

157. Parker WT, Yeung DTO, Yeoman AL, Altamura HK, Jamison BA, Field CR, et al. The impact of multiple low-level BCR-ABL1 mutations on response to ponatinib. Blood. 2016;127(15):1870-80.

158. Yildiz D, Eskazan AE. STAMP inhibitors and their future in CML therapy: a critical analysis. Blood Cancer Journal. 2025;15(1).

159. Patel RK, Weir MC, Shen K, Snyder D, Cooper VS, Smithgall TE. Expression of myeloid Src-family kinases is associated with poor prognosis in AML and influences Flt3-ITD kinase inhibitor acquired resistance. PLOS ONE. 2019;14(12):e0225887.

160. Nam S, Williams A, Vultur A, List A, Bhalla K, Smith D, et al. Dasatinib (BMS-354825) inhibits Stat5 signaling associated with apoptosis in chronic myelogenous leukemia cells. Molecular Cancer Therapeutics. 2007;6(4):1400-5.

161. Hu X, Li L, Nkwocha J, Kmieciak M, Shang S, Cowart LA, et al. Src inhibition potentiates MCL-1 antagonist activity in acute myeloid leukemia. Signal Transduction and Targeted Therapy. 2025;10(1).

162. Smith BD, Brümmendorf TH, Roboz GJ, Gambacorti-Passerini C, Charbonnier A, Viqueira A, et al. Efficacy and safety of bosutinib in patients treated with prior imatinib and/or dasatinib and/or nilotinib: Subgroup analyses from the phase 4 BYOND study. Leuk Res. 2024;139:107481.

163. Shi R, Farnsworth DA, Febres-Aldana CA, Chow JLM, Sheena R, Atwal T, et al. Drug tolerance and persistence to EGFR inhibitor treatment are mediated by an ILK-SFK-YAP signaling axis in lung adenocarcinoma. Oncogene. 2025;44(32):2831-49.

164. Uribe ML, Marrocco I, Yarden Y. EGFR in Cancer: Signaling Mechanisms, Drugs, and Acquired Resistance. Cancers. 2021;13(11):2748.

165. Raji L, Tetteh A, Amin ARMR. Role of c-Src in Carcinogenesis and Drug Resistance. Cancers. 2023;16(1):32.

166. Rubtsova SN, Zhitnyak IY, Gloushankova NA. Dual role of E-cadherin in cancer cells. Tissue Barriers. 2022;10(4).

167. Serrels A, Canel M, Brunton VG, Frame MC. Src/FAK-mediated regulation of E-cadherin as a mechanism for controlling collective cell movement. Cell Adhesion & Migration. 2011;5(4):360-5.

168. Zhe Zhang YT, Canhua Huang, Xiawei We,. Redox signaling in drug-tolerant persister cells as an emerging therapeutic target. EBioMedicine. 2023;89:104483.

169. Haderk F, Chou Y-T, Cech L, Fernández-Méndez C, Yu J, Olivas V, et al. Focal adhesion kinase-YAP signaling axis drives drug-tolerant persister cells and residual disease in lung cancer. Nature Communications. 2024;15(1).

170. Zou H, Poore B, Brown EE, Qian J, Xie B, Asimakidou E, et al. A neurodevelopmental epigenetic programme mediated by SMARCD3–DAB1–Reelin signalling is hijacked to promote medulloblastoma metastasis. Nature Cell Biology. 2023;25(3):493-507.

171. Petersen W, Liu J, Yuan L, Zhang H, Schneiderjan M, Cho YJ, et al. Dasatinib suppression of medulloblastoma survival and migration is markedly enhanced by combining treatment with the aurora kinase inhibitor AT9283. Cancer Lett. 2014;354(1):68-76.

172. Wei J, Ma L, Li C, Pierson CR, Finlay JL, Lin J. Targeting Upstream Kinases of STAT3 in Human Medulloblastoma Cells. Curr Cancer Drug Targets. 2019;19(7):571-82.

173. Kuzmychova H, Chawla, U., Martell, E., Grewal, A., Jain, C., Ramnauth, K., Kaul, E., Senthil, H., Venugopal, C., Anderson, M. C., Singh, K. S., & Sharif, T. Targeting SRC enhances differentiation and promotes multifaceted cell death mechanisms in recurrent group 3 medulloblastoma. Cell Death Dis. 2026.

174. Sharma P, Aaroe A, Liang J, Puduvalli VK. Tumor microenvironment in glioblastoma: Current and emerging concepts. Neuro-Oncology Advances. 2023;5(1).